MECHANICAL AND STRUCTURAL CHARACTERISATION OF EXTRUSION MOULDED SHCC
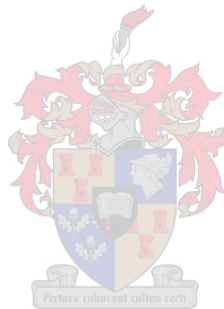
CHRISTO RIAAN VISSER

THESIS PRESENTED FOR THE DEGREE OF MASTER OF SCIENCE AT THE DEPARTMENT OF CIVIL ENGINEERING OF THE UNIVERSITY OF STELLENBOSCH

SUPERVISOR: PROF. G.P.A.G. VAN ZIJL

December 2007

DECLARATION

I, the undersigned, hereby declare that the work contained in this thesis report is my own original work and that I have not previously in its entirety or in part submitted it at any university for a degree.

Signature: _____

Date: _____

SUMMARY

SHCC (Strain-Hardening Cement-based Composite) is a type of HPFRCC (High Performance Fibre Reinforced Cement-based Composite) that was designed and engineered to overcome the weaknesses of ordinary concrete. It shows a high ductility as it can resist the full tensile load at a strain of more than 3%. This superior response is achieved with multiple cracking under tensile loading which has a pseudo strain-hardening phenomenon as a result.

The purpose of the research project reported in this thesis document was to design and build a new piston-driven extruder for the production of SHCC as well as R/SHCC (reinforced SHCC) elements and to investigate and characterise the structural and mechanical behaviour of extrusion moulded SHCC.

A new piston-driven extruder, specifically for academic purposes, was designed based on the principles of fluid flow mechanics. Although fluid flow is not an ideal model to represent the flow of viscous material through an extruder, it was deemed sufficient for this specific study. A new extruder with the capacity to extrude SHCC and R/SHCC was built. Provision was made that this extruder can be fitted with extruder dies and transition zones of varying shapes and sizes.

A comparative study between unreinforced as well as reinforced cast SHCC and extruded SHCC as well as a suitable R/C (Reinforced Concrete) was conducted. Three-point bending tests, representative of the envisioned structural application, were performed on specimens of each of the composites.

The unreinforced cast SHCC and especially the unreinforced extruded SHCC have a comparative level of performance to the cast R/C. These specimens displayed a similar cracking pattern of multiple cracks, although less pronounced in the extruded SHCC. The extruded SHCC has superior first cracking and ultimate strength in comparison to cast SHCC, but with accompanying lower ductility.

The reinforced SHCC specimens failed in a combination of flexure and shear. The extruded R/SHCC specimens formed multiple diagonal cracks before failure, while the cast R/SHCC specimens formed only a few diagonal cracks, before delaminating along the reinforcement. The higher shear capacity and thus the ability to form multiple diagonal cracks of the extruded R/SHCC

can be ascribed to the better fibre orientation of the specimens in the longitudinal direction, while the cast specimens have a random orientation of fibres. R/SHCC and especially extruded R/SHCC could be a far superior structural material to R/C.

Mechanical characterisation of extruded SHCC was done with the use of uni-axial tensile and compressive tests. The results of these tests were compared with the results of uni-axial tensile tests previously performed on cast SHCC as well as uni-axial compressive tests that were performed on cast SHCC in this research study.

The extruded SHCC displayed superior tensile performance in terms of first cracking and ultimate strength in comparison to cast SHCC, but with accompanying lower ductility. In terms of compressive performance the extruded SHCC has a higher ultimate strength, but with a lower ductility than cast SHCC. The extruded SHCC also has a much higher E-modulus than cast SHCC. This can partly be attributed to the difference between the water/binder ratios of the cast and extruded SHCC, but can mainly be ascribed to the lower porosity as a result of high extrusion forces involved in the manufacturing of extruded SHCC.

A simple bending model for SHCC has also been introduced. This model is based on the mechanical characteristics of SHCC. The model somewhat underestimates the resistance moment of the extruded and cast SHCC, but this underestimation is more pronounced in the case of the cast SHCC. Various reasons for the underestimation is discussed, but it is postulated that the main reason for the difference in experimentally determined and the calculated resistance moment of the cast SHCC is the possible variation in ingredient properties and specimen preparation and testing, since the characterisation of the cast SHCC was done over a long period of time and by different researchers. The bending model is however deemed sufficient for the design purposes of SHCC.

OPSOMMING

SHCC ("Strain-Hardening Cement-based Composite") is 'n tipe HPFRCC ("High Performance Fibre Reinforced Cement-based Composite") wat ontwerp is om die swakhede van gewone beton te oorkom. Hierdie materiaal het 'n hoë duktiliteit en kan die volle trekkrag weerstaan met 'n vervorming van meer as 3%. Hierdie uitstaande gedrag word gekenmerk deur meerdere krake wat vorm gedurende 'n trek belasting wat vervormingsverharding tot gevolg het.

Die doel van die navorsingsprojek wat weergegee word in hierdie tesis dokument was om 'n nuwe suier-aangedrewe ekstrueerder vir die produksie van SHCC sowel as R/SHCC (bewapende SHCC) te ontwerp en te bou en om die strukturele en meganiese gedrag van ge-ekstrueerde SHCC te ondersoek en te karakteriseer.

'n Nuwe suier-aangedrewe ekstrueerder, spesifiek for akademiese doeleindes, is ontwerp gebaseer op die beginsels van vloeistof vloeimeganika. Alhoewel vloeistof vloeimeganika nie 'n ideale model is vir die voorstelling van die vloei van 'n viskose materiaal deur 'n ekstrueerder nie, word dit beskou as aanvaarbaar vir die doeleindes van hierdie spesifieke studie. 'n Nuwe ekstrueerder met die kapasiteit om SHCC en R/SHCC te ekstrueer is gebou. Voorsiening is ook gemaak dat ekstrueerder vorms ("dies") en oorgangsones van verskillende vorms en groottes aan die ekstrueerder geheg kan word.

'n Vergelykende studie tussen onbewapende sowel as bewapende gegote en ge-ekstrueerde SHCC, sowel as 'n gepasde R/C ("Reinforced Concrete") is uitgevoer. Drie-punt buigtoetse, verteenwoordigend van die voorgestelde strukturele toepassings vir SHCC, is uitgevoer op proefstukke van elk van die bogenoemde materiale.

Die meganiese gedrag van die onbewapende gegote SHCC en spesifiek die onbewapende ge-ekstrueerde SHCC is vergelykbaar met die meganiese gedrag van gegote R/C. Hierdie proefstukke het ooreenstemmende kraakpatrone van veelvuldige krake getoon, alhoewel dit minder prominent was in die geval van ge-ekstrueerde SHCC. Die ge-ekstrueerde SHCC het hoër eerste kraak- en maksimum sterktes in vergelyking met gegote SHCC, maar met gepaardgaande laer duktiliteit.

Die bewapende SHCC proefstukke het in 'n kombinasie van buig en skuif gefaal. Die ge-ekstrueerde R/SHCC proefstukke het meerdere diagonale krake gevorm voor faling, terwyl die gegote R/SHCC proefstukke slegs 'n paar diagonale krake gevorm het, voordat dit langs die

bewapening gedelamineer het. Die hoër skuifkapasiteit van ge-ekstrueerde SHCC en dus die vermoë om meerdere diagonale krake te vorm, kan toegeskryf word aan die longitudinale orientasie van vesels van die proefstukke, terwyl gegote proefstukke se vesels meer lukraak georienteerd is. R/SHCC en spesifiek ge-ekstrueerde R/SHCC kan 'n superieure strukturele materiaal in vergelyking met R/C wees.

Die meganiese karakterisering van ge-ekstrueerde SHCC is gedoen met die gebruik van direkte trek- en druktoetse. The resultate van die hierdie toetse is vergelyk met die resultate van direkte trektoetse uit 'n vorige studie op gegote SHCC,, sowel as met die uitslae van direkte druktoetse wat op gegote SHCC in hierdie navorsingstudie gedoen is.

Die ge-ekstrueerde SHCC het superieure trekgedrag in terme van eerste kraak en maksimum sterktes in vergelyking met gegote SHCC getoon, maar met gepaardgaande laer duktiliteit. In terme van drukgedrag het die ge-ekstrueerde SHCC 'n hoër maksimum druksterkte, maar met 'n laer duktiliteit in vergelyking met die gegote SHCC. Die ge-ekstrueerde SHCC het ook 'n veel hoër E-modulus as gegote SHCC. Dit is gedeeltelik as gevolg van die verskil in die water/binder verhouding van die gegote en ge-ekstrueerde SHCC, maar kan grootliks toegeskryf word aan die laer porositeit van ge-ekstrueerde SHCC as gevolg van die hoë ekstrusie kragte.

'n Eenvoudige buigmodel vir SHCC word ook voorgestel. Hierdie model is geabseer op die meganiese gedrag van SHCC. Die model onderskat die weerstandsmoment van ge-ekstrueerde SHCC sowel as gegote SHCC, maar hierdie onderskatting is meer prominent in die geval van gegote SHCC. Verskeie redes vir hierdie onderskatting word genoem, maar dit word beweer dat in die geval van gegote SHCC dit grootliks as gevolg van moontlike variasies in die materiaal eienskappe en proefstukke se voorbereiding en toetsing is, aangesien die karakterisering van die gegote SHCC oor 'n lang tydperk en deur verskillende navorsers gedoen is. Die buigmodel word nogtans as voldoende beskou vir die ontwerpdoeleinde van SHCC.

ACKNOWLEDGEMENTS

TABLE OF CONTENTS

LIST OF FIGURES

LIST OF TABLES

NOMENCLATURE

A/B	Aggregate-Binder ratio
A_c	Cross sectional area of concrete
A_s	Cross sectional area of steel reinforcing
c	Crack spacing
C.O.V.	Coefficient of Variation
E	Elastic modulus
E_a	Aggregate elastic modulus
E_c	Elastic modulus of the composite
E_m	Matrix elastic modulus
FA	Fly Ash
FA/B	Fly Ash-Binder ratio
f_{cu}	Ultimate compressive strength
F_{fc}	First cracking force
F_{max}	Maximum force
FRC	Fibre Reinforced Concrete
f_t	Tensile strength
$f_{t,f}$	Tensile strength of fibres
f_{tu}	Ultimate tensile strength
f_y	Yield strength
G_f	Fracture energy
GGCS/B	Ground Granulated Corex Slag-Binder ratio
GGCS	Ground Granulated Corex Slag
HCC	Hybrid Concrete Construction
HPFRCC	High Performance Fibre Reinforced Cement Composite
L_m	Length of multiple cracking zone
M_{max}	Maximum moment
MOR	Modulus of Rupture
Ø	Diameter
OPC	Ordinary Portland Cement
p	Porosity
P(x)	Horizontal pressure at point x
PVA	Poly Vinyl Alcohol
R/C	Reinforced Concrete

R/SHCC	Reinforced Strain Hardening Cement-based Composites
RD	Relative Density
SHCC	Strain Hardening Cement-based Composites
SP	Superplasticiser
StdDev	Standard Deviation
V	Shear force
V_a	Aggregate volume
VA	Viscous agent
v_c	Shear stress capacity
V_f	Fibre volume
V_m	Matrix volume
V_p	Paste volume
W/B	Water-Binder ratio
γ_m	Material factor
δ_m	Crack mouth width
δ_p	Ultimate fibre deformation
δ_{ss}	Steady-state crack width
ε_0	Strain at pre-stress σ_0
ε_c	Compressive strain
ε_{cu}	Ultimate compressive strain
ε_t	Tensile strain
ε_{tmax}	Maximum tensile strain
ε_{tu}	Ultimate tensile strain
$\varepsilon_{u,f}$	Ultimate fibre elongation
η	Efficiency coefficient
μ	Friction coefficient
σ_0	Pre-stress
σ_c	Compressive stress
σ_{ca}	Standardized compressive strength
σ_{cu}	Ultimate compressive stress
σ_{fc}	First cracking strength
σ_{ss}	Steady-state stress
σ_t	Tensile stress
σ_{tf}	Tensile first cracking stress
σ_{tu}	Ultimate tensile stress

$\tau(x)$ Friction surface / shear stress at point x

τ_{max} Maximum shear stress

1 INTRODUCTION

Over the centuries, concrete has been used as a reliable, fairly durable building material. Two of the main advantages of concrete are that it has a high compressive strength and that it can be cast on the construction site into virtually any size and shape. The shortcomings of concrete are becoming more and more prominent in this day and age with the emphasis of design moving towards optimised economical designs. The most prominent disadvantages of concrete are the brittleness during failure and the low tensile strength, which is about one tenth of the compressive strength. The low tensile strength is compensated for with the use of reinforcing steel, but cracking still occurs during the normal use of reinforced concrete. These cracks lead to durability problems as water penetrates the concrete through the cracks and causes the corrosion of the reinforcing steel which in turn leads to structural degradation.

SHCC (Strain-Hardening Cement-based Composite) is a type of HPFRCC (High Performance Fibre Reinforced Cement Composite) that has been engineered to overcome the weaknesses of ordinary concrete as mentioned above. It shows high ductility as it can resist the full tensile load at a strain of more than 3% compared to concrete which fails on average at a strain of 0.01% in tension. When using SHCC instead of ordinary concrete the strain capacity increases more than 300 times. This leads to a high energy absorbing capacity of SHCC.

During the increase of strain under tensile loading of SHCC, a constant strain-hardening effect is found and many, closely spaced, micro-cracks are formed in the material. These fine, multiple cracks reduce the problem of water penetration and thus improve the durability of the structures.

SHCC is more expensive than ordinary concrete, but if the superior material characteristics are exploited, it becomes a competitive material in the building industry. The advantages of SHCC may be exploited in several applications:

- Seismic loading application: Due to the high ductility and flexibility of SHCC it can be used in designated areas in a multi-storey structure to withstand seismic loadings.

- Thin membrane and shell members: Due to the high ductility, thin membrane members, i.e. less than 15 mm thick, can be made e.g. pipes, tiles, etc.

- Repair material: Due to the high strain capacity and energy absorption, SHCC is ideal to be used as repair material, especially for bonded overlays.

- Durable structural application: Due to the fine, multiple cracking phenomenon of SHCC it is an ideal cover material for reinforcing steel in R/C elements.

- Composite application: Applied in combination with R/C, for instance as a permanent formwork shell for (reinforced) concrete members, SHCC adds the benefits of construction time saving and shear steel reduction, as SHCC has a higher shear resistance than ordinary concrete.

South Africa is currently facing a shortage of engineers, technicians and other skilled workers in the construction industry. The shortage of skills clearly places high demands on designers and contractors to provide services and to realise projects in ever reducing time periods and at lower cost. These conditions, in a growing economy, augmented by the shortage of manpower, make it increasingly difficult to maintain quality of construction in an industry where mistakes can lead to disastrous consequences. Hybrid Concrete Construction (HCC) is a type of construction where a combination of prefabricated concrete elements and cast in-situ concrete is used and is seen as a possible solution to these problems that the South African construction industry is facing. This is done by using the optimal combination of both types of concrete construction by considering time and cost reduction, but with increased quality. SHCC is a construction material suitable to this type of construction and can be used for various applications, as mentioned above.

Extrusion is a special type of manufacturing method by which structural elements with complex geometrical cross section can be made to virtually any length, permitting for space restrictions. This type of manufacturing method of SHCC fits in well with the idea of HCC. Not much research has been done on the extrusion of SHCC, especially on piston-driven extrusion. This thesis document reports on research that was done to determine the mechanical properties of extruded SHCC with the structural use thereof in mind. It also contains a description of the new piston-driven extruder that was designed to manufacture extruded SHCC and R/SHCC (steel reinforced SHCC) as well as mechanical tests that were conducted on both types of composites. In addition, a simple bending model is presented for the design/analysis of (R/)SHCC, which uses these characterised properties of SHCC.

In Chapter 2 a theoretical background is given on SHCC, its typical mechanical properties and the properties of its constituent material. The extrusion of SHCC is also covered.

In Chapter 3 a description of the design of the new piston-driven extruder facility is given along with a description of the extruder itself.

In Chapter 4 a comparative study of cast and extruded SHCC and R/SHCC as well as Reinforced Concrete (R/C) is undertaken. This is done by comparing the mechanical properties of the composites in flexure.

In Chapter 5 the tensile and compressive mechanical properties of extruded SHCC are investigated and compared to that of cast SHCC. This is done by comparing responses to uni-axial tests on extruded SHCC.

A simple bending model for SHCC, based on its uni-axial properties as determined in the previous chapter, is introduced in Chapter 6. The results obtained with this model are also compared with experimentally determined results.

Finally, in Chapter 7 conclusions, based on the research study reported in this thesis document, are drawn and recommendations are made for possible future research studies.

2 BACKGROUND OF SHCC AND EXTRUSION

2.1 INTRODUCTION

Concepts about the development of SHCC as a durable building material will be presented in this section. Attention is given to the unique material properties and constituents used to achieve the material behaviour. The concept of the extrusion of SHCC as well as the development thereof thus far is also introduced.

The focus of this literature study will be directed towards characterising SHCC, its constituents and properties. Secondly it will focus on the extrusion of SHCC, the requirements for extrusion and the characteristics of extruded SHCC. The third section contains a discussion of the benefits and applications for reinforced SHCC (R/SHCC).

2.2 PROPERTIES OF SHCC

2.2.1 MATERIAL PROPERTIES

Most of the properties that are discussed in this section are based on work that has been done with SHCC prepared by casting in moulds, since casting has been the preferred way of manufacturing for SHCC thus far. The basic concepts do however apply to SHCC in general. The extrusion of SHCC specifically, will be dealt with in another section of this chapter.

2.2.1.1 Tensile properties

Most of the research that has been done on SHCC has been focussed on the tensile behaviour and tensile characteristics of SHCC. The most fundamental mechanical property of SHCC is the ductile tensile behaviour after the occurrence of the first crack. The fundamental difference between SHCC and ordinary fibre reinforced concrete (FRC) is the strain-hardening response that accompanies the

ductile behaviour of SHCC. FRC displays a decline in strength with an increase in strain beyond the occurrence of the first crack, which is referred to as strain-softening. Strain-hardening behaviour on the other hand is a behaviour that displays an increase in post cracking strength, accompanied by the formation of multiple cracks, not always visible to the naked eye. Multiple cracks are the only means by which a rigid cement-based material can manifest strains larger than elastic strain, with an increase in strength. Note that the notion of strain is used in a macroscopic sense. A non-uniform deformation does occur, with higher local deformation in the vicinity of cracks due to lower stiffness in these regions of bridged cracking. Nevertheless, this non-uniformity is much less pronounced in the case of multiple fine cracks, than in R/C or FRC with localised wide cracks. This multiple cracking is accomplished by means of the capacity of fibres to bridge and transfer the applied stresses over the matrix cracks. As for any material under tensile load, the matrix cracks at the weakest point. If no fibres are present in the matrix, the material would fail completely. In the case of FRC, the crack bridging capacity is less than the cracking strength of the concrete, thus the crack widens and the load is reduced if the deformation is increased, i.e. strain-softening occurs. In the case of SHCC, however, the fibres bridging the crack in the matrix have the capacity to sustain the load. In the case of SHCC however the fibres have the capacity to sustain the load. If the deformation is then increased, the load will increase and the matrix will crack at the next weakest point which is stronger than the first cracking point. Thus an increase of the stress is found, i.e. strain-hardening occurs. The fibres implemented for this research are poly vinyl alcohol (PVA) fibres. Only when strain-hardening reaches its peak at about three to six percent strain does SHCC start to display a strain-softening trend, also exhibited by FRC. At this point a localising crack forms at one of the multiple cracks and strain-softening starts. The cumulative interfacial bond strength between PVA fibres and the matrix over a section controls the ultimate tensile strength of SHCC (f_{tu}). A stress-strain curve similar to that of a ductile metal is achieved. This is illustrated in Figure 2.1 along with a comparison between FRC and ordinary concrete.

Crack widths in the matrix are controlled by the elastic strain and slip of fibres bridging the matrix cracks. The ability of SHCC to control crack width, occurs in the envelope starting from first cracking strength (σ_{fc}) and ending at the ultimate strength (f_{tu}). SHCC, like concrete is a dynamic material in which the hydration process continues for very long periods until most of the free water is incorporated in hydration products. When cracks occur, as they do in all cement-based products, surfaces are exposed to water particles. The ability of SHCC to limit crack widths induces the phenomenon of autogenous healing (formation of $CaO\text{-}SiO_2\text{-}H_2O$ over fine cracks) [Illston and Domone 2001]. This self-healing ability of SHCC, which is currently studied intensely [Yang et al. 2005, Li and Yang 2007], is an added benefit and can be exploited for durability purposes.
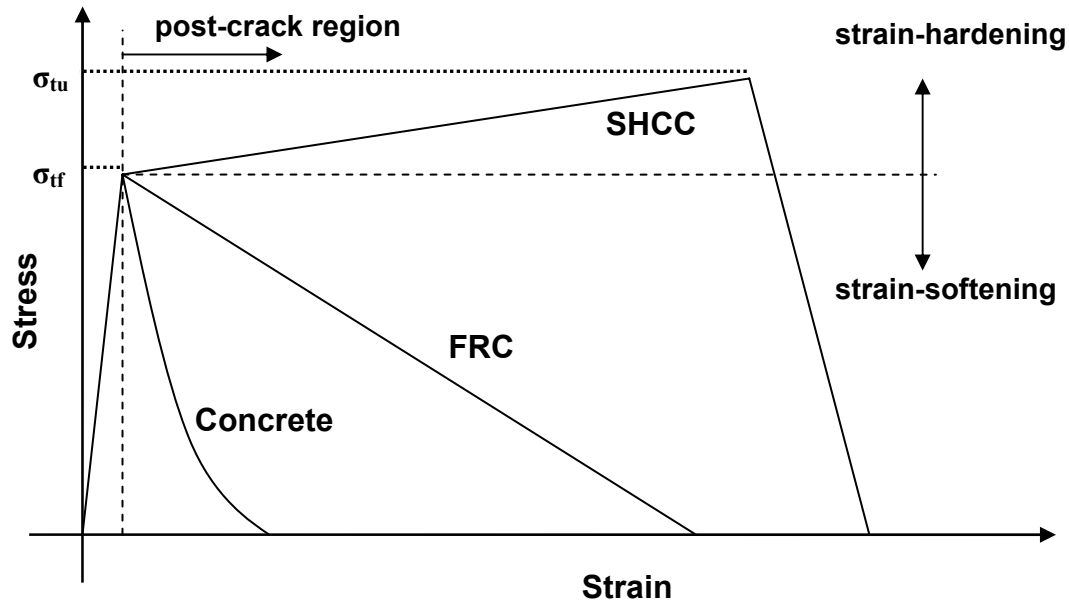
Figure 2.1: The tensile stress-strain behaviour of cement-based composites.

Another important consideration when developing a ductile SHCC, is the fracture energy (G_f) of the cementitious matrix. G_f is an attribute influenced by the micro-structure [Li 2003]. It is measured as the amount of energy dissipated per unit crack surface. High G_f values for the material matrix adversely affect the strain-hardening property. It may lead to non-uniform loading of fibres in a crack, which may cause consecutive, progressive fibre breakage or fibre pull-out, instead of the crack extending in its length. Figure 2.2 illustrates two types of cracks that might occur in SHCC, namely the Griffith crack and the steady-state crack [Li 2003].
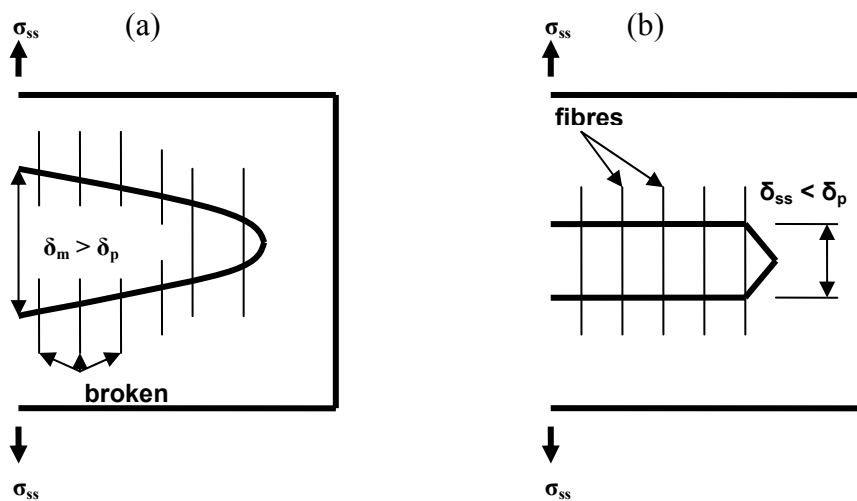
Figure 2.2: Steady-state crack analysis presents two crack propagation scenarios: (a) The Griffith crack, where the fibres slip out or rupture in the mid-crack section where δ_m exceeds δ_p. (b) The steady-state flat crack, where the fibres remain intact as the crack propagates under a constant σ_{ss}, with $\delta_{ss} < \delta_p$ [Li 2002].

In a Griffith crack the fibres slip out or rupture in the midsection, where the crack mouth opening (δ_m) exceeds the fibre deformation at its ultimate resistance (δ_p). The fibres for the steady-state crack remain intact as the crack propagates under a constant steady-state stress (σ_{ss}), with the steady-state crack opening (δ_{ss}) less than δ_p. One way of manipulating G_f in cement-based composites is to vary the aggregate content. Higher aggregate content leads to more complex crack paths and associated high G_f.

2.2.1.2 Compressive properties

Research based on the compressive behaviour of SHCC has been limited to the determination of the ultimate compressive strength thereof and to some extent the determination of the compressive stress-strain response of SHCC. For the most part the compressive response of SHCC has been modelled using a phenomenological approach [Kabele 2000 & 2007, Kanda et al. 2005], where a curve is fitted to the observed response. The compressive response of SHCC up to the ultimate compressive stress can be characterized as linear elastic until the ultimate compressive stress is reached with the slope of the curve determined by the E-modulus of the composite, although the stress-strain curve tends to deviate from its linearity as it reaches the ultimate stress. SHCC displays a strain-softening post-peak response which can be utilized in the post-peak response of structural members.
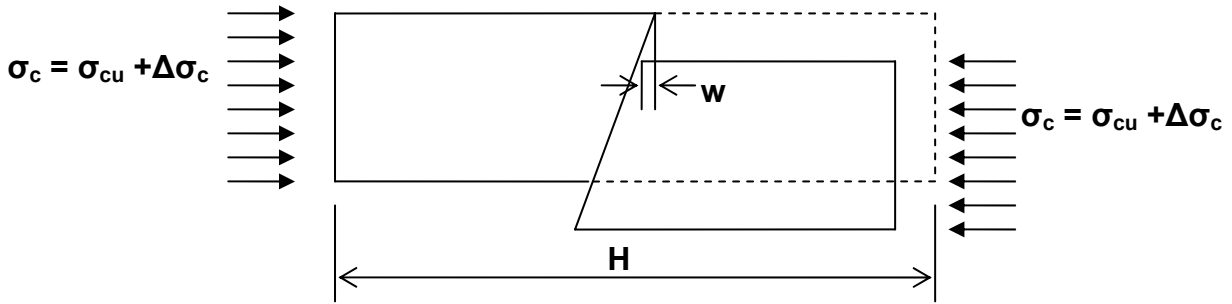
Figure 2.3: Crushing failure in a compressed SHCC specimen [Fantilli et al. 2007].

Recently, efforts have been made to characterize the strain softening part of the compressive stress-strain curve after the peak or ultimate stress is reached [Fantilli et al. 2007], in other words after localized damage has occurred. At this stage, the progressive sliding of two blocks of cement-based material is evident [Figure 2.3]. According to Fantilli et al. this part of the stress strain curve can be represented by the following equation:

$$\varepsilon_c = \varepsilon_{cu} - \frac{\sigma_{cu} \cdot [1 - F(w)]}{E} + \frac{w}{H} \qquad \text{for } \varepsilon_c > \varepsilon_{cu} \qquad (2.1)$$

where ε_{cu} is the strain at the ultimate compressive stress σ_{cu}; w is the inelastic displacement of the specimen as defined in Figure 2.3; H is the height of the specimen; E is the elastic modulus of the composite; and F(w) is a non-dimensional function which connects w and the relative stress σ_c / σ_{cu} during softening. The function F(w) is considered to be a material property and should be determined for the specific SHCC material under consideration.

Research on the compressive behaviour of SHCC at the University of Stellenbosch, up to now, has been limited to the determination of the ultimate compressive strength of SHCC [Stander 2007]. It was found, like in other studies, that the tensile strength is approximately 1/10 of the compressive strength.

2.2.1.3 Shear properties

The main focus of research based on the shear behaviour of SHCC has been on heavily steel reinforced SHCC aimed at replacing concrete in shear-critical structural elements [Shimizu et al. 2006, Kabele 2005, Suwada and Fukuyama 2006]. Efforts have however been made to characterize the shear behaviour of SHCC itself [Li et al. 1994, Shang 2006]. The research by Li et al. was done on SHCC beams containing 2% by volume polyethylene fibres where this material was subjected to an Ohno-type shear beam test, which creates a pure shear plane in the centre of the specimens. While these tests demonstrated the contribution of shear resistance by SHCC to the composite beams, they could however not be used for the objective determination of the shear characteristics of SHCC, because of the use of longitudinal reinforcement to prevent flexural failure.

The research done by Shang was done on SHCC containing PVA-fibres and the aim of the research was to develop a shear test for SHCC and to characterize the shear behaviour of this SHCC. The shear test that was developed is based on the Iosipescu shear test [Iosipescu 1967] that is used for shear testing of metals, fibre reinforced plastics and wood. The SHCC that was tested displayed a ratio between the ultimate shear strength and the first cracking strength of 2.25 and the ratio between the ultimate shear strength and the ultimate uni-axial tensile strength of 1.5. The SHCC forms multiple micro cracks in shear, whereby the true nature of SHCC, as also exhibited in uni-axial tension, is mobilised. The cracks develop at an angle greater than 45° (60°-65°), dominated by the principal stress direction, which in turn depends on the compressive/tensile strength ratio. This can only be realised if sufficient ductility in tension allows the tensile resistance to be maintained at deformations beyond the first cracking deformation, to enable the compressive resistance to be

mobilised. The final failure of the SHCC in shear is when these diagonal micro-cracks are connected with vertical cracks.

2.2.1.4 Elastic Modulus

One hindrance for the structural use of SHCC is its low Elastic Modulus (E-modulus). In various research studies done at the University of Stellenbosch on SHCC [Shang 2006 and Boshoff 2006] the E-modulus of SHCC has been determined to be between 7.5 and 10 GPa. These values were determined by applying a secant method to compute the E-modulus from direct tensile responses at stress levels one third of the first cracking stress and a low pre-stress ($\sigma_0 = 0.1$ N/mm^2) and the corresponding strains as follows:

$$E_c = \frac{\frac{1}{3}\sigma_{tf} - \sigma_0}{\varepsilon_{(\frac{1}{3}\sigma_{tf})} - \varepsilon_0} \qquad\qquad (2.2)$$

The E-moduli of between 7.5 and 10 GPa were computed for cast SHCC specimens that were cured for 14 days and that were subsequently tested at the age of 14 days. Similar tests done on a SHCC at 28 days showed that the E-modulus increases [van Zijl 2005] and may roughly be double at this higher age [Li et al. 1995]. This would suggest that E-modulus of SHCC at 28 days would be roughly between 13 and 20 GPa. This is still significantly less than the 28GPa that is suggested for ordinary concrete with equivalent compressive strength ($\sigma_{cu} = 30$ MPa) by the SABS 0100-1 code [2000]. It has however been shown that by increasing the aggregate content of a SHCC mix, the E-modulus is also significantly increased [van Zijl 2005].

2.2.2 MATRIX CONSTITUENT PROPERTIES

2.2.2.1 General

SHCC utilises the same material ingredients as ordinary FRC's, such as water, cement, sand, fibres and other common chemical additives, but it is rather the optimal combination of these ingredients, based on micromechanical considerations, that affords SHCC its unique ductile, tensile strain-hardening behaviour. Course aggregates are not used as they tend to increase the fracture toughness which negatively affects the unique ductile behaviour of the composite. Larger aggregate particles also prevent effective fibre dispersion and crack bridging. Unlike some high performance FRC's, SHCC does not utilise large amounts of fibres. In general 2% or less by volume of discontinuous fibres is adequate. This relatively small amount of fibres with its short fibre length contributes to the fact that the mixing procedure is similar to that of ordinary concrete.

Hardened SHCC consists of three main components, namely fibres, cement-based matrix and the fibre-matrix interface. Proportioning of each component with the correct mechanical and geometric properties is necessary to attain the unique ductile behaviour. Material design of SHCC is guided by micromechanical principles. Admixtures are incorporated into the mix design, because they enhance the properties of the SHCC in the fresh state, which in turn result in a beneficial hardened state. The beneficial condition is defined by the uniform spread of constituents, causing a resemblance to isotropic material properties. Uniformity of constituent rheology is imperative for the functioning of micromechanical properties.

2.2.2.2 Fibres

Several different types of fibres exist which can be used in SHCC. As stated previously, PVA-fibres were used in this research. These fibres were chosen for their relative high tensile strength (f_t) and E-modulus (E). Thereby the fibre breakage at the crack regions, which will lead to premature brittle behaviour of the composite, can be avoided or restricted. A fibre length of 12mm was chosen to ensure better fibre dispersion and a more workable material in its fresh state. Longer fibres tend to coagulate and form fibre balls. The f_t, E-modulus and other properties of these PVA-fibres are shown in Table 2.1.

Table 2.1: Properties of PVA-fibre [Horikoshi et al. 2006]

Type	Diameter [mm]	Length [mm]	$f_{t,}f$ [GPa]	E [GPa]	$\varepsilon_{u,}f$ [%]
PVA-REC15	0.04	12	1.6	37	6

2.2.2.3 Admixtures

Admixtures are chemicals that are added to the concrete immediately before or during mixing and significantly alter its fresh, early age or hardened state to ensure economic or physical advantages. Normally only small quantities are required, typically 0.1 to two percent by weight of the binder.

Superplasticiser (SP)

Known as workability aids, it increases the fluidity or workability of a cement paste or concrete. They are also referred to as high-range water reducers. It has a high molecular weight and is manufactured to high standards of purity and can therefore achieve substantially greater primary effects without significant side-effects.

The addition of fibres and methyl cellulose lead to an increase in viscosity, thus needing an additive (SP) to improve the workability. The SP also serves to ensure a workable mix in the case of

extrusion where a highly viscous, dough-like mix is required, which is obtained with a low water-binder ratio.

The mode of action induced by SP is purely physical and a combination of mutual repulsion and steric hindrance between cement particles, creating less friction when the particles move. The behaviour of any particular combination of SP and cement will depend on several factors other than the admixture type, including the cement composition, the cement fineness and the water-binder (W/B) ratio.

Substantially increased performance can be obtained if the SP is added a short time (1-2 minutes) after the initial contact between the mix water and the binder [Illston and Domone 2001]. When SP and mix water are added simultaneously, a significant amount of SP is incorporated into the rapid $(CaO)_3 \cdot Al_2O_3$ / gypsum reaction, hence reducing the amount of available to attain workability. The SP action only occurs for a limited time period, usually half an hour to a few hours.

The SP that was used in this research is a product of Chryso, namely Optima 100, with a relative density (RD) of 1.2.

Methyl Cellulose (Viscous Agent)

Chryso Aquabeton ZA is a powder additive necessary to prevent segregation and wash out of the fresh concrete. Also known as viscous agent (VA), it causes an increase of intermolecular shear force of the fresh concrete. Thus it acts as a dispersion agent and assists in the uniform dispersion of the fibres in the mix. VA is also an essential component of an extrusion mix, as it prevents segregation in the form of water being squeezed out under the high extrusion pressure. The addition of the Chryso Aquabeton ZA will tend to reduce the workability of a concrete or cement-based mix. This has to be taken into account when designing a SHCC mix. Workability is compensated for by the use of the correct water-binder ratio and an optimal amount of SP.

2.2.2.4 Binder

The binders considered in this research are Ordinary Portland Cement (OPC – CEM I 42.5N), Fly Ash (FA) and Ground Granulated Corex Slag (GGCS). For the extrusion mixes the binder consisted of a 50:50 combination of FA and OPC, while the composition of the binder for the cast mixes were 50% FA, 45% OPC and 5% GGCS. The cast mix is a standard mix design that was used by Boshoff [2006] in his research at the University of Stellenbosch of which some results were used in the current research for comparison purposes. The slight difference between the binder content of the

two mix designs were deemed minor for the purposes of this research, but will be adequately discussed in the evaluation of results in this thesis.

Ordinary Portland Cement (CEM I 42.5N)

CEM I 42.5N is a hydraulic cement consisting essentially of hydraulic calcium silicates. Since the cement is composed of a heterogeneous mixture of several compounds, the hydration process consists of reactions of the anhydrous compounds with water, occurring simultaneously. As the hydration reaction of cement compounds is exothermic, the compounds of cement are none-equilibrium products of high temperature reactions and are therefore in a high-energy state. The cultivated heat of hydration could lead to cracks in some applications and affect the structural strength and durability. The 42.5 in the name corresponds to the strength in MPa achieved at 28 days after curing with a W/B ratio of 0.5. The letter N for normal depends on the strength after 2 days, in this case equal to or more than 10MPa.

Fly Ash (FA)

FA is collected, by electrostatic precipitator, form the flues of power stations that burn finely ground coal. Being a by-product of an industrial process, it has cost advantages and is readily available in the inland regions (mostly Gauteng) of South Africa, but not at the coastal regions.

FA is a pozzolanic material which, when mixed with Portland cement and water, reacts with calcium hydroxide (product of cement hydration) to produce $CaO\text{-}SiO_2\text{-}H_2O$ gel. Other reasons for the use of this product are that it gives a variety of useful enhancements to the concrete product.

The spherical shape of the particles causes an increase in mix workability. The relative density is also less than that of cement, and therefore the substitution on a weight-by-weight basis will lead to an increased volume. It increases the durability of cement-based products in the sense that it increases the density of the material and improves the mechanical behaviour, in particular in extruded products of SHCC. The addition of FA enhances the ductile behaviour of extrusion composites with long fibres [Shah and Peled 2003]. The FA changes the failure mode form fibre breakage to fibre pull-out and thus enhances the ductile behaviour. The extrusion process provides a strong fibre-matrix bond due to the decreased porosity of the extrudate and the addition of FA reduces the bond strength and changes the mode of failure.

FA also limits the heat exerted during hydration because it prolongs the hydration process. The type of FA implemented in the research was Dura-Pozz, a graded class-F FA product provided by Ash Resources, South Africa.

Ground Granulated Corex Slag (GGCS)

The Corex slag considered in this research is a by-product of the steel manufacturing process at Saldanha steel plant in the Western Cape region of South Africa. Slag is a latent hydraulic binder in that it hardens very slowly in water, but becomes much more reactive when activated by alkalinity of calcium hydroxide, a product of cement hydration. The introduction of Corex slag as a cement extender does not only improve the durability and workability of cement-based materials, but also reduces the cost of the material.

The RD is also less than that of cement and therefore, the substitution on a weight-for-weight basis will lead to a volume increase. The particles are finer than cement particles, which results in better workability, lower bleed rates and shorter setting times than conventional slag [Mackechnie et al. 2003]. Increased durability is achieved via an increased density of the composite. Slag also limits the heat of hydration.

2.2.2.5 Fine Aggregate

An important aspect of a cement-based mix is to ensure the uniform spread of different aggregate grain sizes. This spread of the grain sizes is referred to as the grading of the aggregate. It is important to ensure that the particle sizes are not all the same and that they yield a dense packing of the aggregate, which in turn cultivates workability and durability.

A F95 grading is a fine grading and is used to ensure a good spreading of the fine sand particles, ensuring that the role of the aggregate is optimal. The fine grading ensures a lower matrix fracture toughness, which conforms to micromechanical models of strain-hardening. This suggests that a matrix with lower toughness (in comparison to concrete) should require a smaller amount of fibres to make the transition from brittle to pseudo-strain-hardening mode of failure. The process of grading the sand is expensive, but it is used to ensure the occurrence of the multiple cracking phenomena which yields high ductility and durability. The RD of the sand used in this research is 2.7. It is blended sand prepared by sieving and proportioning local Philippi (dune) sand. Since this sand lacks the required fine particles, crusher dust was used to complete the required F95 grading [Figure 2.4].
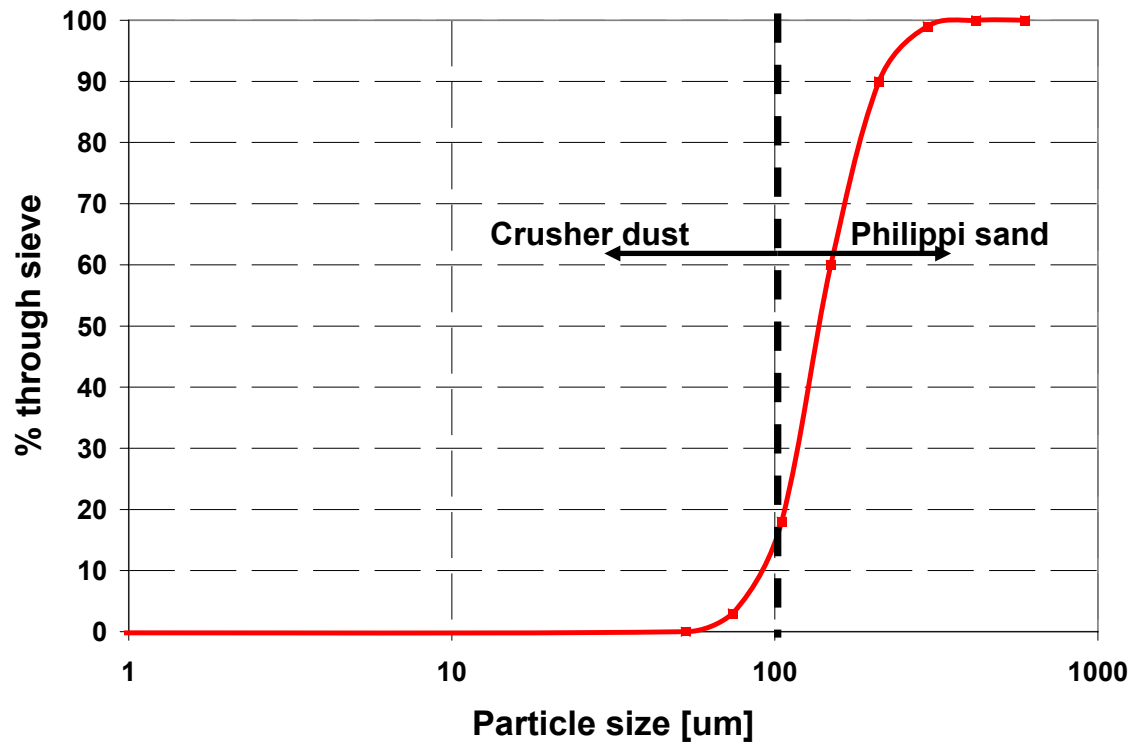
Figure 2.4: Grading of F95 sand, a proportioned blend of Philippi (dune) sand and crusher dust.

2.3 EXTRUSION OF SHCC

2.3.1 INTRODUCTION

Extrusion can be described as a plastic moulding process whereby structural elements are formed under high shear and high compressive forces. An extruder is a machine that forces material through a die by applying pressure. It produces products with a constant cross section and preferably a high symmetry. Extrusion has been used successfully by the ceramic, plastics and even metal and aluminium industries for many years already to produce products such as pipes, facades, balustrades and structural steel members with complex sections. More recently, extrusion is also being used by the prefabrication concrete industry to produce hollow-core slabs and lintels. In this case the concrete is extruded on a flat bed with the extruder moving along the bed. The extrusion of fibre reinforced concretes is still a relatively new concept with various potential applications.

There are two basic types of extrusion that can be used for the extrusion of SHCC, namely wet-mix extrusion like that used by Stang [1999] or dry-mix extrusion. In the wet-mix method extra water is added to the mix to create a flowable, workable mix in the fresh state. The excess water is then forced out during extrusion in a consolidation phase. Dry-mix extrusion can be further subdivided into two categories, namely auger-driven extrusion or piston driven-extrusion. Auger-driven

extrusion uses a screw to convey material toward the extruder die which has a smaller cross section than the screw barrel. Pressure is built up due to this change in cross section, which results in the compaction of the material and the material then being forced through the die. The screw allows material to be constantly fed into the extruder.

Piston-driven extrusion, which is the type of extrusion that is used in this research, uses a piston to force the material forward. Figure 2.5 illustrates a basic piston-driven extrusion set-up.
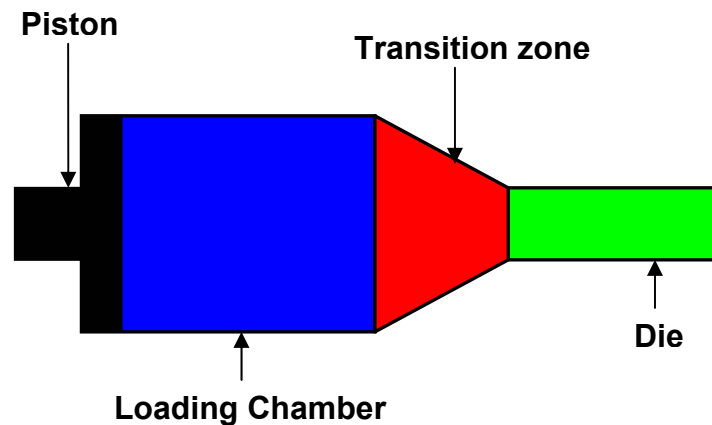
Figure 2.5: Schematic representation of piston-driven extrusion. Material is loaded into the loading chamber and pushed forward by a piston through a transition zone and out through the die.

The fresh material is loaded into the loading chamber and it is then forced forward by means of a piston. The transition zone allows for the change from a large cross section to the smaller, desired cross section. It is in the transition zone that pressure builds up due to the difference in cross section and where the compaction of the material takes place. The material then travels through the die which has the same cross sectional shape as the element that is being produced. The material then exits the die, with the required cross sectional shape afforded to it by the die, and can then be cut into the desired lengths and taken to a curing room to harden.

2.3.2 RHEOLOGICAL REQUIREMENTS FOR PISTON-DRIVEN EXTRUSION

In order to be able to extrude SHCC by means of piston-driven extrusion, the SHCC mix needs to be tailored to ensure extrudability. Aspects such as segregation and form retention need to be considered when tailoring SHCC for extrusion and this was done in designing an SHCC mix for extrusion in previous research [Visser 2005].

Unlike casting, where you need a flowable mix, extrusion requires a stiff, dough-like composite in its fresh state to ensure form retention after extrusion. The most efficient way to ensure a mix with

such a rheology is by reducing the W/B ratio. This is however not sufficient, because such a mix lacks cohesion, for which reason both SP and VA are added. Without fluidity and cohesion in an extrusion mix the material will block in the transition zone and pressure will continue to build up, leading to segregation in the form of water being forced from the mix. The SP helps to ensure that the mix is workable, whereas the VA ensures a stiff cohesive mix and prevents segregation.

2.3.3 Characteristics of Piston-driven Extruded SHCC

Through the process of extrusion the material and mechanical properties of SHCC are significantly altered. This is firstly due to the tailoring of the SHCC mix for extrusion and secondly due to the influence of the extrusion mechanism itself. These changes need to be considered when deciding on an application for products manufactured by extrusion and thus they will be discussed in the following section.

2.3.3.1 Influence of tailoring

In order to ensure extrudability of SHCC, in other words to create a stiff, dough-like mix, the W/B ratio of extrusion SHCC is significantly reduced in comparison to the W/B ratio of cast SHCC. This results in a higher aggregate content for the extrusion SHCC. This increase in aggregate content can result in an increased E-modulus and an increased tensile as well as compressive matrix strength for the extrusion SHCC in comparison to that of the cast SHCC [van Zijl 2005].

2.3.3.2 Orientation of fibres

Structural applications for SHCC may be optimized by improving the performance of the composite in the direction of the critical failure mode. This implies that to make full use of the benefits of SHCC, the fibres need to be orientated in the principle direction of rupture, the reason being that the fibres are aligned optimally for resistance of action in that direction. Fibres need to be orientated in the longitudinal direction for uni-axial structural elements such as bars, beams and one-way spanning plates, but there should also be orthogonally or diagonally orientated fibres for bi-axially loaded elements such as pressure pipes or two-way spanning plates.

By optimizing the fibre orientation a larger resistance for the same fibre volume can be realized, or reduced fibre content can be used to achieve the required resistance. Furthermore, the ductility of the composite can be improved by enhancing the multiple cracking phenomena, which produces strain-hardening behaviour.

It has been proven that the fibre orientation of extruded SHCC containing steel fibres is governed by the extrusion mechanism [De Koker 2004]. This implies that fibres are orientated diagonally (in a helix pattern) for auger-driven extrusion and longitudinally, in the direction of the extrusion force, for piston-driven extrusion. This has also been shown by the author to be true for the extrusion of SHCC containing PVA fibres by means of piston-driven extrusion [Visser 2005]. Three-point bending tests were conducted on specimens cut from the longitudinal as well as the orthogonal direction of extruded plates. This SHCC also contained 12 mm PVA fibres and the specimens had dimensions of 15 mm X 30 mm X 70mm and were tested over a span of 60 mm. A comparison was made between the mechanical responses for both directions, where a good ductile, strain-hardening response indicates good fibre orientation in that direction. Although this is an indirect approach and not just a reflection of the fibre orientation alone, it gives a good indication of fibre orientation.

The results indicated that the fibres are predominantly orientated in the longitudinal direction of extrusion and that the fibres are poorly orientated in the orthogonal direction. This was reflected by the ductile, strain hardening response of the longitudinal specimens which formed multiple cracks in comparison to the orthogonal specimens which had a brittle response and formed one localized crack. The results of these tests are given in Figure 2.6 below.
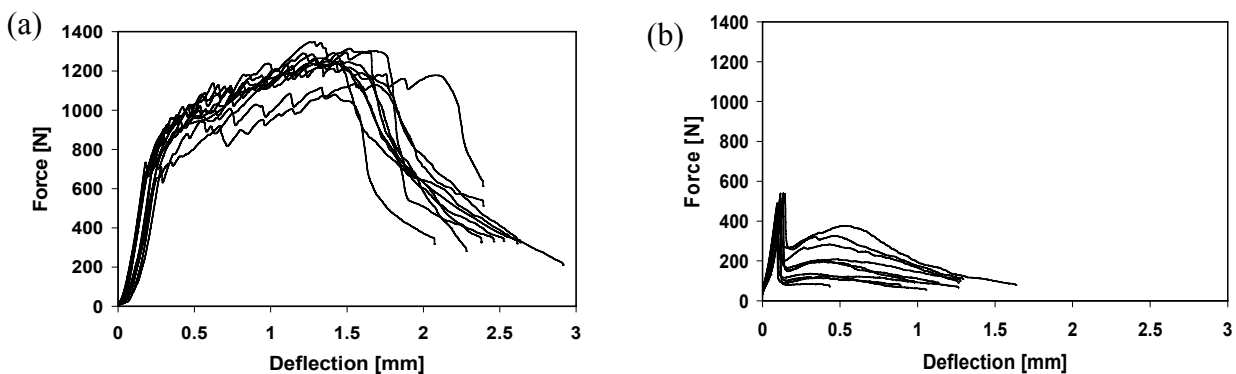
Figure 2.6: Three-point flexural bending in the (a) Longitudinal and the (b) Orthogonal direction [Visser 2005].

It is the author's view that the orientation of the fibres takes place in the extruder transition zone and to an extent in the die. When fibres are dispersed in an infinitely large volume of concrete, they are expected to be randomly orientated, with equal opportunity to be orientated in different directions in space. In the presence of parallel boundaries where the distance between sides are relatively small in comparison to the fibre length, the fibres tend to orientate more two-dimensionally near the boundaries. The boundary effect of the sides of the extruder along with the

high extrusion forces in the direction of material flow in the transition zone and die of the extruder orientates the fibres in the longitudinal direction.

2.3.3.3 Densification and interfacial bond between fibres and the matrix

The performance of SHCC to a large extent depends on the properties of the fibres and the matrix, and those of the fibre-matrix interface. The role of fibres and that of the individual matrix constituents has already been discussed. Here the role of the fibre-matrix interface and influence of the fabrication method on the interfacial bond will be discussed.

Through the process of extrusion the fibre packing and matrix density is increased, resulting in a stronger bond between the fibres and the matrix. This can cause the failure mechanism of the extruded SHCC composite to change from fibre pullout to fibre breakage, which will result in a more brittle type of failure. The addition of FA reduces the bond between the fibres and the matrix [Shah and Peled 2003]. This reduction in bond enhances the ductile behaviour of extruded SHCC by changing the failure mechanism form fibre breakage to fibre pullout.

The extrusion process also serves to enhance the density of the SHCC composite and thus reducing the porosity thereof [de Koker 2004]. It is widely acknowledged that the reduction of porosity leads to increased matrix strength and an increased E-modulus.

2.3.4 APPLICATIONS FOR EXTRUDED SHCC

There are numerous advantages associated with extrusion and the extrusion of SHCC. These advantages range from structural and mechanical advantages, superior to ordinary concrete, to better quality control. Extrusion has all the benefits associated with prefabrication, like better quality control, high geometrical tolerances and better accuracy but with an even higher production rate. It is also possible to create elements with complex geometrical cross sections through extrusion. The superior tensile mechanical characteristics of extruded SHCC in comparison to concrete and in many ways to cast SHCC make it a desirable material for structural use.

One specific application field for extruded SHCC is in permanent formwork. Extruded SHCC panels have been used for permanent formwork in the construction of bridges in Japan [Yamada et al. 2006]. Here, flat and curved panels with ribs were used as permanent formwork for the floor decks of bridges and the guard walls of the bridges. The use of cast SHCC as a permanent formwork has also been investigated at the University of Stellenbosch [Avenant 2005], where rectangular thin-walled, hollow tubes were cast from SHCC and used as permanent formwork for

beams and columns. This research study showed that columns cast from ordinary reinforced concrete and columns cast from ordinary reinforced concrete, but in these prefabricated, hollow SHCC tubes and with 50% less shear reinforcement, are comparable based on axial load and bending moment resistance. The processes of casting and stripping the pre-fabricated SHCC tubes were complicated and remain to be improved if this method is to be used commercially. It is the opinion of the author that extrusion has good potential for manufacturing of such tubes.

The use of prefabricated concrete elements in combination with cast in-situ concrete is a concept called Hybrid Concrete Construction, a concept that is also currently being investigated at the University of Stellenbosch [Jurgens 2006] for the South African construction industry. Hybrid Concrete Construction can be defined as a method of construction which integrates prefabricated concrete and cast in-situ concrete to take best advantage of their different inherent qualities [Goodchild 2004]. It is the opinion of the author that the extrusion of SHCC can be utilized to good effect with this concept in mind. Extrusion can be used to produce uni-axial as well as possible bi-axial flexural members as well as other structural members like balustrades and facades.

Another field of interest for the use of SHCC is in the use of SHCC as a construction material in seismic active areas, due to its superior mechanical response to seismic loading in comparison with ordinary concrete [Fischer and Li 2002]. A lot of buildings that have been built in seismic active areas were not designed to resist seismic loading. One way of enhancing these buildings' seismic resistance is by retrofitting structural members of such a building with SHCC. Extrusion can be used to manufacture SHCC panels that can be used for the epoxy-bonded retrofitting of R/C structural members [Farhat and Karihaloo 2007].

The enhanced performance of cast steel reinforced SHCC to that of ordinary reinforced concrete will be discussed in the next section along with the possible advantages of using extruded steel reinforced SHCC.

2.4 STEEL REINFORCED SHCC

2.4.1 CAST REINFORCED SHCC (R/SHCC)

The contribution of concrete to the load-deformation response beyond first cracking of reinforced concrete (R/C) in uni-axial tension is generally described as the tension-stiffening effect. The response of the R/C is compared with that of the bare steel reinforcement, and the difference is attributed to the tensile stresses in the concrete matrix between transverse cracks. Due to the

brittleness of concrete, these cracks cannot transfer any significant stress across the crack and, consequently, the maximum tensile load of the reinforced composite is limited by the tensile strength of the reinforcement, assuming minimum reinforcement is provided. Besides this limitation on load-carrying capacity, cracking of concrete causes a deformation concentration in the steel that the surrounding concrete is unable to accommodate. In addition, high bond stresses are required to transfer the tensile load into the concrete matrix between transverse cracks. Both phenomena result in deterioration of the concrete matrix and adversely affect the intended composite mechanism.

In order to overcome this inherent weakness, the concrete matrix has been substituted with various fibre-reinforced cement matrices in a number of research studies in which the effect of increased tensile strength and toughness by steel fibre reinforcement of concrete has been investigated. For example Abrishami and Mitchell [1997] reported that after cracking and significant deformation, plain concrete suffered splitting cracks and lost a significant amount of its stiffening contribution. The addition of steel fibres controlled these cracks and resulted in improved tension stiffening behaviour. Other studies similarly observed that high circumferential stresses lead to the development of longitudinal cracks, resulting in splitting and bursting of concrete cover [Krstulovic-Opara et al. 1994]. It has been found that the load level at which longitudinal cracking occurs is dependent on the cover thickness, the average bond stress at interface, and the composite tensile stress-strain response. Furthermore, an increase in bond strength and bond stiffness has been attributed to the presence of steel fibres in the concrete.
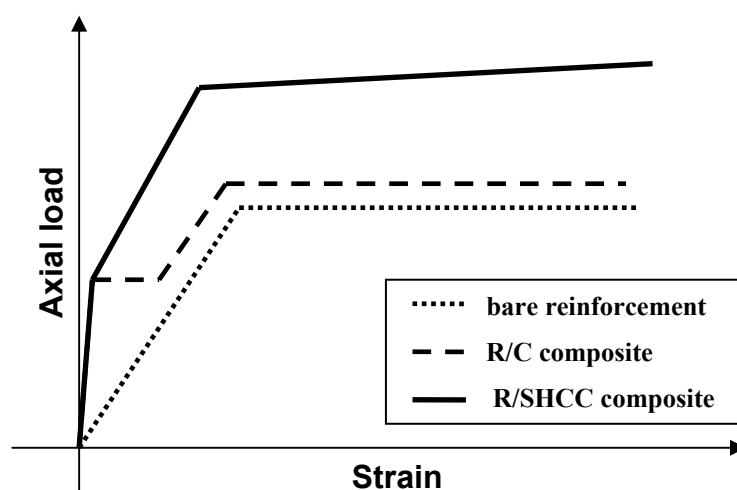
Figure 2.7: Typical load-deformation, tension-stiffening response of R/SHCC in comparison to R/C and the load-deformation response of bare steel [Fischer and Li 2002].

Fischer and Li [2002] conducted an investigation into the influence of matrix ductility on the tension-stiffening behaviour of R/SHCC. An SHCC containing polyethylene fibres, with a tensile stress-strain response very similar to the one used in this research was used to emphasize the importance of the particular deformation characteristics of this SHCC. Uni-axial tensile tests were conducted on R/C and R/SHCC, where the SHCC have ductile deformation characteristics analogous to those of metals. An analysis of the deformation mechanisms suggested that the combination of steel reinforcement and SHCC results in composite action, where unlike R/C and FRC, both constituent materials deform compatibly in the postcracking and postyielding deformation process [Figure 2.7].

a) Composite before   b) R/C after   c) R/SHCC after
matrix cracking   matrix cracking   matrix cracking
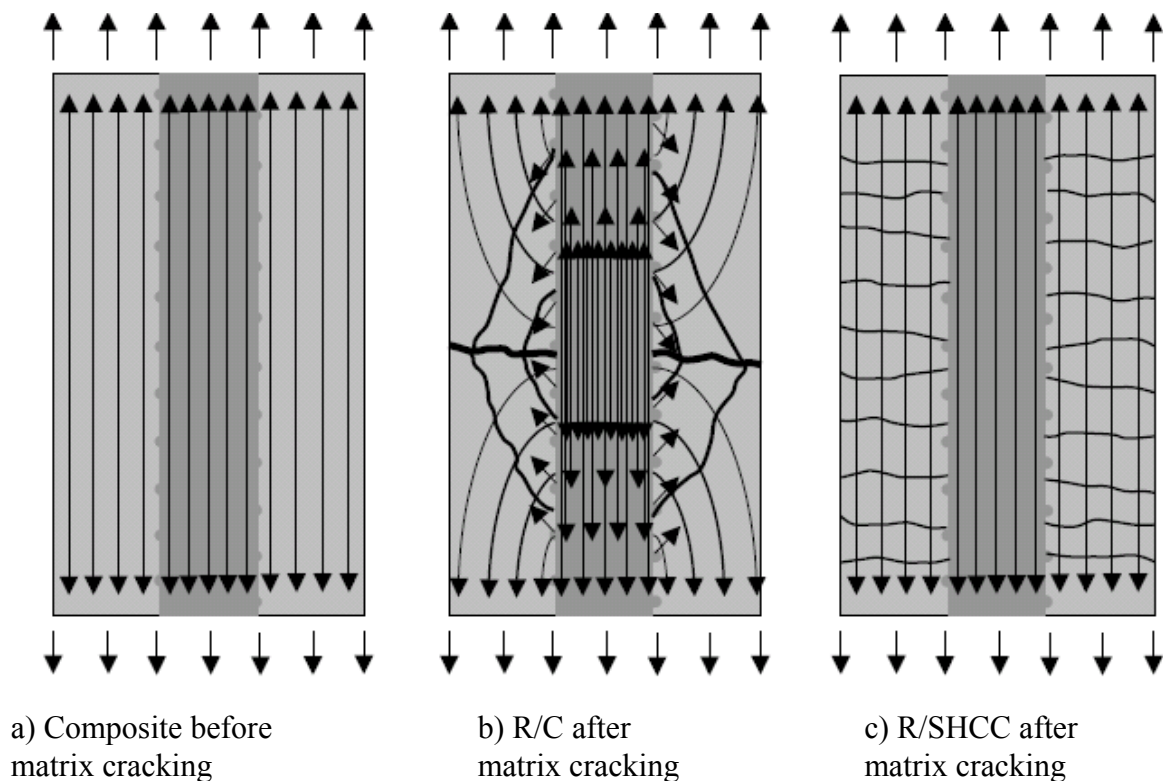
Figure 2.8: Schematic of crack formation and internal stresses in R/C and R/SHCC composites [Fischer and Li 2002].

The comparison of R/C and R/SHCC showed qualitative and quantitative differences in their tension-stiffening behaviours. The combination of reinforcement and matrix material with elastic/plastic stress-strain behaviour results in a composite where both materials are deforming compatibly in the inelastic deformation regime. Consequently, damage induced by local slip and excessive interfacial bond stress between reinforcement and matrix is prevented. The SHCC matrix stiffens the specimen at uncracked sections and also strengthens it at cracked sections. Hence, the composite load-deformation response is significantly improved in terms of axial load-carrying capacity as well as ductility. To maintain this composite action at relatively large inelastic

deformations, strain-hardening and multiple cracking of the SHCC matrix are essential. It is postulated that the resulting composite action is primarily achieved by the reduction of internal stresses. This results in a distribution of internal stresses in the R/SHCC composite as illustrated in Figure 2.8 compared to the internal stress distribution in R/C composites.

2.4.2 EXTRUDED REINFORCED SHCC (R/SHCC)

To the knowledge of the author, no research concerning the extrusion of R/SHCC has been published to date. Thus it is unknown whether any research has been done on this topic or whether the extrusion of SHCC containing reinforcing steel has been attempted before. The prefabrication concrete industry produces hollow-core slabs containing steel reinforcing by means of extrusion. These are however prestressed strands over which ordinary concrete is then extruded and is not comparable to extruded SHCC containing ordinary reinforcing bars.

When taking the enhanced mechanical performance of extruded SHCC that was mentioned in the previous sections into consideration, it can be postulated that the extrusion of R/SHCC can lead to even better composite action than cast R/SHCC. This postulation is based on the fact that the tensile behaviour of extruded SHCC is even closer to the tensile behaviour of steel. The extrusion forces can also ensure a denser packing of the SHCC around the reinforcement, which can lead to a better bond between the reinforcement and the SHCC material.

The enhanced mechanical properties of extruded SHCC can also contribute to a higher moment resistance of R/SHCC which will allow smaller cross sections than R/C to be used for the same resistance. The SHCC can also act as shear reinforcement reducing or even eliminating the amount of shear reinforcement required for structural elements. The formation of small micro cracks can reduce or prevent the penetration of harmful chlorides, protecting the steel reinforcement.

The extrusion of R/SHCC and the investigation thereof will thus be one of the main objectives of this research study. The rest of this report documents the various research studies that were undertaken with the main focus being on the extrusion of SHCC and R/SHCC.

3 EXTRUSION OF SHCC

3.1 EXISTING EXTRUSION EQUIPMENT

The investigation into the concept of extrusion and the extrusion of SHCC at the University of Stellenbosch was first begun by Don De Koker under the guidance of Prof Gideon PAG van Zijl in 2003 [De Koker 2004]. During this research period [2003 – 2004] two piston-driven extruders were designed and built as part of a larger research program on SHCC. The first extruder was a pipe extruder that can produce pipes with an inside diameter of 150 mm and a wall thickness of 15 mm. The other extruder is plate extruder that is able to produce sample plates suitable for testing purposes with dimensions 15 mm X 70 mm [Figure 3.1].

Figure 3.1: Piston-driven plate extruder developed by De Koker [2004].

Both extruders were built with a fixed transition zone and die size and with the loading chambers, transition zones and dies permanently welded together. Thus the extruders are only able to produce elements with a fixed cross sectional size. They also do not allow for easy modifications of the extruders like changing the transition zone size or the die length, or for introducing reinforcement steel into the extruded elements. The pistons of these extruders are also powered by a Loosenhauser hydraulic pump system, which does not allow for sufficient force or displacement control of the pistons.

It was consequently decided to design and build a new piston-driven extruder, to extend the experimental research capabilities. The design specifications and the final design of this extruder are discussed in the following sections.

3.2 DEVELOPMENT AND DESIGN OF A NEW EXTRUDER

The inability of the existing extruders to be easily modified is cited as one of the main reasons for designing a new piston-driven extruder. This was also then the starting point for setting specifications and requirements that the new facility had to adhere to.

3.2.1 REQUIREMENTS AND SPECIFICATIONS FOR DESIGN

It was a requirement that transition zones with varying sizes as well as dies with varying shapes and lengths can be fixed to a universal loading chamber. This will enable the investigation of the effect of varying transition zone sizes on for instance the fibre orientation of an extruded element and the difference in extrusion pressure that it induces. The ability to fix different dies onto the extruder will allow for the production of elements with different shapes and sizes and also the investigation of the effect that different die lengths has on the extruded composite.

The ability to control the extrusion piston displacement and speed was also seen as an essential requirement. It is necessary to be able to stop the extruder while extruding and also to control the speed at which the extruder is extruding and thus the speed at which the extrudate exists the die. It also enables the investigation of the effect that different extrusion speeds and thus extrusion forces have on for instance the density and fibre orientation of extruded elements.

Lastly, as was mentioned in Chapter 2, there are various potential benefits that can be cited as reasons for extruding R/SHCC. Consequently it was decided to design the new extruder with the ability to extrude SHCC and R/SHCC. This posed to be the most challenging part of the design requirements. In order to prevent differential slip between the steel and the extrudate, both the steel and the extrudate need to be travelling at the same speed. Since the extrudate undergoes an increase in travelling speed due to the change in cross section when the material is moving in the transition zone, i.e. from the loading chamber to the die, the steel needs to be introduced just before the die. Another challenge was the fact that the piston has to be able to move within the loading chamber and thus there is limited space left in which to actually introduce the steel.

It has to be stated that not all the possible investigations that was mentioned in this section have been done in this research, but was taken into consideration for future research. The main focus here is to develop and design an extruder that can be successfully used for the purposes of this research study, but with the ability to be adapted for other research studies on piston-driven extrusion.

3.2.2 MECHANICAL DESIGN EQUATIONS

Since the existing piston-driven extruders and extrusion process have been refined in previous studies [De Koker 2004, Visser 2005] to be suitable for the extrusion of SHCC it was decided to base the new extruder on the same concepts. Thus measurements that were obtained from the plate piston-driven extruder were used to set up governing differential equations that could be used in the design of the new extruder. In order to set up these equations, the flow of the material through an extruder during the extrusion process was regarded as fluid flow. This required some assumptions and simplifications to be made and these will be discussed next.

The SHCC material that is extruded is not actually a fluid, but it is rather a type of material that falls between a fluid and a rigid body i.e. a viscous material. Thus, the assumption of fluid flow is not accurate, but it was seen as the simplest way to set up design equations. The major assumption that follows from this simplification of the material behaviour is the fact that it is assumed that the pressure at a point in space within the extruder is the same in all directions while the extrusion process is underway. In consideration of force equilibrium, the next assumption is that all the forces that are involved are equal to the sum of all the applied forces (piston forces), the friction forces and the forces that act on the inside surface of the extruder. It is also assumed that the applied forces and thus also the reaction forces are distributed equally across the cross section of the extruder.

In Figure 3.2 (a), it can be seen that two basic sets of equations has to be set-up for this type of extruder. The first set of equations would be for the loading chamber and die which has a constant cross section and the second set of equations would be for the transition zone where there is a constant change in cross section over the length of the transition zone. Firstly, the constant cross section will be dealt with.

Figure 3.2 (b) illustrates the free-body diagram for an infinitesimal element of the loading chamber and die section, with all the forces that act in on this element. In this diagram P(x) is the horizontal pressure at a distance x from the starting point and P(x) + dP is the pressure in the horizontal direction at a distance x + dx from the starting point. The frictional surface stress at a point x is given by τ(x). The vertical pressure is not included in this diagram as horizontal action is of interest

here. Nevertheless, the pressure P(x) is considered also to act vertically, but in opposite directions at the upper and lower edges, giving vertical force equilibrium if the self weight is considered negligible.
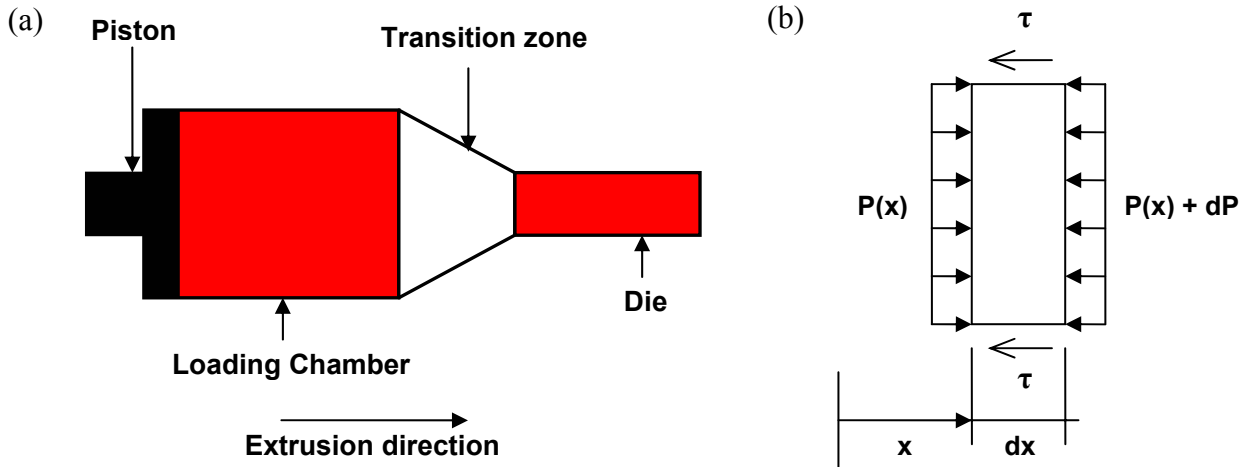
Figure 3.2: The different zones within an extruder (a) and the free-body diagram for an infinitesimal sized element of the loading chamber and die (b).

The sum of all the horizontal forces can then be shown to be as follows:

$$\sum F_x = 0 \tag{3.1 (a)}$$

$$P(x) \cdot h \cdot w = (P(x) + dP) \cdot h \cdot w + \tau(x) \cdot 2(h + w) \cdot dx \tag{3.1 (b)}$$

In this equation w is the inner width and h the inner height in the extruder cross section, which is constant for the die and transition sections respectively. The frictional surface stresses, $\tau(x)$, can be expressed in terms of the vertical pressure acting on the surface of the extruder and a friction coefficient. Due to the assumption of fluid flow the vertical pressure at a point is equal to the horizontal pressure at that point. Thus, $\tau(x)$ can be expressed as:

$$\tau(x) = \frac{1}{2}(P(x) + (P(x) + dP)) \cdot \mu \tag{3.2 (a)}$$

$$\tau(x) = P(x) \cdot \mu \tag{3.2 (b)}$$

Not that adhesion is considered negligible and not included in eq. (3.2). By substitution of eq. (3.2b) into eq. (3.1) and algebraic manipulation, the differential equation follows:

$$\frac{dP(x)}{dx} = \frac{-2 \cdot \mu \cdot P(x) \cdot (h+w)}{h \cdot w}$$
(3.3)

With the aid of MATLAB R2006a the solution of eq. (3.3) was found to be as follows:

$$P(x) = c \cdot e^{\frac{2 \cdot \mu \cdot (h+w) \cdot x}{h \cdot w}}$$
(3.4)

In this equation c is a constant. By assuming that the horizontal pressure at the starting point of the loading chamber or die, in other words at $x = 0$, is P_0. Then the constant, c is equal to P_0. The final expression of the horizontal pressure in terms of x at a point is given as follows:

$$P(x) = P_0 \cdot e^{\frac{2 \cdot \mu \cdot (h+w) \cdot x}{h \cdot w}}$$
(3.5)

Secondly, governing equations for the transition zone are developed. Two cases are considered. The first is a transition zone that has a constant width or height with a linear reduction in either the height or width over the length of the transition zone. This will be referred to as a transition zone with a single slope. The second case is a transition zone, where both the width and the height reduce linearly over the length of the transition zone. This will be referred to as a transition zone with a dual slope. The single slope transition will be dealt with first.

Figure 3.3 (a) illustrates a single slope transition where the width stays constant, but the height reduces in the x-direction. It can thus be seen that height of this transition can be written as a function of x as follows:

$$h(x) = h_i - \frac{h_i - h_L}{L} \cdot x$$
(3.6 (a))

$$h(x) = h_i - 2 \tan \theta \cdot x$$
(3.6 (b))

In this equation, L is the length of the transition, h_i is the height of the transition at $x = 0$ and h_L is the height of the transition at $x = L$ [Figure 3.3]. The angle θ is the angle that the top and bottom of the transition makes with the horizontal.
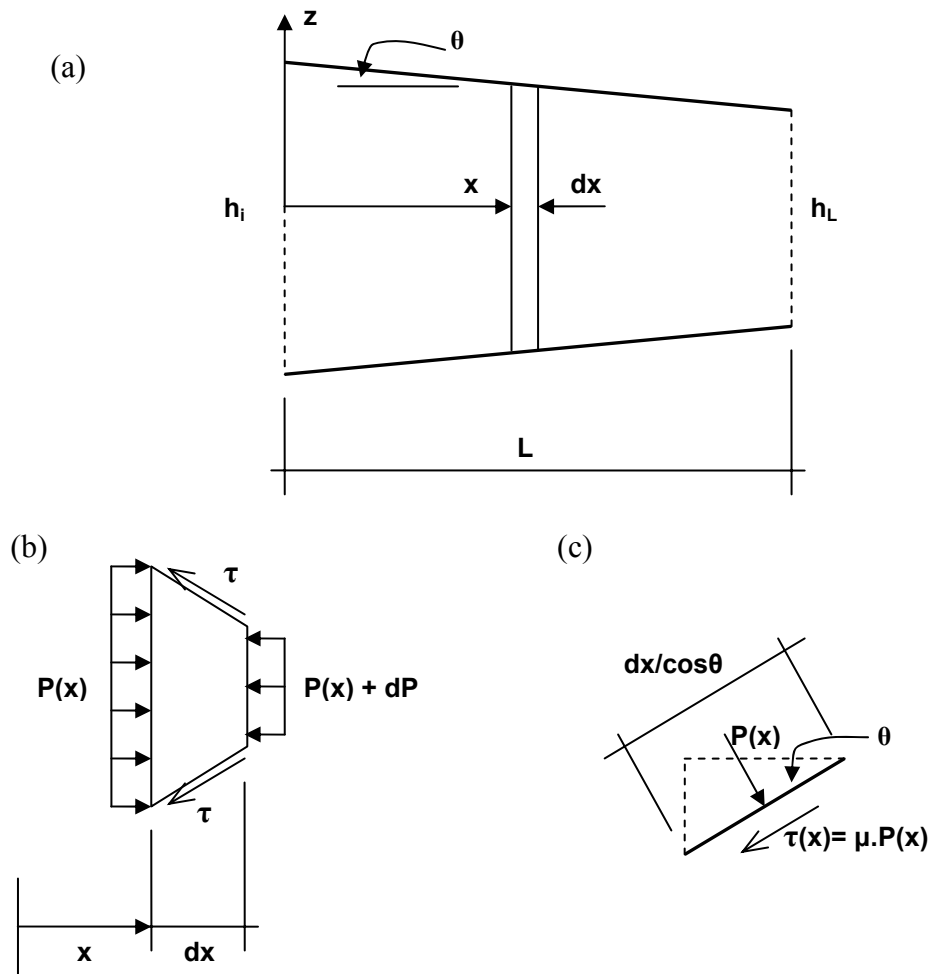
Figure 3.3: (a) A diagram of a single slope transition zone with the height reducing and (b) & (c) free-body diagrams of an infinitesimal sized element of a single slope transition.

When all the horizontal forces are summed together as was done previously for the loading chamber and die, the resulting equation is as follows:

$$P(x) \cdot h(x) \cdot w = (P(x) + dP) \cdot h(x) \cdot w$$
$$+ 2 \cdot \tau(x) \cdot h(x) \cdot dx$$
$$+ (2 \cdot \tau(x) \cdot w \cdot \frac{dx}{\cos\theta}) \cdot \cos\theta$$
$$- 2 \cdot P(x) \cdot w \cdot dx \cdot \tan\theta \tag{3.7}$$

From eqs. (3.6), (3.7) and (3.2), the governing differential equation is found as follows:

$$\frac{dP(x)}{dx} = \frac{2 \cdot P(x) \cdot \tan\theta}{h_i - 2 \cdot \tan\theta \cdot x} - \frac{2 \cdot P(x) \cdot \mu}{h_i - 2 \cdot \tan\theta \cdot x} - \frac{2 \cdot P(x) \cdot \mu}{w} \tag{3.8}$$

The solution of eq. (3.8), with boundary value that the pressure at x = 0 is P₀, is as follows:

$$P(x) = \left(\frac{-P_0}{-h_i^{1/\tan\theta \cdot \mu}} \right) \cdot h_i \cdot (-h_i + 2 \cdot \tan\theta \cdot x)^{\left(\frac{\mu - \tan\theta}{\tan\theta} \right)} \cdot e^{-\left(\frac{2 \cdot \mu \cdot x}{w} \right)}$$

(3.9)

The same diagram that was used for the single slope transition [Figure 3.3] can be used for the dual slope transition. In this case however the width of the transition can also be written as a function of x [eq. (3.10)] and the angle that the sides of the extruder make with the horizontal is written as Ø.

$$w(x) = w_i - \frac{w_i - w_L}{L} \cdot x$$

(3.10 (a))

$$w(x) = w_i - 2 \tan\phi \cdot x$$

(3.10 (b))

where w_i is the width of the transition at x = 0 and w_L is the width of the transition at x = L. When horizontal force equilibrium is considered for the dual slope transition the resulting equation is:

$$\begin{aligned}
P(x) \cdot h(x) \cdot w(x) = {} & (P(x) + dP) \cdot h(x) \cdot w(x) \\
& + 2 \cdot \tau(x) \cdot h(x) \cdot dx \\
& - 2 \cdot P(x) \cdot h(x) \cdot dx \cdot \tan\phi \\
& + 2 \cdot \tau(x) \cdot w(x) \cdot dx \\
& - 2 \cdot P(x) \cdot w(x) \cdot dx \cdot \tan\theta
\end{aligned}$$

(3.11)

By substitution of eqs. (3.2), (3.6) and (3.10) into eq. (3.11), the following governing differential equation is derived:

$$\frac{dP}{dx} = \frac{2 \cdot P(x) \cdot (\tan\phi - \mu)}{w_i - 2 \cdot \tan\phi \cdot x} + \frac{2 \cdot P(x) \cdot (\tan\theta - \mu)}{h_i - 2 \cdot \tan\theta \cdot x}$$

(3.12)

The solution of this differential equation, again assuming that the pressure at x = 0 is P₀, is as follows:

$$P(x) = \left[(-h_i + 2 \cdot \tan\theta \cdot x)^{\frac{(-\tan\theta + \mu)}{\tan\theta}} \right] \cdot \frac{P_0 \cdot h_i \cdot b_i}{\left[(-h_i)^{\frac{\mu}{\tan\theta}} \right] \cdot \left[(-b_i)^{\frac{\mu}{\tan\phi}} \right]} \cdot \left[(-b_i + 2 \cdot \tan\phi \cdot x)^{\frac{(-\tan\phi + \mu)}{\tan\phi}} \right] \quad (3.13)$$

It has to be recognized that the governing equations (3.5), (3.9) and (3.13) are simplified representations of the extrusion process. But, similar to the assumption of an ideal fluid when studying the concept of fluid flow, certain assumptions and simplifications are made, in order to obtain simple, understandable equations. These equations are considered as a starting point for the design of an extruder. They can be refined in further research in order to more accurately capturing the physical process, for instance to study the influence of the fresh material rheology on the forming process. For the purpose of this research, the simplified equations are deemed sufficient to assist in the design of a new extruder facility.

3.2.3 FINAL DESIGN

In the previous sections some specifications were set for the design of the new extruder facility. Equations were also developed that can be used for this purpose. In this section the final design of this new extruder are introduced and discussed.

In order to address the issue of better control in terms of extrusion pressure, speed and displacement, a hydraulic actuator and control system were used as the driving mechanism for the piston. A 5 ton Instron Hydraulic Actuator with a maximum stroke length of 250 mm was used. This actuator can be controlled by means of force or displacement, with the ability to adjust the stroke length, speed and wave-type.

The actuator is mounted vertically, with the piston pressing down vertically into the loading chamber. The loading chamber has a 90° angle change, which creates space for reinforcing steel to be introduced horizontally without being hampered by the piston. In other words, the material is loaded vertically into the loading chamber, and it is then forced by the piston to go through the 90° circular bend and to then travel horizontally towards the transition zone and die. Tubes were placed horizontally in the loading chamber for the purpose of introducing the reinforcing steel into the extrusion process.

It was calculated that the pressure in the transition zone will be sufficient for the material to grip around the reinforcing steel and thus pull the steel along with it. The tubes are placed in the correct

position to ensure the correct concrete cover for the reinforcing steel of a specimen. These tubes run from the loading zone to the edge where the transition zone and the die meet and are tapered to ensure a gradual transition along the length of the tube. The steel is then pushed through these tubes, with its openings at the back of the extruder, until the material grips and pulls it along.

The loading chamber, transition zone and die are designed individually so that different transitions and dies can be fitted onto the loading chamber. This is made possible by the designed concept of simple bolted connection through flanges on each of these three parts. Thus a universal loading chamber with a constant cross section of 200 mm X 200 mm exists onto which a transition can be bolted and a die can then be bolted onto this transition in turn. For the design of the transition and the die the governing equations (3.5), (3.9) and (3.13) are used.

As will be explained in the following section, it was decided to create a transition and die that will produce SHCC beams with a cross section of 100 mm X 100 mm. Some of these beams will have to be extruded with two Ø8 mm Y-steel tensile reinforcing bars with a concrete cover of 20 mm.

The design of the new extruder consisted of the mechanical and the structural design thereof. The equations that were set-up in the previous section were used for the mechanical design of the extruder and will be briefly discussed below. The structural design of the extruder falls outside the scope of this report and will not be discussed here. It can however be said that the necessary calculations were made and the correct design procedures followed to ensure a structurally sound extruder.

As it was mentioned previously, measurements that were obtained in previous research from the existing plate piston-driven extruder [Visser 2005] were used for the design of the transition and die of the new extruder. The criterion that was set was that the same drop in pressure that was obtained in the existing extruder has to be obtained in the new extruder, in other words, the drop from the applied pressure, in the loading chamber, to atmospheric pressure, as the material exits the die, had to be the same for both extruders. Thus, eqs. (3.5) and (3.13) were used to compute the pressure in the plate extruder along the horizontal axis by using its dimensions and angles and the extrusion pressure that was measured from the piston. Thereby the pressure at the start of the plate extruder die was computed and assigned as the die entry pressure (P_0) for the new extruder. With this pressure and the known new die dimensions (100 mm X 100 mm) the required new die length of 500 mm was computed with eq. (3.5). Eq. (3.13) was then used to calculate the length and angle of the transition that reduces the inlet chamber cross section of 200 mm X 200 mm to the die cross

section of 100 mm X 100 mm. The required length for the transition [L] was calculated to be 176 mm, corresponding with the angles [θ and $\varnothing$] as 15.86°. Figure 3.4 shows an illustration of the new piston-driven extruder. Note that the length and angles are not unique, but other combinations can be computed from eq. (3.13).
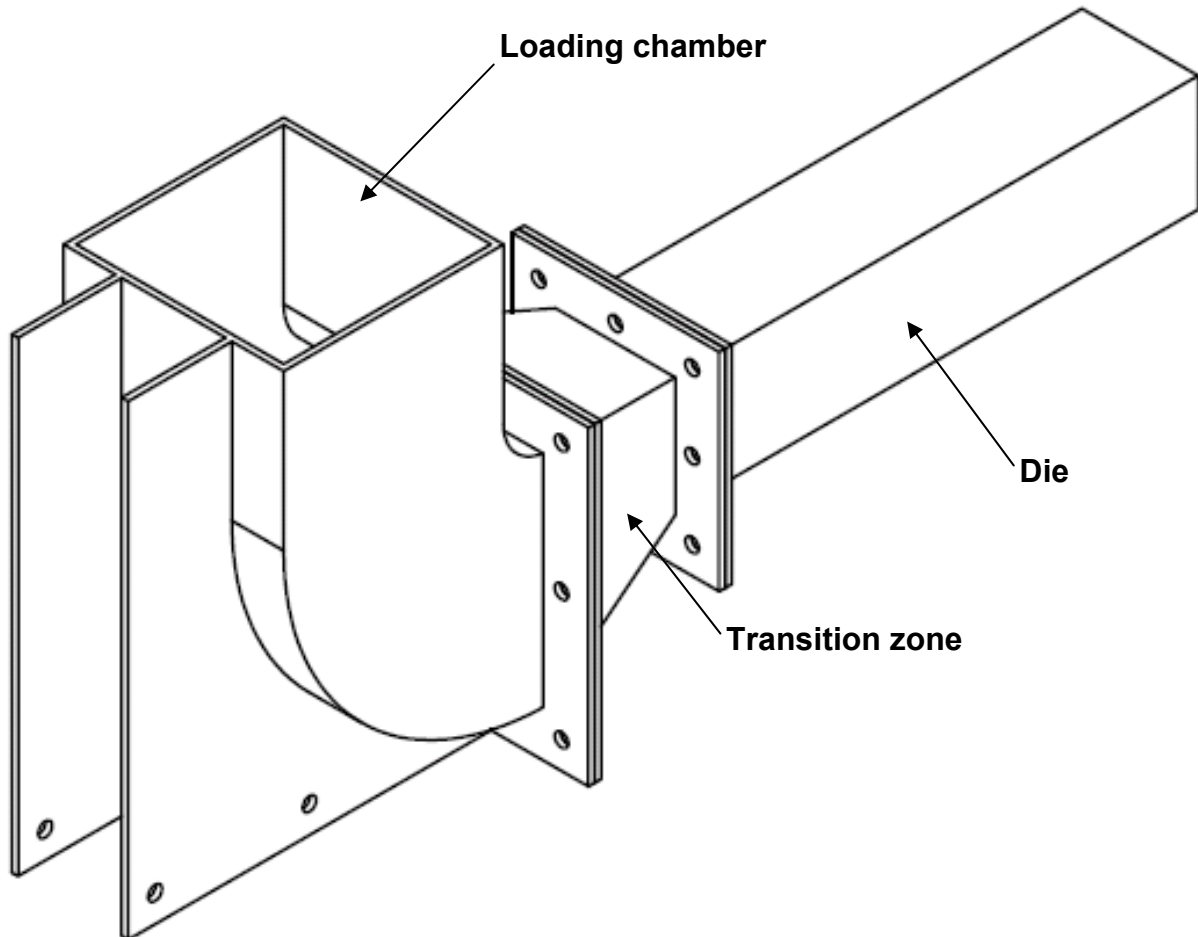
Figure 3.4: An isometric view of the new piston-driven extruder.

4 COMPARATIVE STUDY OF CONCRETE AND EXTRUDED & CAST SHCC

Due to the enhanced resistance of extruded SHCC in uni-axial loading (uni-axial tension and bending), as a result of fibre orientation, the most beneficial application thereof will be for elements exposed to such loads. This includes, but is not limited to, beams, bars and one-way spanning plates. In order to investigate whether or not such postulations are indeed true and whether such enhanced benefits are indeed realized, it was decided to conduct a comparative study between concrete, cast SHCC and extruded SHCC. This study will include non-reinforced as well as reinforced elements for each type of composite.

4.1 INTRODUCTION: THREE-POINT FLEXURAL BENDING TESTS

Three-point flexural bending tests are suitable and easy tests to conduct in order to investigate the mechanical behaviour of a cement-based composite. Since it is also a representative test for the type of uni-axial applications including bending moment and shear that are envisioned for these extruded SHCC and R/SHCC composites, it was decided use three-point bending tests for the comparative study. A standard R/C composite was also tested in order to compare the SHCC and R/SHCC composites with generally used concrete composites. The basis for the design of ordinary concrete is its 28 day compressive strength and this was also the basis for choosing a suitable concrete for comparison to SHCC. In other words the cast SHCC and concrete had to have to same ultimate compressive strength. This section will contain a description of the test set-up and the experimental test program that was followed as well as the results that were obtained and a brief discussion.

4.2 TEST SET-UP

The dimensions for the beams to be tested in three-point flexural bending were set at 100 mm X 100 mm with a testing span of 400 mm. The unreinforced specimens were produced to be 500 mm long. A standard 30 MPa concrete mix was chosen for the manufacturing of the R/C specimens based on previously obtained compressive strength measurements of cast SHCC specimens of the same mix design as the cast SHCC used in this research [Stander 2007]. Cube crush tests were also carried out on 100 mm X 100 mm cubes of the concrete and cast SHCC in this study to verify their comparable compressive strengths.

According to the SABS 0144 code [1995] an anchorage length of at least 34 times the bar diameter is needed for 30 MPa concrete in order to convey the tensile force in the bar. The reinforcing steel chosen for these tests were 8 mm Y-steel reinforcing bars. This translates into an anchorage length of at least 272 mm. This means that the length from the mid-point, where the maximum force will be applied, has to be more than an anchorage length of 272 mm. It was decided to produce R/C specimens with a length of 650 mm. This ensured an anchorage length more than efficient for the transfer of the maximum force. Since there are not any codes or guidelines available for the required anchorage length of reinforcing steel in SHCC, it was judged that the anchorage length for the SHCC has to be the same as for the concrete. Thus, R/SHCC specimens with a length of 650 mm were also produced. Wooden moulds with dimensions 100 mm X 100 mm X 650 mm were made for the casting of the R/C and R/SHCC specimens [Figure 4.1 (a) and (b)].

(a)   (b)

(c)
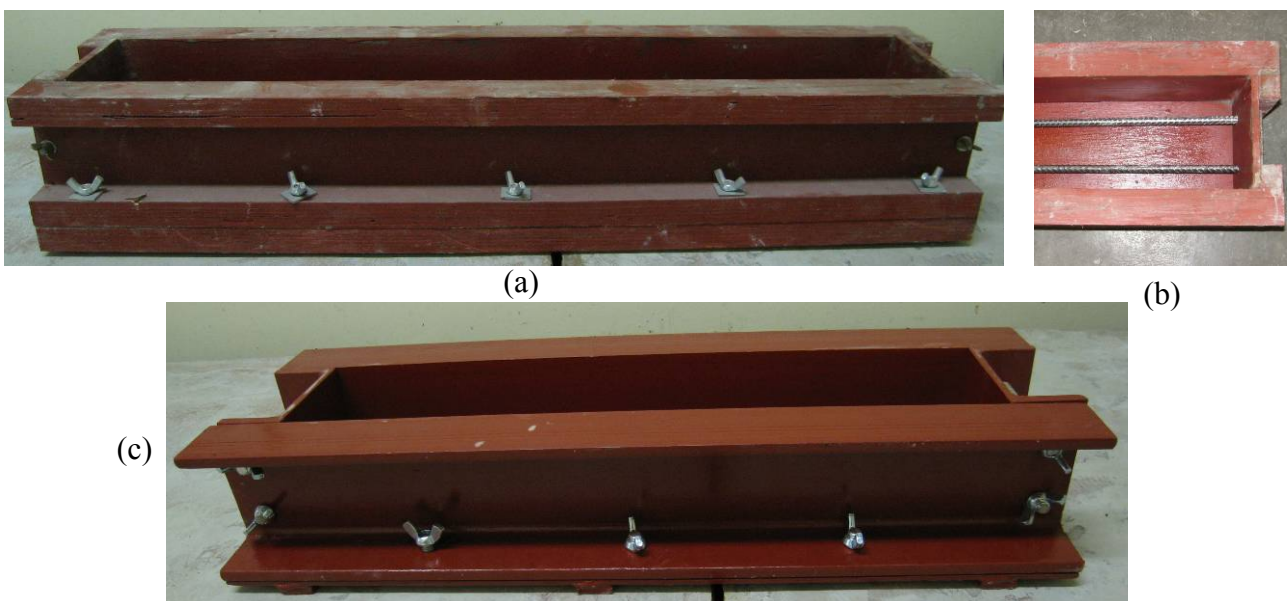
Figure 4.1: Beam moulds for the casting of bending specimens. (a) & (b) Wooden moulds for reinforced specimens and (c) standard steel moulds for unreinforced specimens.

Holes were drilled in the moulds to ensure that the two tensile, 8 mm reinforcing bars can be placed precisely every time. The reinforced specimens were all produced with a concrete cover of 20 mm, which is the minimum cover prescribed by SABS 0100-2 code [1992]. The unreinforced SHCC specimens were cast in standard steel moulds with dimensions 100 mm X 100 mm X 500 mm [Figure 4.1 (c)]. The specimens were cast horizontally on a vibrating table.

The extrusion SHCC specimens, namely the R/SHCC and SHCC specimens were produced with the new piston-driven extruder designed for this research study, as discussed in Chapter 3. The specimens were extruded onto base plates and the specimens were cut to the correct lengths as soon as enough material was extruded, 500 mm for ordinary SHCC specimens and 650 mm for R/SHCC specimens. The velocity of the extruder piston was set at 7 mm/s. This causes the specimen to exit the extruder at 28 mm/s. The 8 mm reinforcing bars for the R/SHCC specimens were cut to correct lengths of 650 mm beforehand. The reinforcing bars were evenly pushed in at the back of the extruder before the extrusion process was begun. When the extrusion process began they were gripped by the SHCC-material and were then automatically pulled through by the material. Figure 4.2 shows photos of the new piston-driven extruder.

(a)

(b)
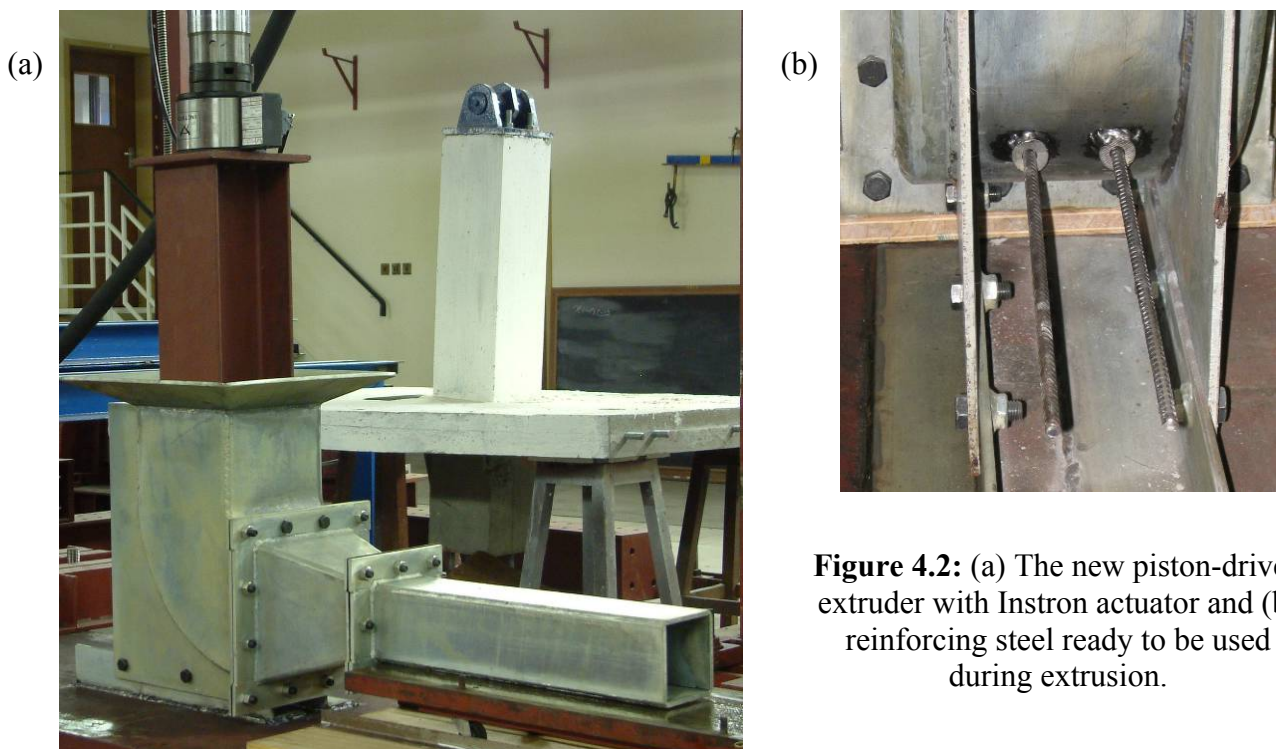
Figure 4.2: (a) The new piston-driven extruder with Instron actuator and (b) reinforcing steel ready to be used during extrusion.

The three-point flexural bending tests were conducted in a Zwick Z250 Universal Materials Testing Machine which has a capacity of 250 kN. A base plate is bolted onto the top and bottom crossheads. A frame with two adjustable rollers (diameter 50 mm) is bolted onto the bottom base plate. The

rollers can be adjusted to equal distances from the centre of the frame for the required testing span length. A fixed roller (diameter 30 mm) is bolted onto the centre of the top base plate. A schematic and a photo of the set-up are given in Figure 4.3.
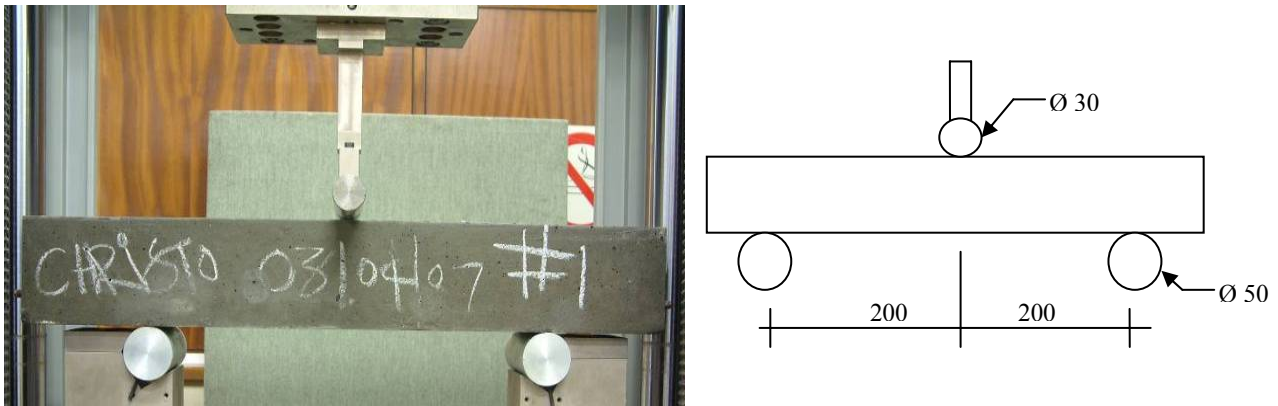
Figure 4.3: Three-point flexural bending test set-up and bending specimen.

The tests were controlled by means of the displacement rate of the crosshead, and the force and deflection measurments of the internal load cell and the crosshead displacement of the Zwick were recorded. A pre-load of 20 N was applied to the specimens and the tests were subsequently conducted at a displacement rate of 5 mm/min. The readings were converted to a data file that was later used to produce graphs of applied load versus mid-span deflection.

4.3 EXPERIMENTAL TEST PROGRAM

This section will be divided into three sub-sections according to the different mix designs and specimen fabrication method used for this part of the research.

4.3.1 CAST SHCC AND R/SHCC

The different mix constituents for SHCC have already been discussed in Chapter 2. The SHCC mix design for casting was acquired form a previous research project conducted by Boshoff [2006]. The mix proportions are given in Table 4.1.

Table 4.1: Cast SHCC mix design [Boshoff 2006]

W/B	A/B	CEM I/B	FA/B	GGCS/B	SP	VA	V_f
[by mass]	[by mass]	[by mass]	[by mass]	[by mass]	[% by B mass]	[% by B mass]	[% by volume]
0.4	0.5	0.45	0.5	0.05	1	0.3	2

Care was taken to ensure that the mixer was saturated with water, but dry to the touch before the execution of all the mixes. This ensured minimum loss of water during the mixing due to the

absorption by the mixer. A pan-type mixer with a capacity of 50 litres was used. The mixing procedure and mixing times are shown schematically in Figure 4.4.
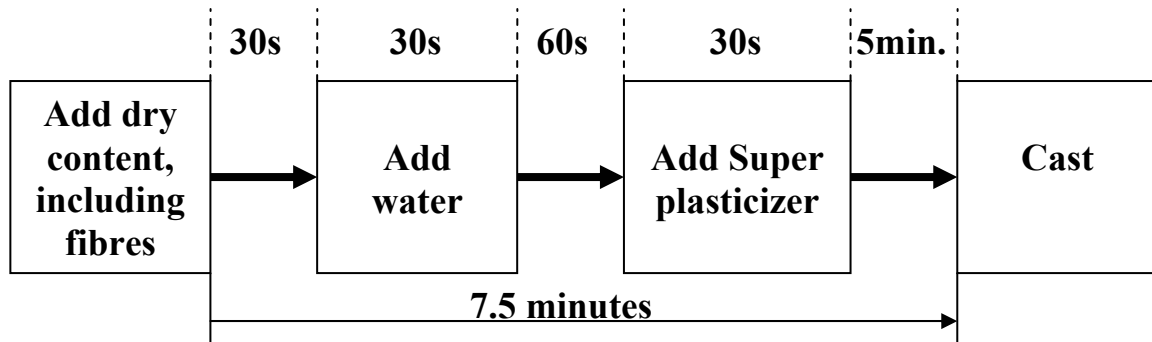
Figure 4.4: Mixing procedure with time shown for each step of mixing cast SHCC.

The specimens were cast horizontally on a standard vibrating table. The reinforcement for the R/SHCC specimens were placed and sealed in the wooden moulds the day before casting, to allow the sealant to set adequately before casting. The correct amount of material was placed in the moulds, in three roughly equal thick layers, while vibrating. This was done to enable entrapped air to escape from the fresh material. After the entire mould was filled, the specimens were vibrated for another minute after which the surface was smoothed over.

The moulds were placed in a temperature controlled humidity room at 100% humidity and 23°C after casting. The specimens were left to cure in the moulds for 72 hours before they were stripped. The specimens were then submerged in clean potable water at 23°C until an age of 14 days. At this stage the specimens were removed from the water and towel dried before testing.

Six R/SHCC and six SHCC beam specimens were cast and tested. The data form all the tests were captured on a computer and graphs were produced for further analysis. The results will be discussed in one of the following sections.

Eight SHCC cubes of dimension 100 mm X 100 mm were also made for comparison of the compressive strength to that of the ordinary concrete. They were cast in steel moulds on the vibrating table, and kept in the moulds in a temperature controlled room at 23°C for 72 hours before they were stripped and submerged in clean potable water at 23°C until the day of testing. Four specimens were tested at 14 days and four specimens were tested at 28 days after curing. The specimens were tested in a Contest Crushing Machine.

4.3.2 EXTRUDED SHCC AND R/SHCC

The SHCC mix used for extrusion was designed in a previous research study [Visser 2005]. The mix proportions are given in Table 4.2.

Table 4.2: Extrusion SHCC mix design [Visser 2005]

W/B	A/B	CEM I/B	FA/B	SP	VA	V_f
[by mass]	[by mass]	[by mass]	[by mass]	[% by B mass]	[% by B mass]	[% by volume]
0.25	0.5	0.5	0.5	1	0.3	2

The same pan-type mixer that was used for the cast SHCC specimens was used for the mixing of the extrusion SHCC. The mixer was again saturated with water and towel dried to minimise water loss. The mixing procedure and mixing times are shown schematically in Figure 4.5.
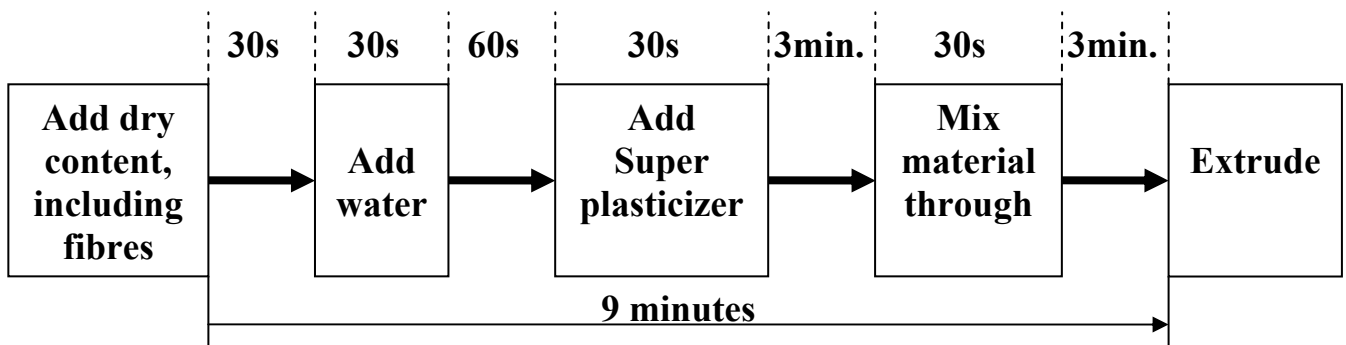
Figure 4.5: Mixing procedure with time shown for each step of mixing extrusion SHCC.

The extrusion SHCC requires a longer mixing time to ensure that all the material is properly mixed and the fibres evenly dispersed. Due to the dry, dough-like mix the mixer has to be stopped during the mixing process to remove the material that is stuck to the blades. The material is then all thrown together and the mixing process is then continued again.

The mix was then taken to the extruder to be extruded. The material was placed in the loading chamber until the entire loading chamber was filled. The material was then extruded onto a base plate that moves along on rollers. The specimens were than cut to length, 500 mm for ordinary SHCC specimens and 650 mm for R/SHCC specimens. Figure 4.6 shows photos of the extrusion process in progress and of the final product.
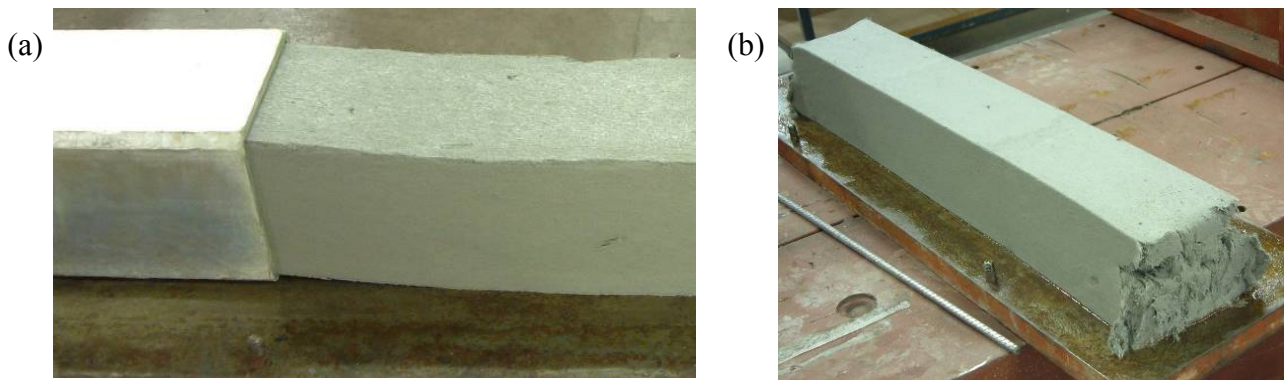
Figure 4.6: (a) Extrusion process in progress and (b) an extruded specimen just after extrusion.

The base plates with the specimens on them were then placed in a temperature controlled humidity room at 100% humidity and 23°C. The specimens were left in the humidity room for 72 hours. They were then removed from the humidity room, taken off the base plates and cured in exactly the same way as the cast specimens, i.e. submerged in clean potable water at 23°C until an age of 14 days. At this stage the specimens were removed from the water and towel dried before testing.

Six R/SHCC and six SHCC beam specimens were extruded and tested. The data form all the tests were captured on a computer and graphs were produced for further analysis. Form retention of specimens after extrusion is also an important requirement and, thus this was also studied. Another important requirement is that the correct concrete cover for reinforcing bars is achieved and that this stays constant. For this reason concrete cover was also measured and was included in the results. All the results will be discussed in one of the following sections.

4.3.3 CAST R/C

A standard 30 MPa concrete mix was designed using standard mix design procedures [Addis 1998]. The aggregate consisted of 13 mm Greywacke stone and Malmesbury sand, local dune sand with an even grading. The binder that was used was CEM I 42.5N (OPC). The mix proportions are given in Table 4.3.

Table 4.3: R/C mix design

W/C	Water content	A/B	Sand/B	Stone size
[by mass]	[L]	[by mass]	[by mass]	[mm]
0.64	195	6.05	2.61	13

A 50 litre pan-type mixer was used to mix the concrete. Standard concrete mixing procedures were used. The specimens were cast horizontally on a standard vibrating table. The reinforcement had to be placed and sealed in the moulds a day before mixing. After the correct amount of material was

placed in the moulds, the moulds were left to vibrate for another minute, after which the surface was smoothed over.

The moulds were placed in a temperature controlled humidity room at 100% humidity and 23°C after casting. The specimens were left to cure in the moulds for 72 hours before they were stripped. The specimens were then submerged in clean potable water at 23°C until an age of 14 days. At this stage the specimens were removed from the water and towel dried before testing.

Six R/C beam specimens were cast and tested. The data form these tests were captured on a computer and graphs were produced for further analysis. The results will be discussed in one of the following sections.

Eight concrete cubes of dimension 100 mm X 100 mm were also cast on the vibrating table for comparison of the compressive strength to that of the cast SHCC. These cubes were kept in the steel moulds in a temperature controlled room at 23°C for 72 hours before they were stripped and submerged in clean potable water at 23°C until the day of testing. Four specimens were tested at 14 days and four specimens were tested at 28 days after curing. The specimens were tested in a Contest Crushing Machine.

4.4 RESULTS

The results of the three-point flexural bending tests will be given according to the different mix designs and specimen fabrication methods. The results will be discussed and interpreted in the next section.

The important characteristics determinable from flexural tests results are the ultimate flexural strength [F_{max}] commonly expressed as the modulus of rupture [MOR], the first cracking strength [F_{fc}] as well as the ductility. Even though these parameters can not directly be used as material parameters as they strongly depend on the geometry and boundary conditions, they are useful in this case for comparing the different materials' structural and mechanical responses.

The first crack strength was found by investigating the curves of flexural tests results and identifying the first drop in the force reading on the elastic part of the curve which can be interpreted as a drop in the force resistance and thus a crack that formed. Where such a drop in force could not be identified for a specimen, the first crack strength was taken as the strength at which a significant reduction in the stiffness of the specimen could be detected. The ultimate strength is

determined from the highest force resisted by the specimen. The ultimate strength is expressed as a force in kN and the MOR in MPa. The definition of the modulus of rupture is the tensile stress resistance that the material would require to resist the applied load if the material behaviour is purely elastic. This can be calculated as follows:

$$MOR = \frac{3}{2} \cdot \frac{PL}{bh^2}$$

(4.1)

where P is the applied force, L is the distance between the supports, b is the depth of the beam section and h is the height of the section. The ductility was taken as the deflection that corresponds to a force that is equal to 75% of the ultimate strength, but which occurs after the ultimate strength was achieved, i.e. in the softening branch.

Table 4.4: Ultimate compressive strengths of cast concrete and SHCC

Specimen [#]	Concrete [14days] [MPa]	Concrete [28days] [MPa]	SHCC [14days] [MPa]	SHCC [28days] [MPa]
1	22.5	32.4	22.3	30.6
2	23.5	32.8	22.6	32.7
3	23.6	33.1	23.0	32.7
4	23.7	33.9	23.4	33.3
Average	23.3	33.1	22.8	32.3
StdDev	0.48	0.55	0.41	1.03
C.O.V.	2.06%	1.66%	1.82%	3.17%

In order to verify the validity of the choice of the concrete as basis for comparison to SHCC, based on ultimate compressive strength, the results of the compressive strengths are given in Table 4.4. This table shows the 14day compressive strength and 28 day compressive strength of the cast SHCC and concrete cubes. The average values and the standard deviations [StdDev] are also provided along with the coefficients of variation [C.O.V.] in percentile form, which serves as an indication of the spread of the results of a characteristic and can be directly compared with the C.O.V. of other characteristics.

The results of these compressive tests are summarized in Figure 4.7 which shows the average ultimate compressive strengths of the cast concrete and SHCC along with the spread (maximum and minimum value) of each. It can be seen that these values compare well. Thus the chosen concrete is considered suitable for comparison to SHCC in the subsequent flexural tests.
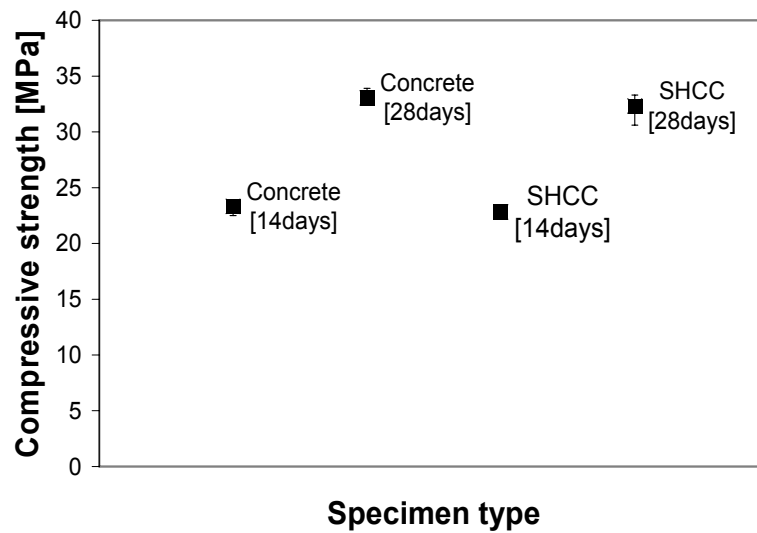
Figure 4.7: The ultimate compressive strength of cast concrete and SHCC.

4.4.1 CAST SHCC AND R/SHCC

The results for the three-point flexural bending tests for the cast SHCC and R/SHCC are shown in Figure 4.8. The graph is given as the mid-span deflection in mm vs. the applied load at the centre of the specimen in kN.
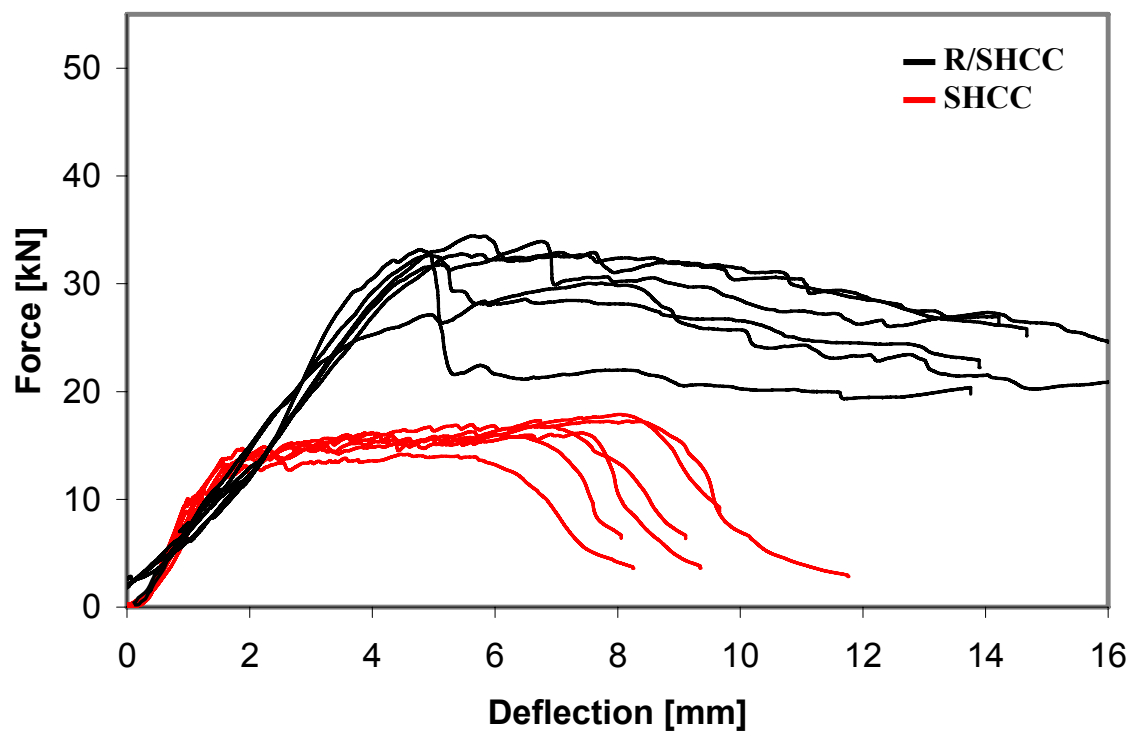
Figure 4.8: Three-point flexural bending test results of cast SHCC and R/SHCC.

The aforementioned characteristics, first cracking force, ultimate strength and ductility, were determined for the cast SHCC and R/SHCC specimens and are given in Table 4.5 and Table 4.6. The average values and the standard deviations are also provided along with the coefficients of variation.

Table 4.5: Flexural characteristics of cast SHCC specimens

Specimen [#]	F_{max} [kN]	MOR [MPa]	F_{fc} [kN]	Ductility [mm]
1	17.308	10.385	10.320	9.03
2	15.970	9.582	9.950	7.28
3	16.182	8.508	8.911	7.64
4	14.181	9.709	8.757	6.56
5	17.882	10.729	9.963	8.72
6	16.773	10.064	9.346	7.93
Average	16.383	9.830	9.541	7.86
StdDev	1.290	0.774	0.633	0.92
C.O.V.	7.87%	7.87%	6.63%	11.64%

Table 4.6: Flexural characteristics of cast R/SHCC specimens

Specimen [#]	F_{max} [kN]	MOR [MPa]	F_{fc} [kN]	Ductility [mm]
1	31.788	19.073	9.264	11.22
2	27.128	16.277	9.995	9.53
3	34.460	20.676	7.692	10.79
4	32.906	19.744	10.85	11.89
5	33.163	19.898	8.654	10.97
6	33.930	20.358	11.182	12.56
Average	32.229	19.337	9.606	11.16
StdDev	2.661	1.597	1.332	1.03
C.O.V.	8.26%	8.26%	13.86%	9.25%

4.4.2 EXTRUDED SHCC AND R/SHCC

Apart from the flexural test results there are other results that were obtained and studied, specifically for the extruded specimens. These results pertain to the extrusion process itself and include the form retention of all the extruded specimens as well as the concrete cover to the steel reinforcing bars of the extruded R/SHCC specimens. For the form retention the height, top and bottom width of all the specimens were measured. The steel cover to the bottom of the R/SHCC specimens, in other words the thickness of the concrete between the bottom edge of a specimen and the reinforcing bars, was also measured on the day of testing. These results are shown in Table 4.7 and Table 4.8 as well as the average values along with the standard deviations and coefficients of variation. The results of the three-point flexural bending tests for the extruded SHCC and R/SHCC are shown in Figure 4.9.

Table 4.7: Form retention measurements for the extruded SHCC specimens

Specimen	Top width	Bottom width	Height
[#]	[mm]	[mm]	[mm]
1	100.1	101.5	97.2
2	100.1	104.2	98.0
3	100.2	104.5	97.4
4	99.9	104.1	97.0
5	100.0	104.6	96.9
6	100.0	103.0	97.5
Average:	100.1	103.7	97.3
StdDev:	0.1	1.2	0.4
C.O.V.:	0.10%	1.16%	0.41%

Table 4.8: Form retention and steel cover measurements for the extruded R/SHCC specimens

Specimen	Top width	Bottom width	Height	Steel cover
[#]	[mm]	[mm]	[mm]	[mm]
1	99.3	106.7	96.9	18.4
2	99.4	105.6	97.0	19.5
3	99.0	105.0	97.2	18.0
4	99.5	105.0	97.0	19.7
5	99.7	106.2	97.2	19.1
6	99.8	107.0	96.1	19.3
Average:	99.5	105.9	96.9	19.0
StdDev:	0.3	0.9	0.4	0.7
C.O.V.:	0.29%	0.81%	0.42%	3.49%
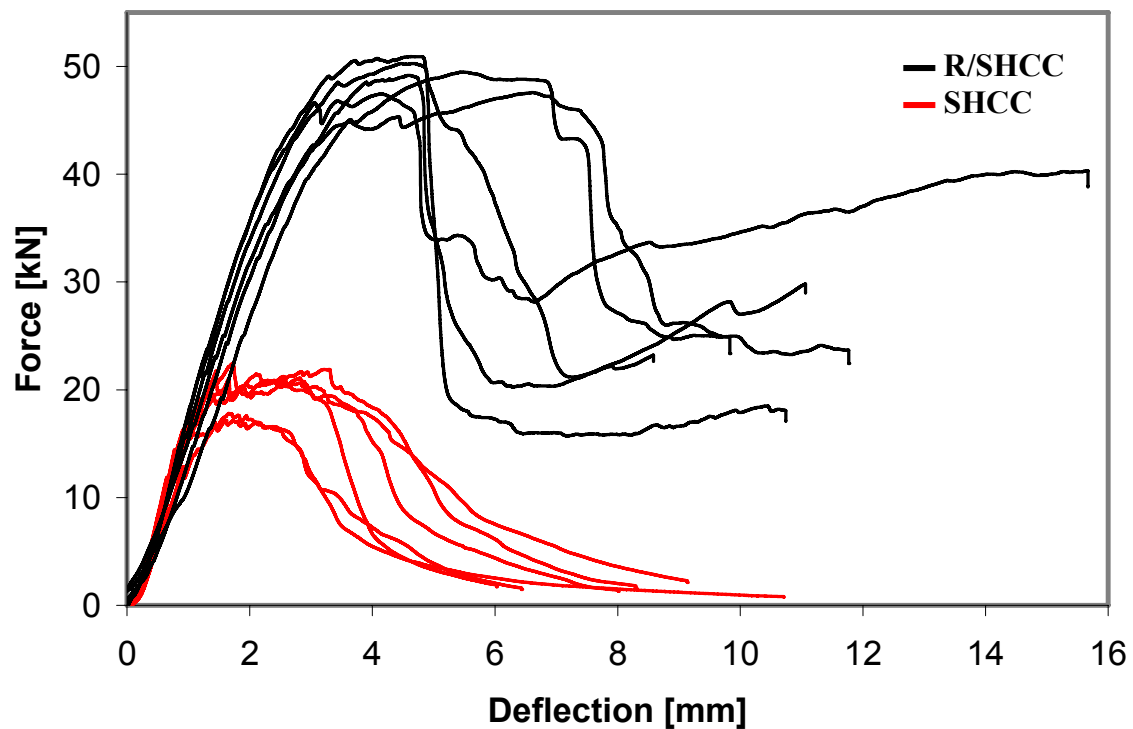
Figure 4.9: Three-point flexural bending test results of extruded SHCC and R/SHCC.

The flexural characteristics of the extruded SHCC and R/SHCC specimens were determined and are shown in Table 4.9 and Table 4.10. The average values along with the standard deviations and coefficient of variations are also provided.

Table 4.9: Flexural characteristics of extruded SHCC specimens

Specimen [#]	F_{max} [kN]	MOR [MPa]	F_{fc} [kN]	Ductility [mm]
1	17.163	10.30	11.696	2.95
2	21.763	13.06	13.172	4.12
3	17.808	10.68	12.868	2.89
4	21.244	12.75	14.434	3.93
5	22.436	13.46	11.928	4.34
6	20.608	12.36	13.613	3.45
Average	20.170	12.102	12.952	3.61
StdDev	2.175	1.305	1.031	0.61
C.O.V.	10.78%	10.78%	7.96%	17.00%

Table 4.10: Flexural characteristics of extruded R/SHCC specimens

Specimen [#]	F_{max} [kN]	MOR [MPa]	F_{fc} [kN]	Ductility [mm]
1	49.493	29.70	15.792	7.56
2	47.458	28.47	15.572	4.83
3	50.270	30.16	15.167	4.98
4	50.922	30.55	16.836	5.95
5	47.573	28.54	12.491	7.93
6	49.177	29.51	14.941	4.91
Average	49.149	29.489	15.133	6.03
StdDev	1.404	0.843	1.452	1.40
C.O.V.	2.86%	2.86%	9.60%	23.21%

4.4.3 CAST R/C

The purpose of testing R/C specimens was to compare a standard reinforced concrete with the cast SHCC and the extruded SHCC composites. For this reason two graphs are given in Figure 4.10 and Figure 4.11. Figure 4.10 shows the three-point flexural bending test results of the R/C specimen in comparison to the unreinforced cast and extruded SHCC specimens. Figure 4.11 shows the test results of the R/C specimens in comparison to the cast and extruded R/SHCC specimens.
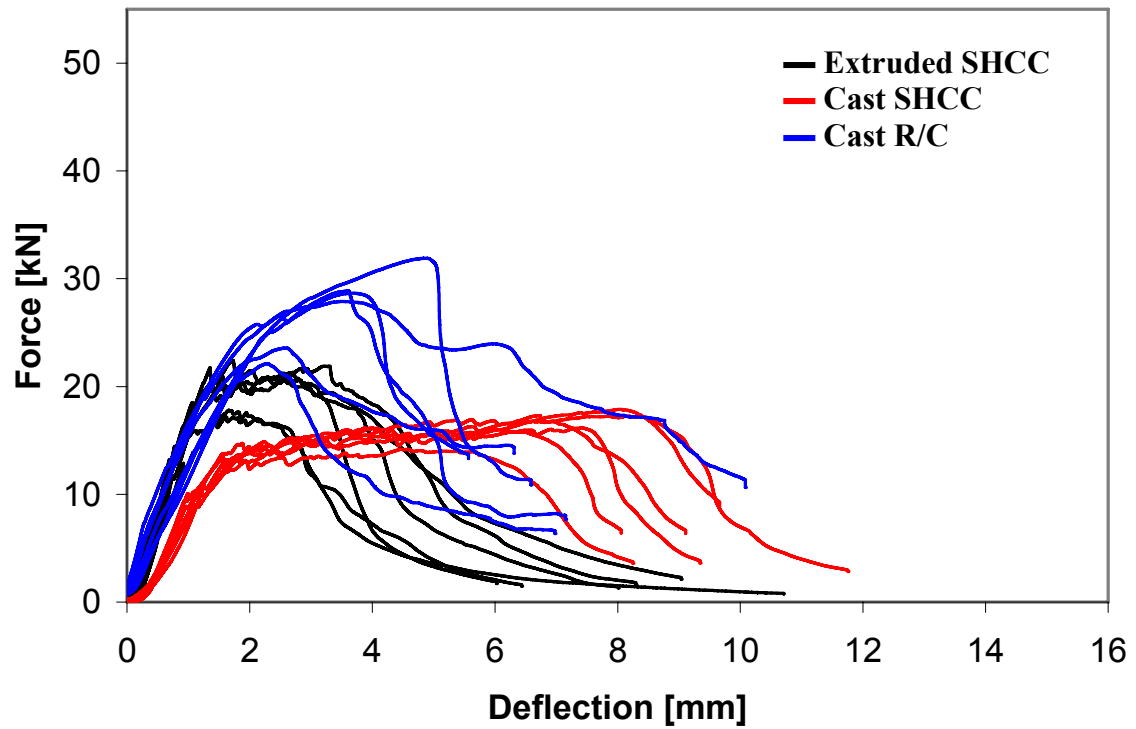
Figure 4.10: Three-point flexural bending test results of cast R/C vs. that of cast and extruded SHCC.

.
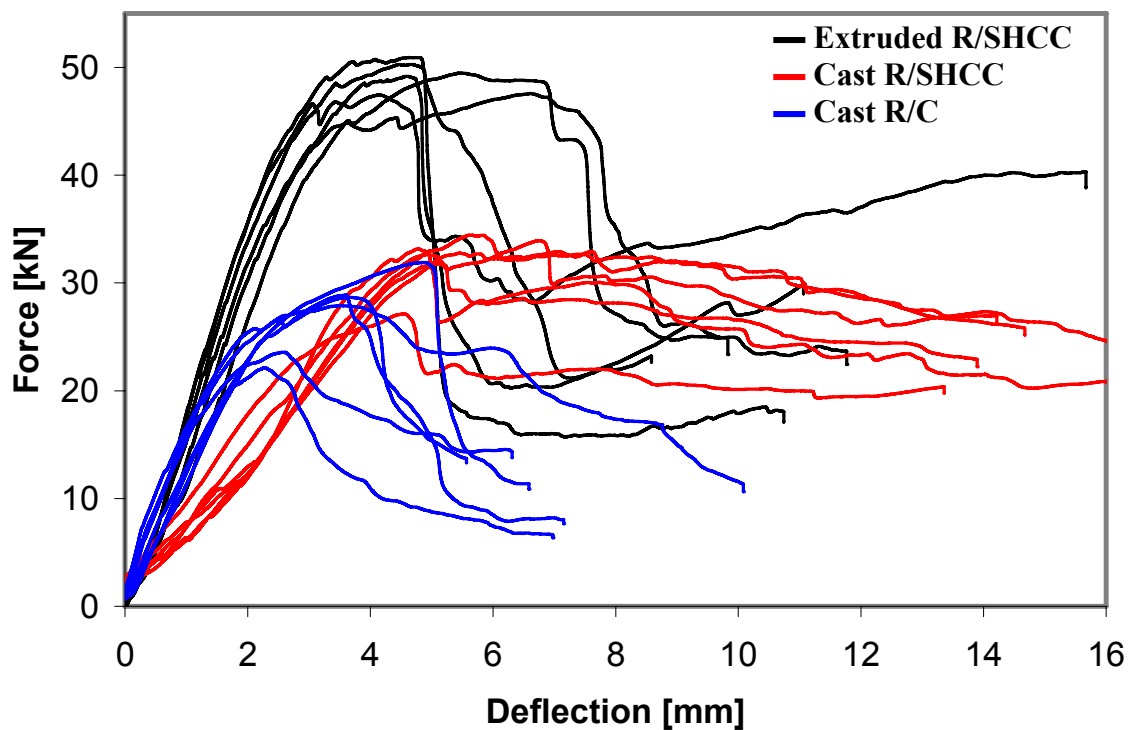
Figure 4.11: Three-point flexural bending test results of cast R/C vs. that of cast and extruded R/SHCC.

The flexural characteristics of the R/C specimens were determined and are shown in Table 4.11. The average values along with the standard deviation and coefficient of variation are also provided.

Table 4.11: Flexural characteristics of cast R/C

Specimen [#]	F_{max} [kN]	MOR [MPa]	F_{fc} [kN]	Ductility [mm]
1	28.887	17.332	7.885	4.19
2	27.896	16.737	7.881	6.63
3	22.128	13.277	6.932	3.01
4	28.668	17.201	7.294	4.24
5	31.898	19.139	7.277	5.12
6	23.573	14.144	6.047	4.00
Average	27.175	16.305	7.219	4.53
StdDev	3.645	2.187	0.685	1.23
C.O.V.	13.41%	13.41%	9.49%	27.15%

4.5 DISCUSSION

4.5.1 GENERAL

To explain the differences in the mechanical behaviour of the various composites, it is required to first look at the differences in the composition of the composites. As it was mentioned in the previous chapters, SHCC is an engineered composite that can specifically be designed for a required application and fabrication method. The differences between SHCC and ordinary concrete are clear and have been discussed previously, thus only the differences between the two SHCC's (produced by extrusion and casting) will be discussed here.

When looking at the mix designs for the cast and extrusion SHCC's there are two notable differences in their compositions. Firstly, unlike in the extrusion mix, a portion of the cement of the cast mix is replaced by slag (GGCS). There is no particular reason for this except that the two mix designs were obtained form separate research studies [Visser 2005 and Boshoff 2006]. The second and more significant difference between the two SHCC's is the difference in the W/B ratios. The cast mix has a higher W/B ratio (W/B^{cast} = 0.4) to establish a more workable wet mix for casting, while the low W/B ratio for extrusion (W/B^{extrude} = 0.25) ensures a stiff, dough-like and dry mix. The lower W/B ratio however also establishes a higher aggregate content in the extrusion mix in comparison to the casting mix, which in turn causes higher matrix strength of the extrusion mix.

The various influences of the fabrication methods have already been discussed in the previous chapters, but some of the observations of the composites in the fresh state will be discussed here.

Due to the fine-grained nature of the casting mix the material has a so-called "stickiness" which makes it difficult to place the material. Heavy vibration is needed to place the material, but care also has to be taken when placing the material in moulds so that excess air is not entrapped in the composite. When the material is not placed correctly and air is entrapped, it could cause weak spots within the matrix, which can lead to premature failure. This was however not found to be a problem in this case, as can be seen from the low C.O.V. for the first cracking force and ultimate strength of the cast composites.

Figure 4.12: Surface flaws on extruded specimens.

Specimens that were produced with the current extruder transition zone and die set-up of the new piston-driven extruder exhibited some surface flaws [Figure 4.12]. It is the opinion of the author that these flaws are a result of the discontinuous nature of the loading of the material into the extruder. These flaws are not seen as detrimental to the mechanical performance of the composite, since no cracks originated from these flaws when tested. The flaws are however aesthetically unpleasing. It can be corrected when industrializing the extrusion process by ensuring a continuous feed of the material. It is also possible that the transition zone is not long enough to provide enough time and pressure for the material to be compacted properly. This will have to be investigated in further research.

Another observation that was made is that the extruded specimens did not retain their cross sectional shape, but sagged out under their own weight [Tables 4.7 and 4.8]. There are solutions to this problem. An even stiffer mix can be used for extrusion. This can be obtained by decreasing the SP content, but this will also alter the rheology of the mix and might have an effect on the mechanical performance of the composite. The specimens can be extruded onto plates onto which retaining sides can be fixed to prevent the specimens from sagging. This is however not the most economically viable alternative since extra moulds and space will be required. Another alternative is to design a die with a compensating, deformed cross sectional shape which can produce specimens that can sag out into their intended shape. Measurements form this study can be used in the initial design of such a die, but the shape will most probably have to be perfected in a further study through a series of trial and error test iterations.

4.5.2 MECHANICAL RESPONSE

The results from the three-point bending tests are summarized in Figure 4.13. The averages along with the maximum and minimum values for each specimen type are shown.
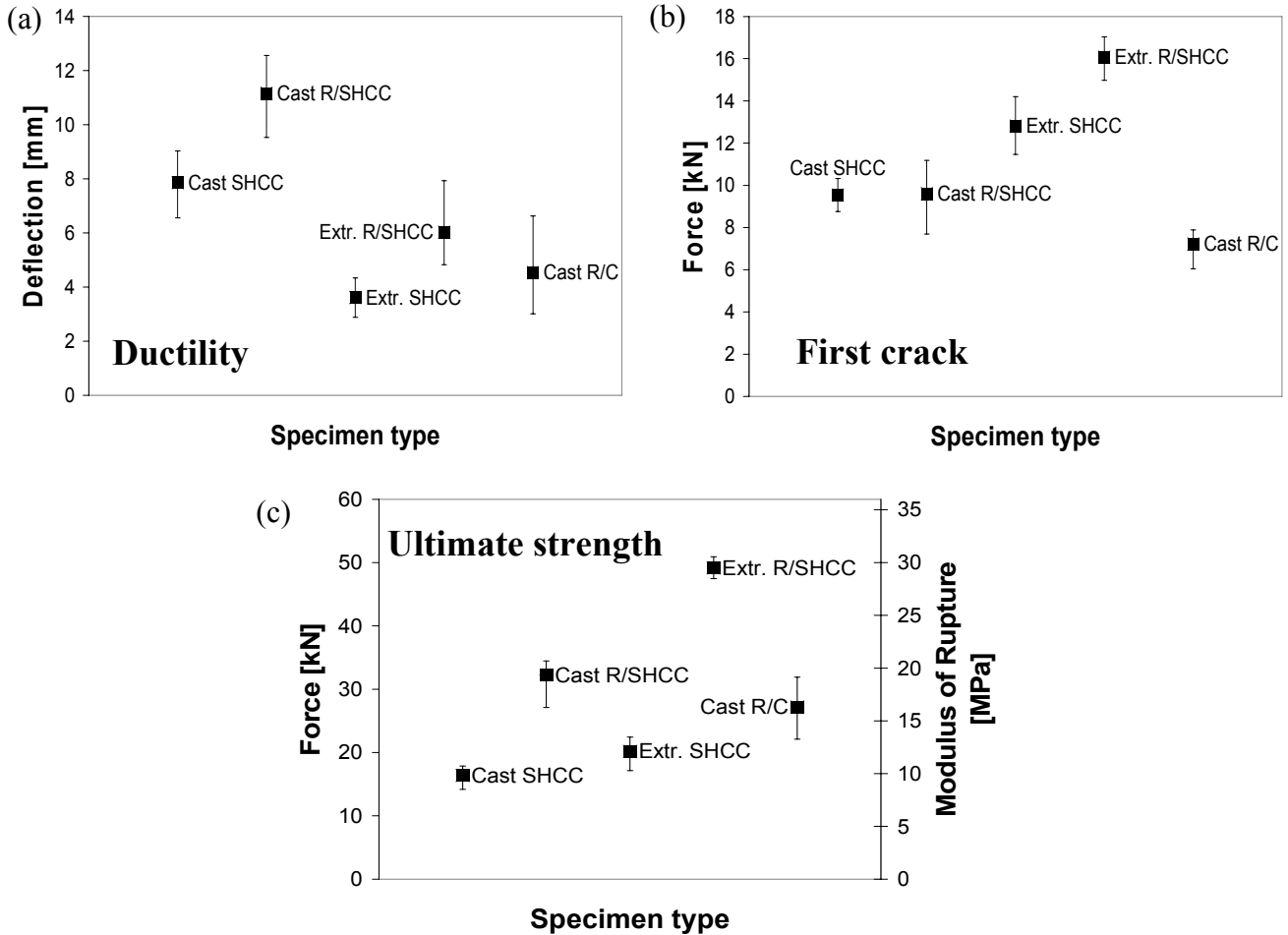
Figure 4.13: Comparison of (a) ductility, (b) first cracking force and (c) ultimate resistance.

The various composites that were tested exhibited different cracking patterns and modes of failure. These cracking patterns and modes of failure along with the test results will be discussed here in an effort to clarify the results that were obtained for the different composites.
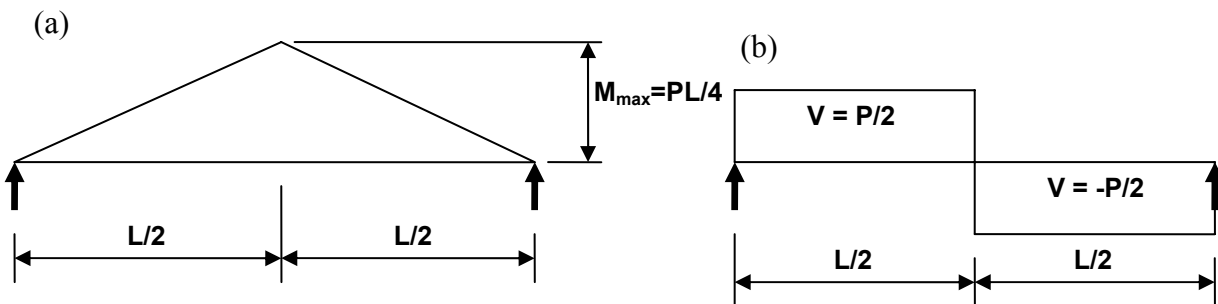
Figure 4.14: (a) Bending moment diagram and (b) shear force diagram for three-point bending tests.

The three-point bending test results in a bending moment diagram with a maximum moment in the centre of a specimen while a constant shear force is obtained between the first support and the centre and a constant shear force of the same magnitude, but opposite sign is obtained between the centre and the second support [Figure 4.14]. Thus, in the absence of significant weak spots, a specimen that fails due to flexure fails in the centre of the specimen, while the failure of a specimen away from the centre of the specimen is due to shear or a combination of shear and flexure.

(a)   Micro cracking   (b)   Crack localization
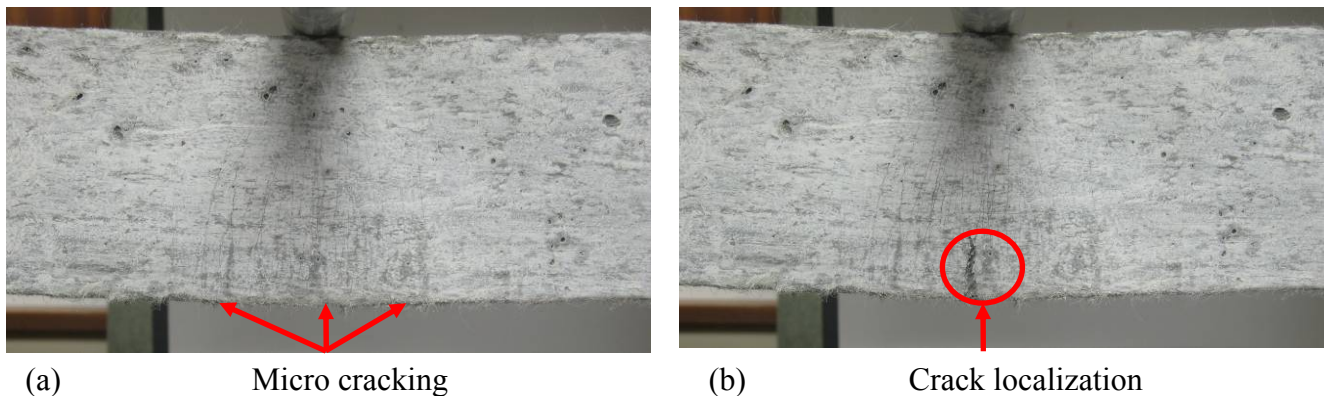
Figure 4.15: Crack formation and cracking pattern of a typical cast SHCC beam.

4.5.2.1 Unreinforced specimens

The cast SHCC and extruded SHCC specimens exhibited very similar cracking patterns although a more pronounced cracking pattern was displayed by the cast SHCC specimens. Both types of specimens formed multiple micro cracks at the bottom of the specimen in the centre. The specimens failed in flexure when one of these micro-cracks localized and continued to open while the rest of the cracks stayed constant. The crack formation and cracking pattern of a typical cast SHCC specimen are shown in Figure 4.15.

The extruded SHCC specimens had fewer micro cracks and these cracks were also barely visible to the naked eye. Extrusion specimens have an increased matrix strength which is caused by a higher aggregate content and a significantly reduced porosity through high extrusion forces. In this test series the W/B ratio was also lower for the extruded mix, also contributing to the higher strength.

The centre area of the beam undergoing flexural testing is shown schematically in Figure 4.16 [Boshoff 2006]. Note that the figure is not intended to be on scale. L_m is defined, as shown in Figure 4.16, as the length at the bottom of the beam that undergoes multiple cracking. It can also be defined as the area of which the tensile stress exceeded the first cracking tensile strength of the material.
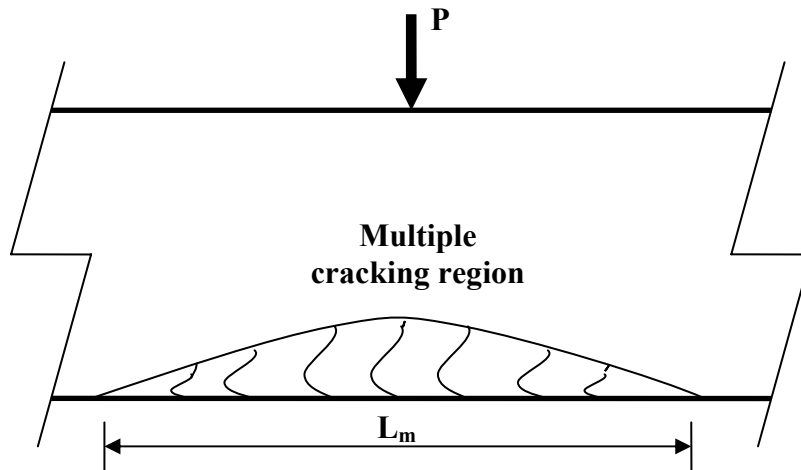
Figure 4.16: Graphical representation of the area of multiple cracking in a flexural test [Boshoff 2006].

It follows that the larger L_m, the higher the ductility of the flexural test as the multiple cracking is the reason for the ductile behaviour in bending. Due to the higher cracking strength of the extruded matrix, the area of multiple cracking will be less and thus it will have less flexural ductility as a result. This can also be seen as the reason why the cracks are less visible, since they have less opportunity to widen before one of them localizes.

(a)   Multiple cracking region   (b)   Crack localization
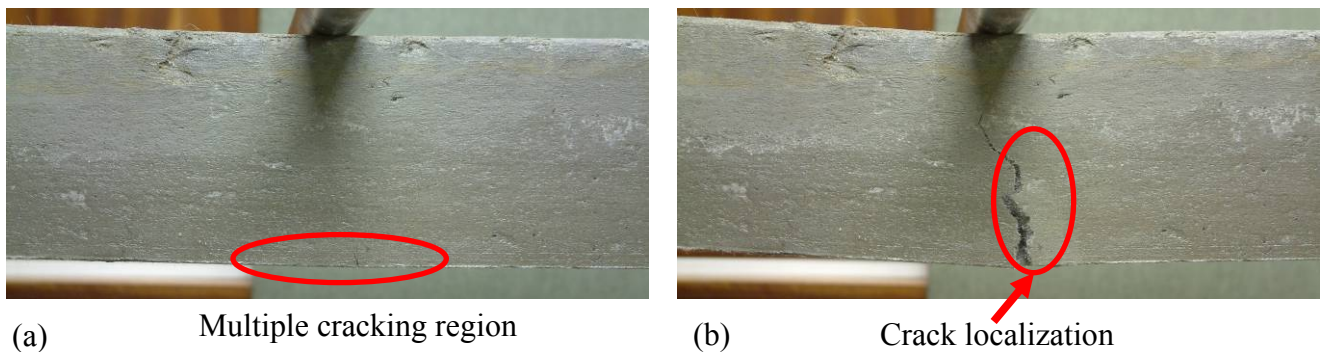
Figure 4.17: Crack formation and cracking pattern of typical extruded SHCC beam.

Figure 4.17 shows the crack formation and cracking pattern of a typical extruded SHCC specimen. The micro cracks are hardly visible, unlike in the cast specimens shown in Figure 4.15.

It can be seen from Figure 4.17 (b) that cracks that form in an extruded composite have a much more tortuous crack path. There are fewer voids in extruded composites than in cast composites, causing these voids to be situated less uniformly throughout the composite. When the composite cracks the cracks form by connecting these weak spots and a tortuous crack path is created.

When studying the flexural characteristics results of the cast SHCC and extruded SHCC it can be seen that the extruded SHCC performed better than the cast SHCC in all but the ductility. The reason for the reduced ductility has already been explained in terms of the smaller "plastic" zone of multiple cracking. The increased matrix strength and ultimate strength of the extruded SHCC specimens are due to the higher aggregate content which leads to higher compressive and tensile (increased tortuosity of cracks) strength, resulting in better flexural performance. These mechanisms will be discussed in the following chapter. It can be seen that cast SHCC and especially the extruded SHCC has a comparative level of performance as the cast R/C.

4.5.2.2 Reinforced specimens

The cast R/SHCC specimens and the extruded R/SHCC specimens both failed in a combination of shear and flexure. In both types of specimens some micro-cracking in the centre at the bottom of the specimens could be observed, but then diagonal shear cracks started to form. It is the opinion of the author that the addition of steel reinforcement changes the failure mechanism from flexural to a combination of shear and flexure. The flexural resistance is increased by such an amount that the composite reaches its shear capacity before the flexural capacity is reached.

The diagonal cracks start at a weak point at mid-height in the beam, on a line that goes roughly through the centre of gravity, at an angle of 45°, like normal shear cracks in the elastic region. These are however micro-cracks, barely visible to the naked eye. The fibres arrest the crack and another radial-type crack forms at another weak point at an angle smaller than 45°. This concept is illustrated in Figure 4.18 at the hand of a Mohr circle. When the section is still in an elastic state, the maximum shear stress (τ_{max}) is located at the centre of gravity of the equivalent section, which for the elastic case coincides with the neutral axis. Thus at this point there are only shear stresses present, as depicted in Figure 4.18 (b), causing the principal stresses, which in turn cause cracking at an angle of 45° to the horizontal axis. When the applied load is increased and the section enters the pseudo-plastic, multiple-cracking state, the neutral axis moves upwards towards the compression zone to maintain equilibrium. The point of maximum shear stress also shifts upwards away from the centroid, but the points of maximum shear stress and the neutral axis no longer coincide. This causes a stress state as depicted in Figure 4.18 (c), where shear stresses as well as horizontal tensile stresses are present. The angle between the horizontal axis and the principal stress direction decreases to an angle (θ') smaller than 45°. Thus another crack is formed at a higher shear stress, but at a reduced angle. More diagonal cracks form until the ultimate shear resistance of the composite is reached. At this stage no more cracks are formed, but the weakest crack starts to localize.
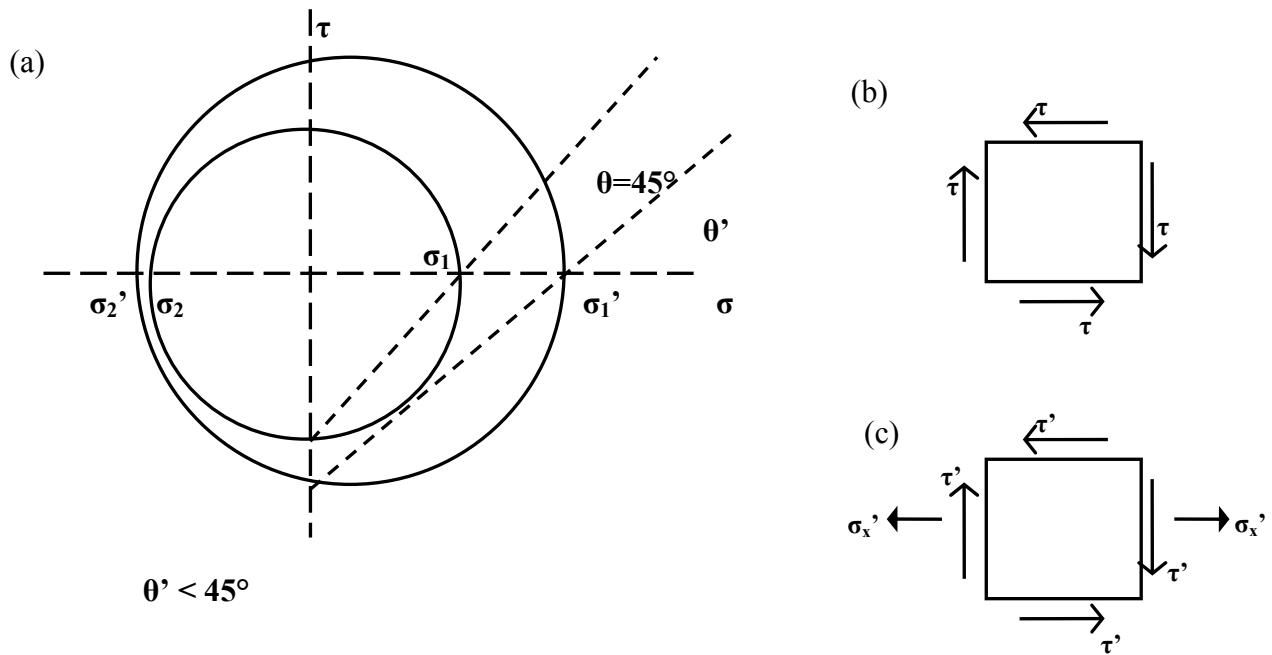
Figure 4.18: Illustration of principal stress rotation and crack alignment using a Mohr circle.

Diagonal cracking could be observed on both sides of the centre of the specimens for both the cast and the extruded R/SHCC specimens. The cast R/SHCC specimens however only formed two or three of these diagonal cracks per side before one of these cracks started to localize. The crack formation and cracking pattern of a typical cast R/SHCC specimen are illustrated in Figure 4.19.

(a)   First diagonal crack   (b)   More diagonal cracks

(c)   Delamination and crack localization.
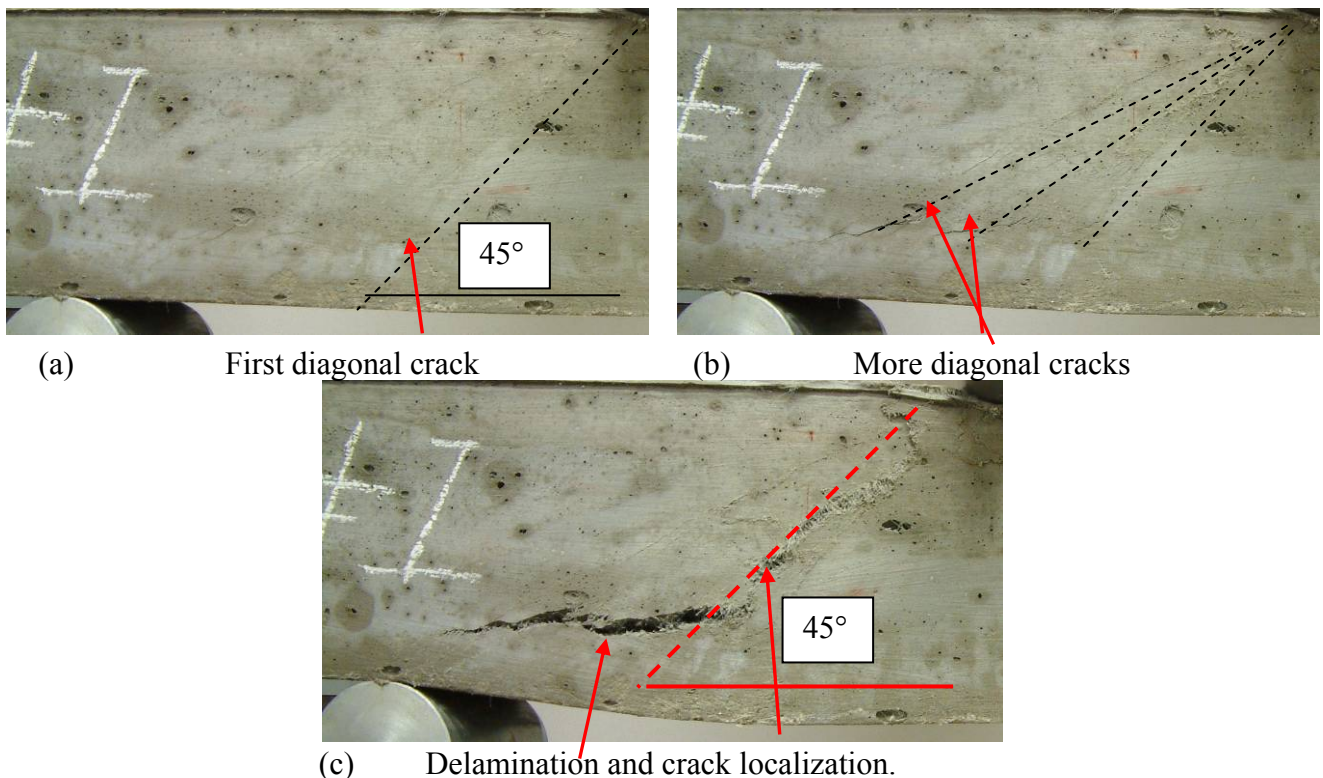
Figure 4.19: Crack formation and cracking pattern of a cast R/SHCC beam.

As it was stated in Chapter 2, the fibres of cast SHCC are more randomly orientated than the fibres of extruded SHCC. As a result there are only a few fibres available to bridge the diagonal cracks that form in a specimen and these cracks start to localize earlier than those of extruded SHCC specimens, which are able to form more diagonal cracks. As it is shown in Figure 4.19 (c), the diagonal cracks are unable to cross the reinforcing bars and the specimen starts to delaminate along the bars as a result. This is the same type of cracking that was observed by Kabele et al. [2007] for cast R/SHCC specimens that were tested in bending shear (the so-called Ohno method) which contained no shear reinforcement.

The extruded R/SHCC specimens however formed multiple diagonal cracks before the weakest of these localized. The orientation of the fibres of the extruded SHCC ensured that there were enough fibres to bridge and arrest the diagonal cracks. This allows more of these cracks to be formed. The crack formation and cracking pattern of a typical extruded R/SHCC specimen are shown in Figure 4.20.

(a)   Diagonal crack formation   (b)   Crack localization

(c)   Total cracking pattern
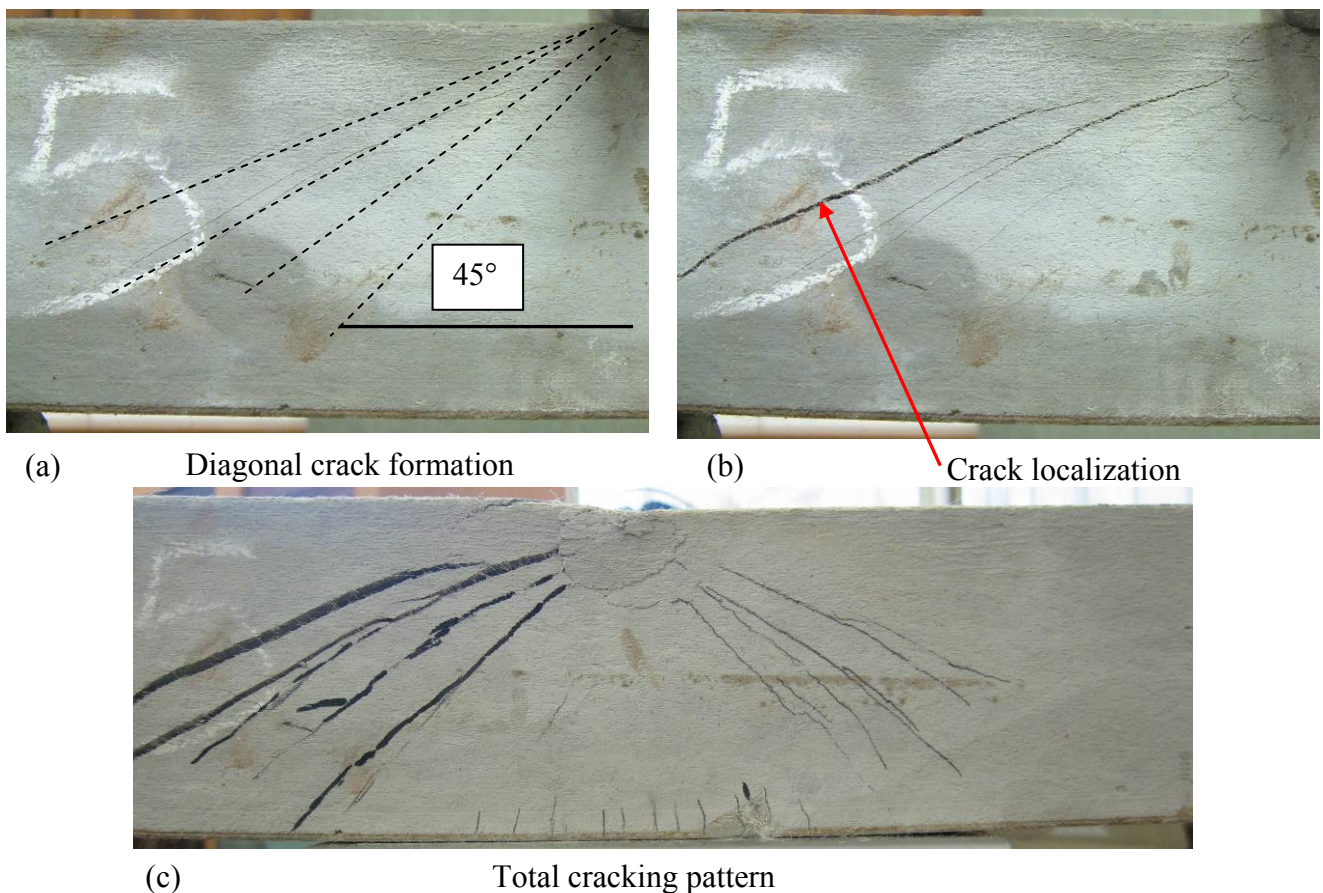
Figure 4.20: Crack formation and cracking pattern of a typical extruded R/SHCC beam.

It can be seen that the extruded R/SHCC results for the flexural characteristics are by far superior to all the other composites, except for its ductility. The ductility and ultimate strength of the cast R/SHCC and the extruded R/SHCC are higher than their ordinary SHCC counterparts as a result of the reinforcement. The first cracking strength of the cast SHCC and cast R/SHCC average at about the same value which is to be expected, since it is the same type of matrix. The first cracking strength of the extruded R/SHCC is slightly higher than that of the extruded SHCC, which is unusual. This can however be a result of the manner in which the first cracking strengths were determined in that the first cracks were too small to register on the graphs.

The cast R/C results will also be discussed for the sake of completeness. The SABS 0100-1 code [1994] prescribes a minimum amount of reinforcing steel (Yield Strength (f_y) = 450 MPa) for rectangular beams subjected to flexure as follows:

$$100A_s/A_c > 0.13 \tag{4.2}$$

where A_s is the cross sectional area of the reinforcing steel and A_c is the cross sectional area of the concrete. The R/C specimens that were tested complied with this standard ($100A_s/A_c$ = 1.0053 > 0.13).

Furthermore the method described in the SABS code 0100 [1994] for computing the ultimate strength as illustrated in Figure 4.21 was used to calculate the ultimate force that can be resisted by the R/C beams. In Figure 4.21, f_{cu} is the ultimate compressive strength of the concrete, which in this case was measured to be 23,3 MPa at 14 days (the age of testing). The factor of 0.67 accounts for the fact that the compression block is not actually square. Further, x is the height of the compression block and b is the width of the section. The depth from the top to the centre of the reinforcing steel is represented as d, A_s is the area of the steel and f_y is the yield strength of the steel. The yield strength of the steel that was used is given as 450 MPa, but this was measured to be 550 MPa and is the value that was used. Basic force equilibrium equations and equations for calculating moments were used to calculate an ultimate force of 32.23 kN that can be resisted by the beam when subjected to three-point bending. The SABS code prescribes material and safety factors to be used, but these were ignored since the calculations are for experimental and not design purposes. The calculated ultimate force is higher than the average ultimate force of 27.175 kN that was measured. This is due to the fact that the beams failed in shear and not in flexure.
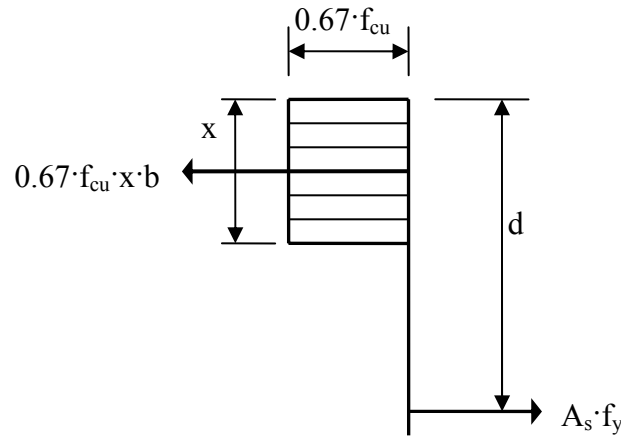
Figure 4.21: Diagram of force equilibrium of a reinforced concrete beam at the ultimate limit state [SABS 0100 1994].

The equation for calculating the shear capacity of a beam given in the SABS code is as follows:

$$v_c = \frac{0.75}{\gamma_m}\left(\frac{f_{cu}}{25}\right)^{\frac{1}{3}}\left(\frac{100 A_s}{b \cdot d}\right)^{\frac{1}{3}}\left(\frac{400}{d}\right)^{\frac{1}{4}}$$

(4.3)

where v_c is the shear capacity in MPa and the rest of the parameters are the same as above. The material factor γ_m was again ignored in this case. The shear capacity that was calculated for the R/C beams was 1.218 MPa. The average ultimate force that was measured can be used to calculate the average ultimate shear stress in the beams by taking the resulting shear force as acting across the entire section of a beam and thus dividing by the area of the beam. This results in an average ultimate shear stress of 1.378 MPa. This is not far off from the shear capacity that was calculated for the beams, thus the beams failed in shear.

The cast R/C specimens first formed a flexural crack in the centre, at the bottom of the specimen. Then it formed diagonal shear cracks which progressed until it reached the reinforcement, at which point the concrete delaminated along the reinforcement as the specimens failed. The crack formation and cracking pattern of a typical R/C specimen is shown in Figure 4.22.

Flexural crack Shear crack Delamination
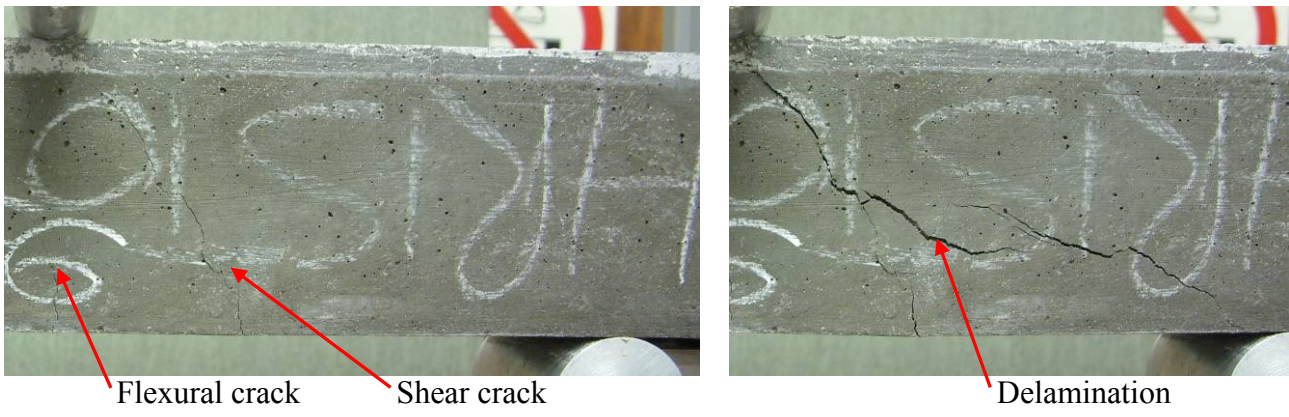
Figure 4.22: Crack formation and cracking pattern of a typical cast R/C beam.

5 MECHANICAL CHARACTERISTICS OF EXTRUDED SHCC

This part of the research is aimed at determining and documenting the uni-axial mechanical characteristics of extruded SHCC and to compare it with known uni-axial mechanical characteristics of cast SHCC. To this end, uni-axial tensile and compression tests were conducted on extruded SHCC. This chapter describes the test methods that were used as well as the results that were obtained. The results will also be used in the following chapter where a basic bending model will be proposed for SHCC.

5.1 TENSILE MECHANICAL TESTS

An uni-axial tensile test is the only type of test that can be used to obtain the tensile material parameters of SHCC directly. Inverse calculation methods that deduce the tensile parameters from flexural test results, e.g. Østergaard et al. [2005], have had limited success. The uni-axial tensile test is however still a point of controversy as many research based opinions exist as to how such a set-up should look, e.g. fixed or rotational boundary conditions. The standard set-up that has been used at the University of Stellenbosch uses a dumbbell-type specimen. This specimen is easy to produce by casting SHCC, but it becomes more difficult to use for the uni-axial testing of extruded SHCC.

The uni-axial tensile testing of extruded SHCC along with its results and the results of uni-axial tensile tests that were previously performed on cast SHCC [Boshoff 2006] will be provided and discussed in this section.

5.1.1 TEST SET-UP

The uni-axial tensile tests were designed to produce objective material properties, but that at the same time are simple and practical to perform. Flat dog bone shaped specimens are tested in direct tension. When cast SHCC is tested, the specimens are cast horizontally in steel moulds with removable studs in the middle of the enlarged end parts, as shown schematically in Figure 5.1. The

specimens are cast with these studs in place. They create holes of 16 mm diameter through which bolts are placed that assist with the gripping of the specimen in the test set-up. The dimensions of the specimens are shown in Figure 5.1 and the steel mould in Figure 5.2.
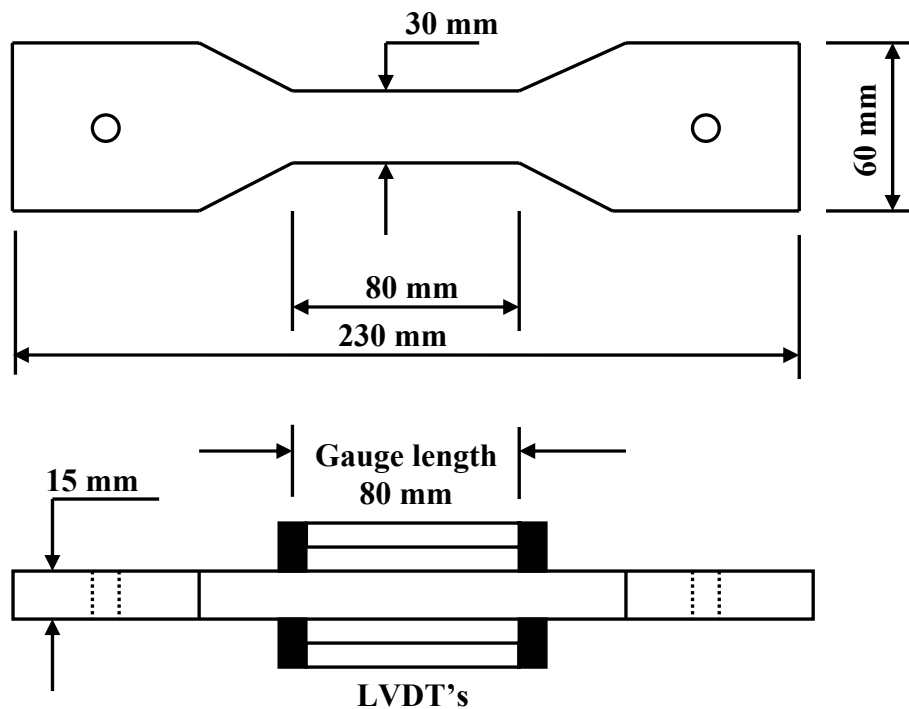
Figure 5.1: The dimensions of the flat dog bone specimen.

Figure 5.2: The steel mould used for casting of flat dog bone specimens with the two removable studs.

To obtain dog bone shaped specimens from extruded SHCC is however not as simple as it is for casting. The specimens have to be cut from the extruded specimens in the desired shape. A circular saw with a diamond cutting blade is used to cut out plate specimens with the correct width and length. An angle grinder is then used to cut out the sides that create the narrower neck section in the centre of the specimen. Cutting out these sections is a delicate and difficult process and care has to

be taken not to cut too deep into the specimens which will create flaws and lead to premature failure in testing.

In this research program two types of specimens were tested. Firstly, plate specimens were produced with the plate piston-driven extruder. Dog bone specimens were then marked out onto these specimens and cut from them two days before testing the specimens. Secondly, beam specimens (100 mm X 100 mm cross-section) were produced with the new piston-driven extruder. Plates of the correct thickness (15 mm) were cut form the bottom and some from the middle of the beams two days before testing. The dog bone specimens were then marked out onto these plates and cut from them. Since these extruded beams will mostly be used as structural elements subjected to uni-axial bending, the tensile specimens were sampled from the bottom of these specimens where the tensile strength is most crucial. However it was decided to sample some specimens from the middle as well to verify whether the tensile characteristics vary over the cross section of the beam.
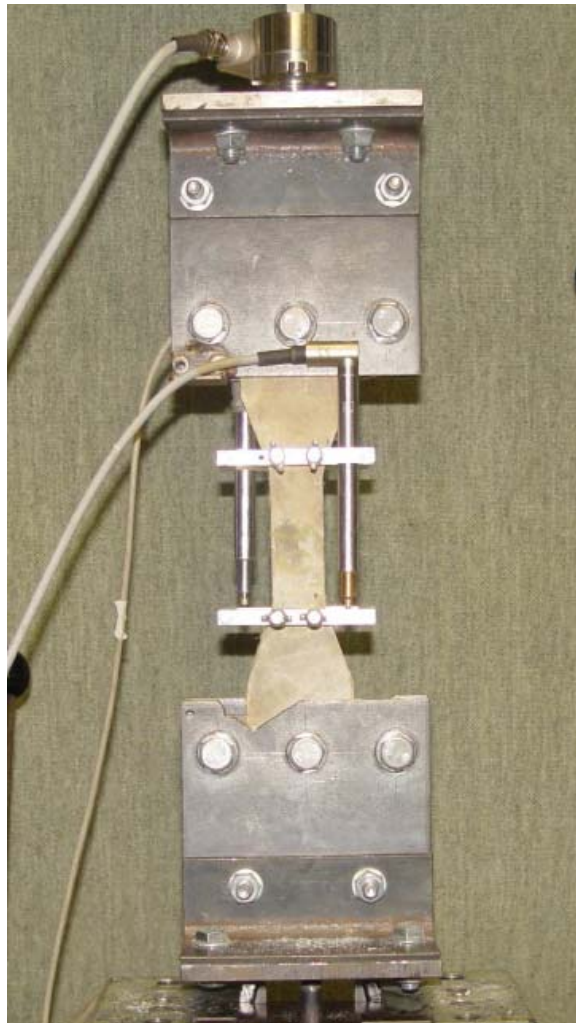
Figure 5.3: The tensile test set-up in the Zwick Z250 and the aluminium frame with the two LVDT's that were used to measure the deformation over the gauge length.

The tensile tests were performed in a Zwick Z250 Universal Materials Testing Machine which has a capacity of 250 kN. Two clamps are fixed to the grips of the machine as shown in Figure5.3. This method does not produce fully rigid boundary conditions, but has some rotational stiffness at the bottom and the top. An HBM 5 kN load cell is connected in line and is used to take the force readings during the tests. The strain is measured by means of two LVDT's fixed on a removable aluminium frame, shown in Figure 5.3, which is attached over the gauge length during the test. The machine is controlled by the speed of the crossheads.

5.1.2 EXPERIMENTAL TEST PROGRAM

The same mix design as the one that was used in Chapter 4 to produce the extruded SHCC was used again in this instance to produce extruded plates and beams from which dog bone specimens were cut. The mix proportions for this mix design are given in Table 5.1.

Table 5.1: Extrusion SHCC mix design [Visser 2005]

W/B	A/B	CEM I/B	FA/B	SP	VA	V_f
[by mass]	[by mass]	[by mass]	[by mass]	[% by B mass]	[% by B mass]	[% by volume]
0.25	0.5	0.5	0.5	1	0.3	2

Exactly the same mixing and extrusion procedures were used as in the case of the flexural tests performed on beams in Chapter 4. The specimens were placed in a temperature controlled humidity room at 100% humidity and 23°C after extrusion for a period of 72 hours. They were then removed from the humidity room and submerged in clean potable water at 23°C until two days before the day of testing. At this time the dog bone shaped specimens were cut from the plate and beam specimens and holes with a diameter of 16 mm were drilled in the middle of the enlarged end parts. These holes serve the same purpose as the ones in the cast specimens which assist with the gripping of the specimens in the test set-up. The dog bone specimens were then placed back in the water until the day of testing. All the specimens were tested at an age of 14 days when they were removed from the water and towel dried before testing.

All the specimens were tested at a displacement rate of 0.5 mm/min. The readings from the load cell and the LVDT's were collected by a Spider8 data logger and converted to a data file on a computer. The data was then used to draw tensile stress-strain graphs for which the average reading of the two LVDT's was taken as the elongation of the specimen over the gauge length. The number of specimens that were tested is given in Table 5.2.

Table 5.2: Test program for the uni-axial tensile tests

Specimen type	Plate	Beam [bottom]	Beam [middle]
Number of specimens	5	6	2

5.1.3 RESULTS

The results of the uni-axial tensile tests for the extruded SHCC are shown in Figure 5.4 to Figure 5.6. The strain is expressed as a percentage and is measured over a gauge length of 80 mm. The stress is calculated as the force reading divided by the actual dimensions of the section in the gauge area.

Uni-axial tensile tests have been preformed on cast SHCC with exactly the same mix design as the cast SHCC mix that was used in Chapter 4 in a previous research study [Boshoff 2006]. This has become a standard cast SHCC mix design that is used at the University of Stellenbosch [Stander 2007, Shang 2006]. The results of these tensile tests will be used for comparison purposes and are also included in this section [Figure 5.7].
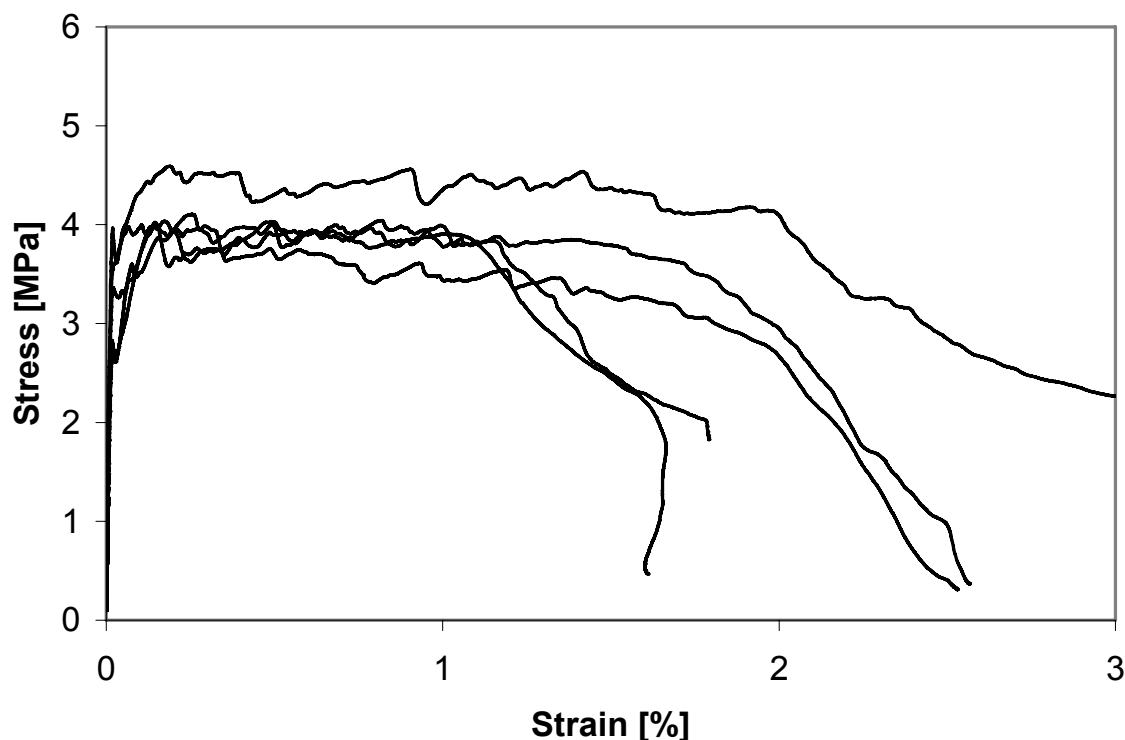
Figure 5.4: Direct tensile response of SHCC specimens cut from extruded plate specimens.
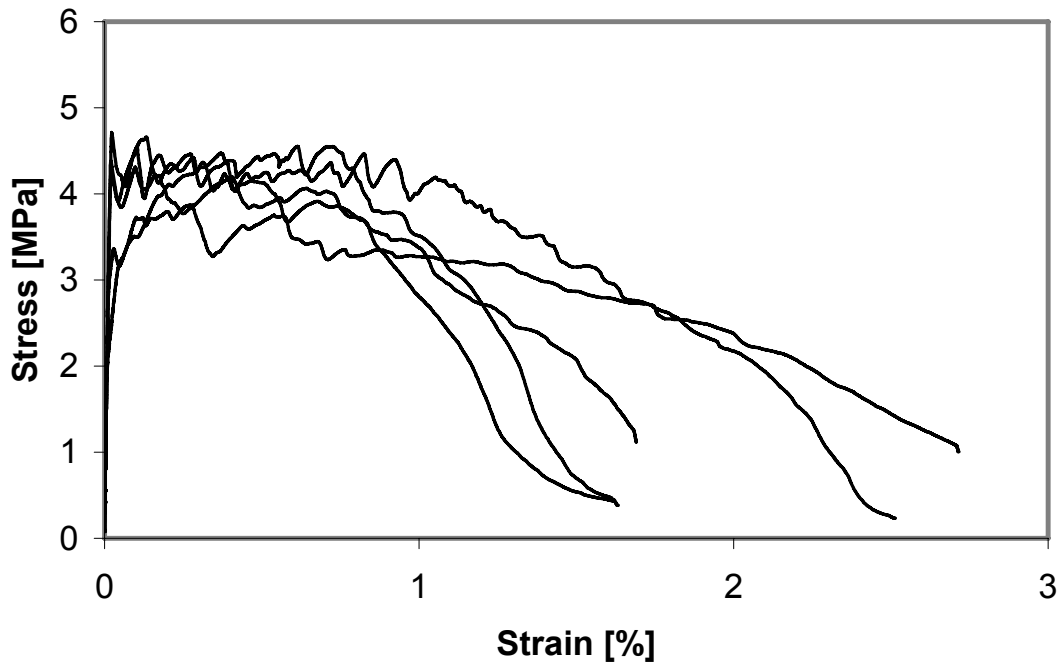
Figure 5.5: Direct tensile response of SHCC specimens cut from the bottom of extruded beam specimens.
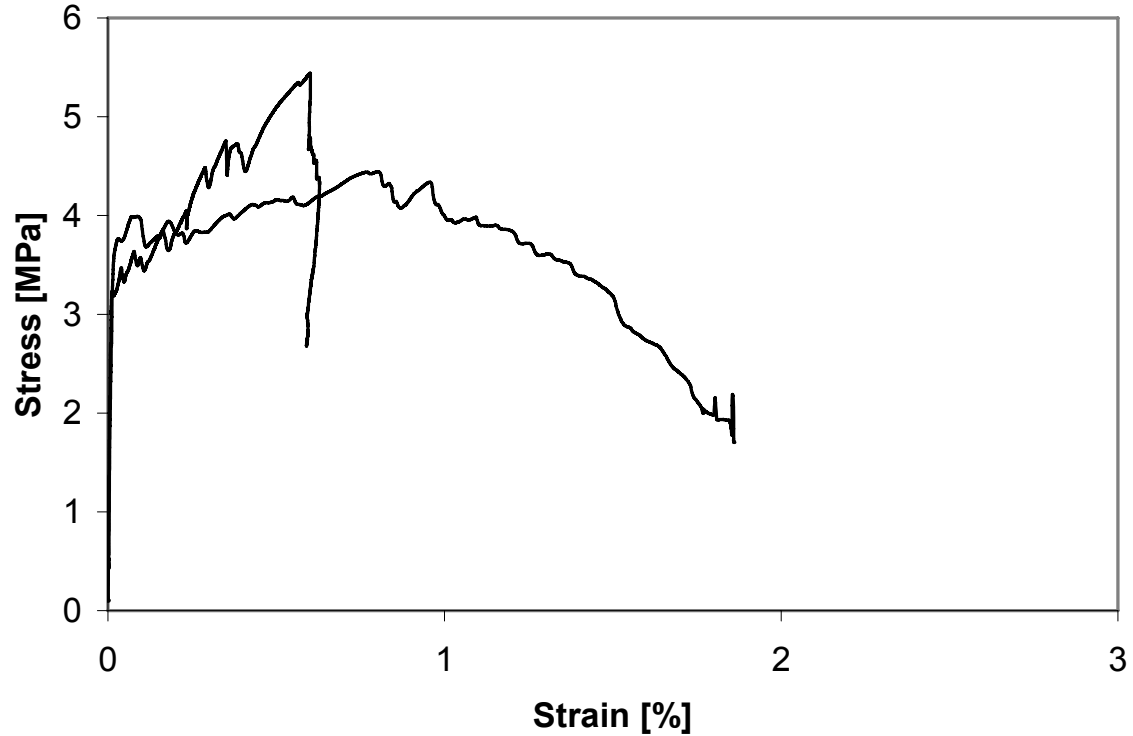
Figure 5.6: Direct tensile response of SHCC specimens cut from the middle of extruded beam specimens.
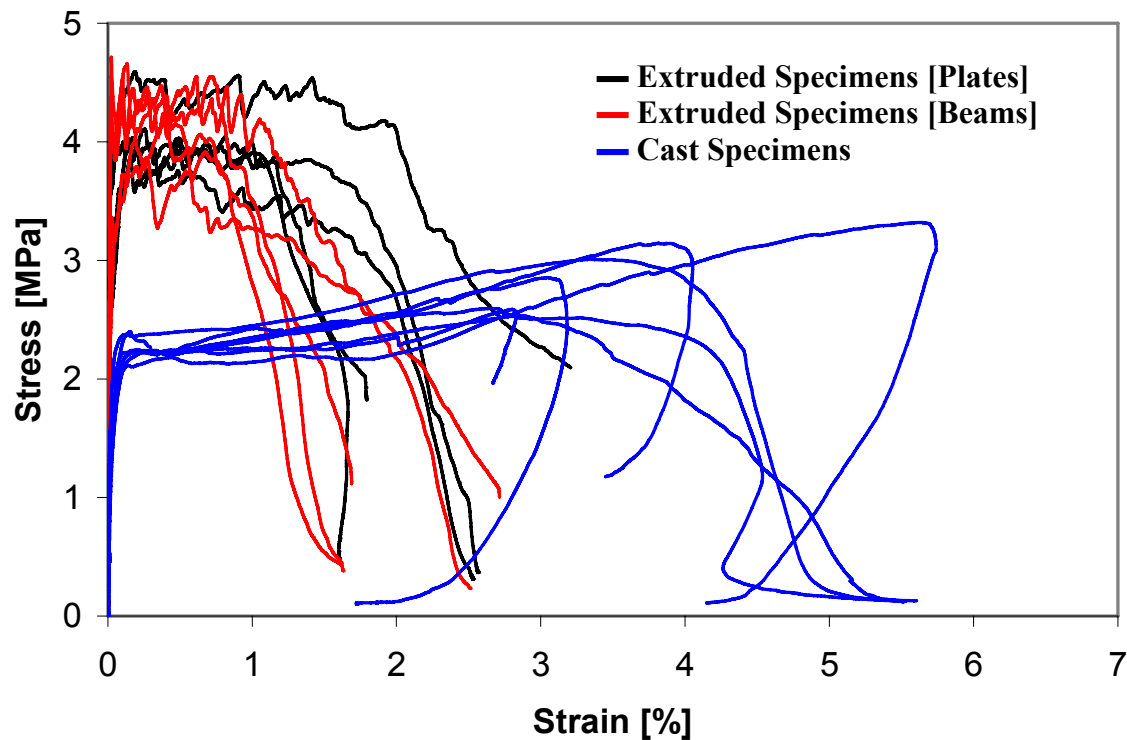
Figure 5.7: Direct tensile response of cast SHCC specimens in comparison with the direct tensile responses of the various extruded SHCC specimens.

There are three main tensile characteristics that are of importance, namely the first cracking strength, the ultimate strength and the ductility. The first cracking strength was determined as the point on the tensile stress-strain curve where the first significant deviation in stiffness, or drop in strength occurs on the elastic part of the graph. This strength can be seen as the strength of the matrix. The ultimate strength is the highest stress that was resisted by the specimen. The ductility is taken as the strain that coincides with a stress equal to the first cracking strength, after the ultimate strength was achieved. The E-modulus is another parameter that can be determined from the tensile curves, but it will be discussed in a separate section of this chapter. The tensile characteristics of the various types of specimens are shown in Table 5.3 to Table 5.5, along with the average values, standard deviations (StdDev) and coefficients of variation (C.O.V.) of each parameter. It should be noted that the actual cross sectional dimensions of the specimens that were cut from the extruded SHCC specimens were recorded and used to calculate the stresses for these specimens.

Only two specimens were produced from plates that were cut out from the middle of extruded beams [Figure 5.6]. The one specimen displayed a very high ultimate strength but this coincided with a low ductility. The other specimen on the other hand displayed very similar response to those of the specimens that were cut from the bottom of the beams. No valid conclusions can be made about the tensile behaviour in the middle of an extruded beam due to a lack of sufficient data. Thus

the results of the tensile characteristics of these two specimens will not be included in the data set for further comparison or discussion in this thesis. Due to time constraints, a further investigation of the tensile behaviour in the middle of an extruded beam was also not possible. Such an investigation is recommended for further research. It can however be said that the ultimate strength is not less than that of the lower part of the beam. A lower strength could be expected, due to the potential of less oriented fibres away from the beam faces. This may be an indication that the fibres are also orientated in the extrusion direction in the middle of the beam. This would imply that the extrusion forces and the boundaries of the extruder still influence the orientation of the fibres, even to a depth of 50 mm.

Table 5.3: Tensile characteristics of SHCC specimens cut from extruded plate specimens

Specimen	σ_{tf}	σ_{tu}	Ductility
[#]	[MPa]	[MPa]	[%]
1	2.80	4.04	1.42
2	2.68	4.11	2.07
3	3.54	4.59	2.20
4	3.65	4.01	1.15
5	3.29	4.04	1.48
Average	3.19	4.16	1.66
StdDev	0.44	0.25	0.45
C.O.V.	13.63%	5.91%	27.05%

Table 5.4: Tensile characteristics of SHCC specimens cut from the bottom of extruded beam specimens

Specimen	σ_{tf}	σ_{tu}	Ductility
[#]	[MPa]	[MPa]	[%]
1	2.78	4.55	1.19
2	3.34	4.38	0.90
3	2.62	4.17	1.26
4	3.20	4.71	1.46
5	3.03	4.55	0.95
Average	2.99	4.47	1.15
StdDev	0.30	0.21	0.23
C.O.V.	9.86%	4.64%	20.08%

Table 5.5: Tensile characteristics of cast SHCC specimens

Specimen	σ_{tf}	σ_{tu}	Ductility
[#]	[MPa]	[MPa]	[%]
1	2.15	2.59	2.80
2	1.96	3.32	5.64
3	2.37	3.01	3.56
4	2.01	2.86	3.05
5	1.91	3.14	3.82
6	2.02	2.60	2.87
7	1.85	2.53	3.69
Average	2.04	2.86	3.63
StdDev	0.17	0.31	0.97
C.O.V.	8.54%	10.78%	26.80%

It can be concluded from Figure 5.7 and the results from Table 5.3 to Table 5.5 that extruded specimens, whether cut from extruded plates or cut from the bottom of extruded beams, display similar tensile responses. These tensile responses are however in contrast to the tensile responses of the cast SHCC specimens. The first cracking strength and ultimate strength of the extruded specimens are significantly higher than that of the cast specimens, while the cast specimens have significantly higher ductility than the extruded specimens. These results will be discussed in more depth in the next section.

5.1.4 DISCUSSION

The tensile parameters of the cast and extruded SHCC are summarized in Figure 5.8 which shows the average values as well as the maximum and minimum values.
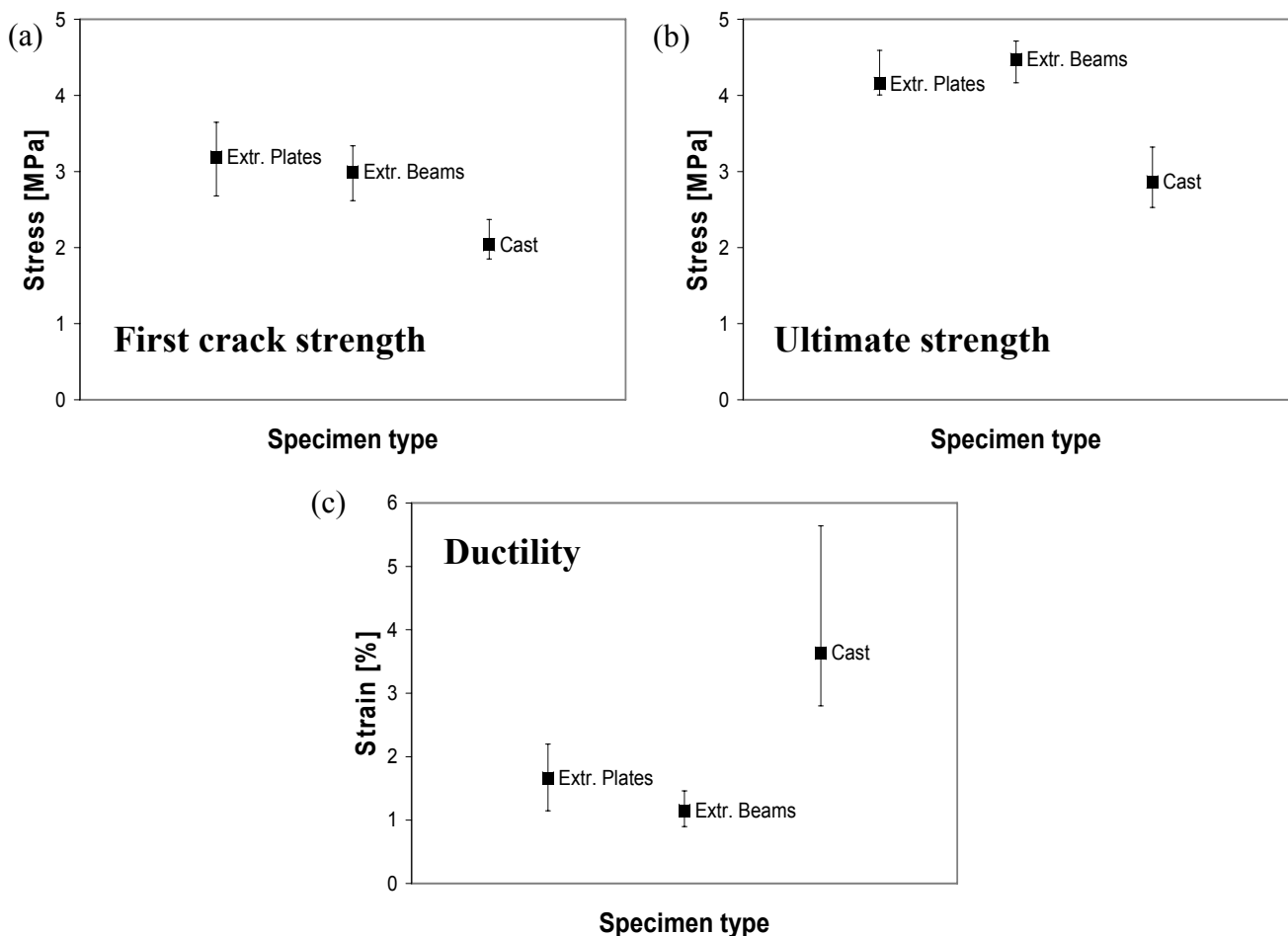
Figure 5.8: Comparison of (a) first cracking strength, (b) ultimate strength and (c) ductility.

It can be seen from Figure 5.8 that the first cracking strength and ultimate strength of the extruded SHCC specimens is much higher than that of the cast specimens. As it was mentioned in Chapter 4

the major difference between the mix designs of the extrusion SHCC and cast SHCC is the lower W/B ratio of the extrusion mix (W/B^{extrude} = 0.25 and W/B^{cast} = 0.4). In addition to the known influence on the matrix strength of cement-based composites, the lower W/B also results in a difference in aggregate content of the two types of SHCC's, where the extrusion mix has a higher aggregate content (V$_a^{extrude}$ = 0.23) than the cast mix (V$_a^{cast}$ = 0.194). An increased aggregate content, or an increased A/B ratio for the same mix design, causes an increase in matrix strength, as represented in this research by the first cracking strength. It is believed that the increased tortuosity of cracks, caused by higher aggregate content, leads to higher matrix tensile strength. This was confirmed in an experimental program [van Zijl 2005] for the same cast SHCC as the one used in this research study, but for various Aggregate/Binder ratios (A/B), Figure 5.9. Typical stress-strain results are shown in Figure 5.9 for cast SHCC with varying A/B ratios. Figure 5.10 shows the trend of increased first cracking strength with increased A/B ratio. The higher ultimate strength of extruded specimens in comparison to that of cast specimens [Figure 5.8] is caused by an increased bond that is a result of the extrusion process. This higher ultimate strength is not a result of the increased A/B ratio as is evident from Figure 5.9, where no significant change in ultimate strength can be detected for varying A/B ratios.
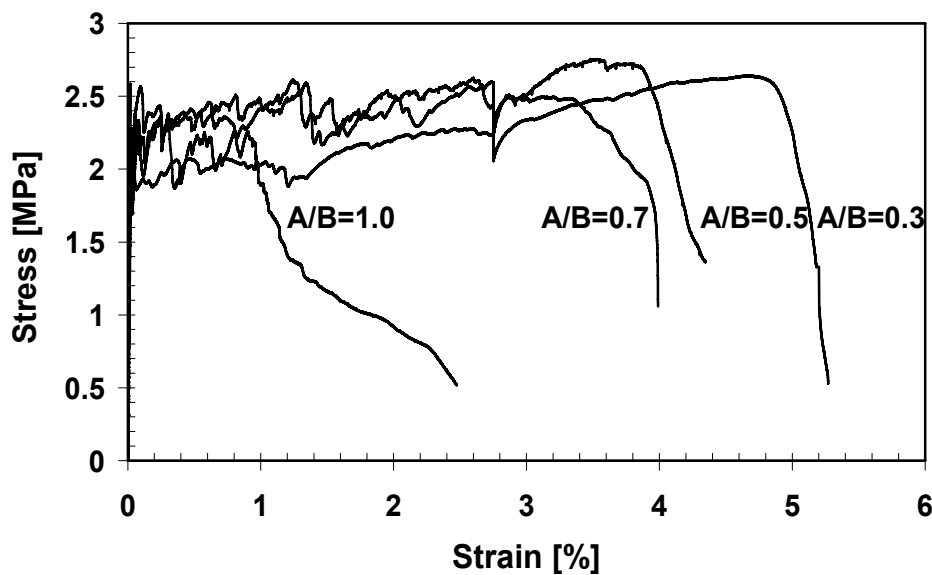
Figure 5.9: Cast SHCC tensile response versus A/B ratio [van Zijl 2005].

However it is believed that the matrix strength and composite strength increase by extrusion is beyond that expected from the above mentioned mechanisms. Another possible reason for the increase in tensile strength is the higher density and thus reduced porosity of the extruded SHCC. It is commonly agreed that reduced porosity leads to increased strength. It is thus argued that the significant reduction in porosity caused by high pressure extrusion leads to the observed strong increase in first cracking strength and ultimate strength.
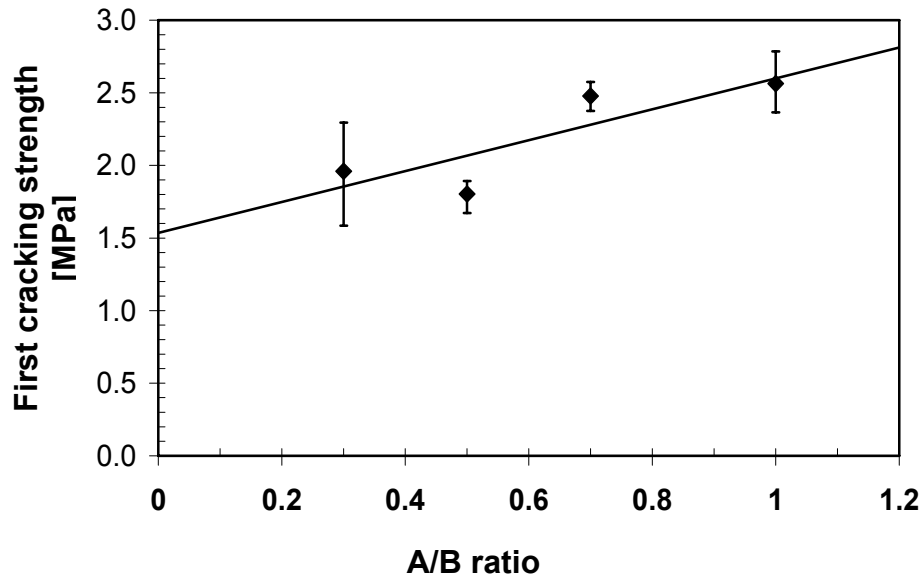
Figure 5.10: Cast SHCC matrix strength versus aggregate content [van Zijl 2005].

From Figure 5.7 and Figure 5.8 it is apparent that increased matrix strength, be it through increased A/B ratio or by reduced porosity caused by extrusion, causes reduced tensile ductility. This is in agreement with micro-mechanical considerations, whereby increased crack tip toughness relative to fibre pullout complimentary energy requires a larger critical fibre volume, i.e. a larger fibre content is required to ensure tensile strain hardening.

5.2 COMPRESSIVE MECHANICAL TESTS

In the case of ordinary concrete the main compressive characteristic that is usually determined is the ultimate compressive strength. Sometimes also the elastic modulus (E-modulus) is determined. The compressive characteristics of cast and extruded SHCC will be investigated briefly in this section. In this case the focus will also be on the ultimate compressive strength, while the E-modulus will be discussed in a separate section of this chapter. Due to the energy absorbing capacity of SHCC the shape of the compressive stress-strain curve after the ultimate compressive strength has been reached will also be of interest.

The means for determining the compressive characteristics is the uni-axial compressive test. The uni-axial compressive testing of cast and extruded SHCC composites will be described in this section. The results of these tests will also be provided and discussed.

5.2.1 TEST SET-UP

The uni-axial compressive test was designed, based on the same principles of the uni-axial tensile tests in terms of the type of test set-up. Round cores were tested in direct compression. When testing the compressive strengths of ordinary concrete, cubes with dimensions 100 mm X 100 mm are usually tested. It was decided to conduct the uni-axial compressive tests in a Zwick Z250 Universal Materials Testing Machine, which allows for better and more accurate control over the tests. To stay within the capacity of the Zwick, it was however required that core specimens of relative small diameter be tested instead of cubes. When cast SHCC was tested, the specimens were cast vertically in a copper mould. The dimensions of the core specimens are shown in Figure 5.11 and the steel mould in Figure 5.12.
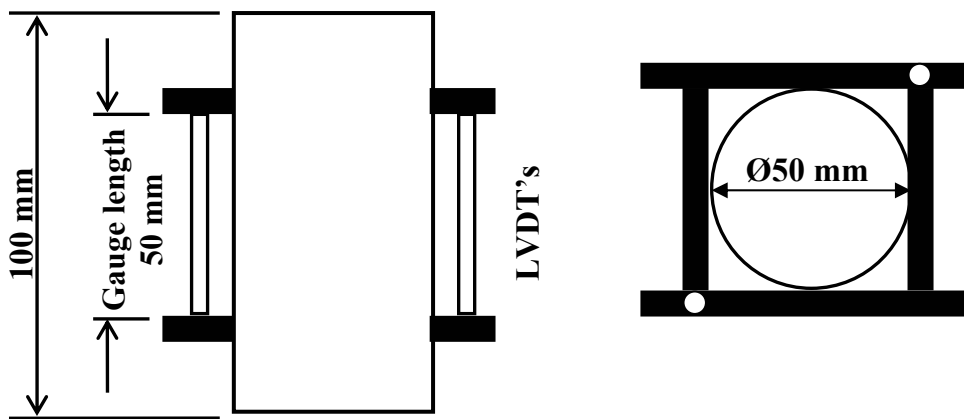
Figure 5.11: Dimensions of the core specimens.

Figure 5.12: Copper mould used for casting SHCC cores.

For the uni-axial compressive testing of extruded SHCC, core specimens had to be drilled from extruded beams produced with the new piston-driven extruder. The cores were drilled with the use of concrete core drill with the appropriate drill size, three days before testing. The cores were taken vertically, in the direction perpendicular to the extrusion action. For the purpose of characterising the compressive behaviour in flexure in the extruded specimens, cores should be drilled parallel to the extrusion direction. Due to the aligned fibres, it is possible that the compressive strength in the longitudinal direction will be different to the compressive strength in the orthogonal direction, but this remains to be tested. The cores were drilled perpendicular to the beams due to difficulty of coring parallel to the beam axis with existing equipment. All the core specimens that were tested for the compressive characterisation of the SHCC's had a height/diameter ratio of two.

Figure 5.13: The compressive test set-up in the Zwick Z250 and the aluminium frame with the two LVDT's that were used to measure the strain over the gauge length.

The compressive tests were performed in a Zwick Z250 Universal Materials Testing Machine with a capacity of 250 kN. A flat base plate is fixed to the bottom grip, while a swivel head with a flat surface is fixed to the top grip as shown in Figure 5.13. The swivel head ensures that the force is applied perpendicular to the surface of the core. An HBM 200 kN load cell is connected in line and is used to take the force readings during the tests. The strain is measured by means of two LVDT's fixed on a removable aluminium frame, shown in Figure 5.13, which is attached over the gauge length during the test. The machine is controlled by the speed of the crossheads, i.e. the displacement control of the machine.

5.2.2 EXPERIMENTAL TEST PROGRAM

The same mix designs that were used in Chapter 4 and the previous section for the extruded and cast SHCC were used for this part of the research as well. Exactly the same mixing, casting and extrusion procedures were followed as in the case of the flexural tests of Chapter 4.

The extruded SHCC beam specimens and the cast SHCC core specimens were all placed in a temperature controlled humidity room at 100% humidity and 23°C for 72 hours. They were then stripped and submerged in clean potable water at 23°C. The extruded beam specimens and the cast core specimens were removed from the water two days before testing. Cores, also with diameter 50 mm and length 100 mm, were then drilled from the beams. All the cores were then capped with high alumina cement [SABS method 865 1994] to ensure flat end surfaces which are perpendicular to the central axis of the core. The cores were then submerged in water again until the day of testing. The specimens were tested at an age of 14 days when they were removed from the water and towel dried before testing.

All the specimens were tested at a displacement rate of 0.5 mm/min. The readings from the load cell and the LVDT's were collected by a Spider8 data logger and converted to a data file on a computer. The data was then used to draw compressive stress-strain graphs for which the average reading of the two LVDT's was taken as the elongation of the specimen over the gauge length.

Based on SABS method 865 [1994] core specimen with a height/diameter ratio of one and a diameter of 70 mm were also drilled from the extruded beams. This was done to enable the comparison of the ultimate compressive strength of cast SHCC based on cube strength (Chapter 4) with the ultimate compressive strength of extruded SHCC. This will be discussed further in later part of this section. These cores were also capped and then submerged in water again until the day of testing at the age of 14 days. The specimens were tested in a Contest Crushing Machine and the

ultimate compressive strengths were recorded. Three core specimens for each type of composite, extruded SHCC and cast SHCC were tested in the Zwick Z250 while four core specimens of the extruded SHCC were tested in the Contest Crushing Machine.

5.2.3 RESULTS

The results of the uni-axial compressive tests for the cast and extruded SHCC are shown in Figure 5.14 and Figure 5.15. The strain is expressed as a percentage and is measured over a gauge length of 50 mm. The stress is calculated as the force reading divided by the actual dimensions of the section in the gauge area.
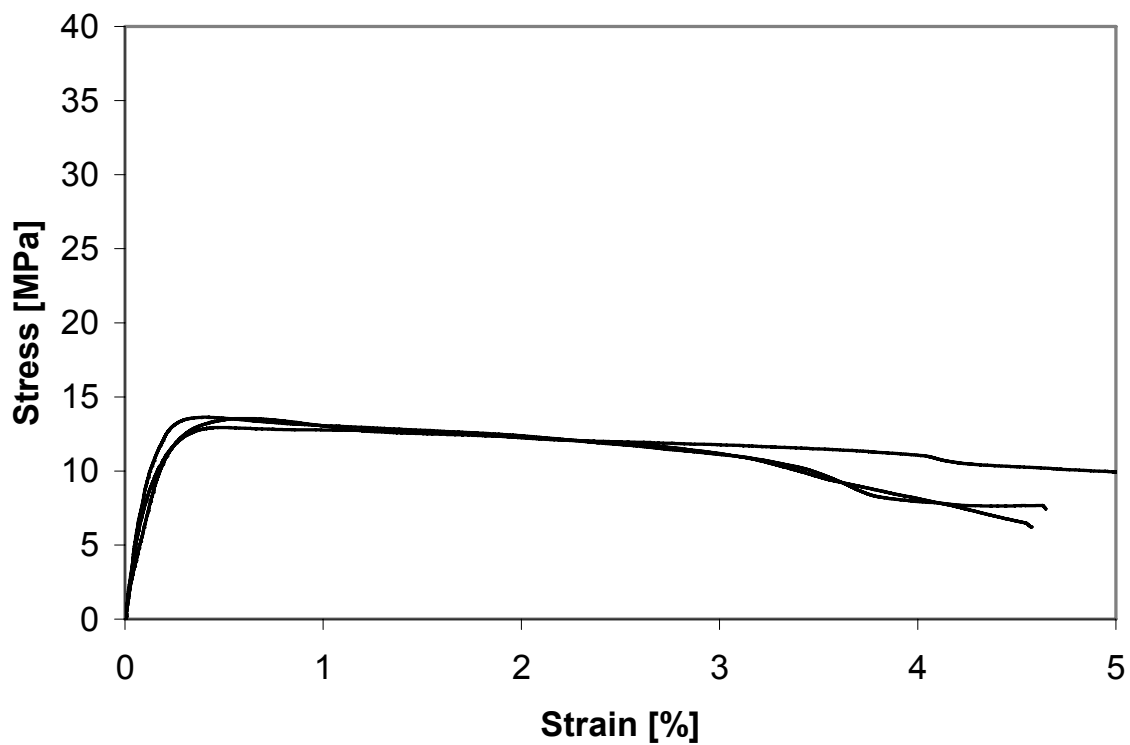
Figure 5.14: Direct compressive response of cast SHCC cores (height: 100 mm; diameter: 50 mm).
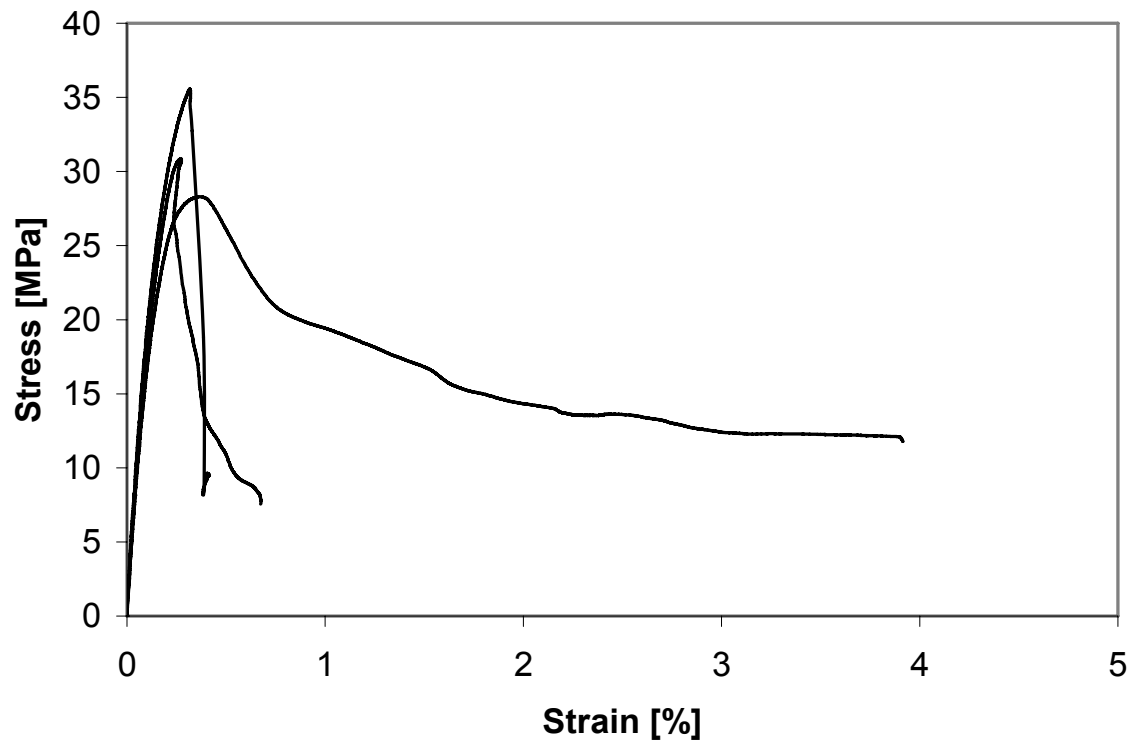
Figure 5.15: Direct compressive response of extruded SHCC cores (height: 100 mm; diameter: 50 mm).

The cast SHCC shows good comparability of the results [Figure5.14], while there is some variability in the results of the extruded SHCC [Figure 5.15]. This variability can be due to the sampling method of drilling cores. Since only three specimens could be tested for each composite, the two specimens displaying the best correlation in Figure 5.15 was seen as representative of the compressive behaviour.

As it was previously mentioned, the main compressive characteristics that are of importance are the ultimate strength and E-modulus. The E-modulus will be dealt with in a separate section of this chapter. As it was also previously mentioned, the shapes of the compressive stress-strain curves are also of interest and will be discussed in the next part of this section.

The ultimate compressive strengths of the various specimens that were tested are shown in Table 5.6 along with the average values, the standard deviations and the coefficients of variation. The compressive strengths for the cast SHCC determined from 100 mm X 100 mm cubes (Chapter 4) are also provided.

Table 5.6: Ultimate 14day compressive strengths of cast and extruded SHCC

Specimen [#]	Cast Specimens		Extruded Specimens	
	Core (h:100 mm; Ø:50 mm) [MPa]	Cube (100 mm X 100 mm) [MPa]	Core (h:100 mm; Ø:50 mm) [MPa]	Core (h:70 mm; Ø:70 mm) [MPa]
1	12.94	22.3	28.30	40.7
2	13.63	22.6	30.85	41.7
3	13.54	23.0	35.57	42.9
4		23.4		44.2
Average	13.37	22.8	31.57	42.4
StdDev	0.38	0.5	3.69	1.5
C.O.V.	2.83%	2.10%	11.68%	3.55%

5.2.4 DISCUSSION

There is a strong of variability in the ultimate compressive strengths that were measured for various test sample geometries. This is due to the different types of specimens that were tested to determine these values. These values need to be adjusted to the same standard to enable a comparison of the values. SABS method 865 [1994] prescribes core specimens to have a height/diameter ratio of 0.9 to 1.1. It does however provide an equation (eq. (5.1)) that can be used to standardize the compressive strength of non-standard cores that fall outside this height/diameter ratio.

$$\sigma_{ca} = \sigma_{cu} \times \frac{2.5}{1.5 + (d/h)} \qquad (5.1)$$

In this equation σ_{ca} is the adjusted or standardized compressive strength, σ_{cu} is the ultimate compressive strength that was measured, d is the diameter of the core and h is the height of the core.

When the average compressive strength of the cast SHCC cores with diameter 50 mm and height 100 mm is adjusted using eq.5.1, the standardized compressive strength (σ_{ca}) for cast SHCC is calculated as 16.71 MPa. According to the SABS 0100-2 code [1994], standardized strengths determined with the use of cores [SABS method 865 1994] should not be below 70% of the intended compressive cube strength. If the standardized compressive strength is then taken as 70% of the compressive cube strength, a compressive cube strength value of 23.88 MPa is calculated. This compares well with the actual average compressive cube strength of 22.8 MPa that was measured for cast SHCC. This should however not be seen as a rule for obtaining the compressive cube strength of a composite from the compressive strength of cores, since it is based on statistics rather than actual material characteristics.

When the average compressive strength of the extruded SHCC cores with diameter 50 mm and height 100 mm (aspect ratio = 2) is adjusted with the use of eq. (5.1), the standard compressive core strength for extruded SHCC is calculated as 39.46 MPa. This also compares well to the average standard compressive core strength of 42.37 MPa that was actually measured for the cores with diameter 70 mm and height 70 mm (aspect ratio = 1). These values can be compared with the standardized compressive strength of the cast SHCC specimens (16.71 MPa). It can be seen that extruded SHCC has a much higher compressive strength than cast SHCC. It should be noted that the SABS method allows for comparison, but does not reflect the real strength, due to the low (1.0) aspect ratio. The strength determined with aspect ratio of 2 is more accurate, as the boundary effects are reduced. Table 5.7 shows the compressive strength values for the cast SHCC cores with an aspect ratio of 2 (measured) and an aspect ratio of 1 (calculated with eq. 5.1) in comparison to that of the extruded SHCC cores with an aspect ratio of 2 (measured) and an aspect ratio of 1 (measured).

Table 5.7: Ultimate 14day compressive strengths of cast and extruded SHCC with various aspect ratios

Specimen	Cast Specimens		Extruded Specimens	
	Aspect ratio = 2	Aspect ratio = 1	Aspect ratio = 2	Aspect ratio = 1
	(measured)	(calculated – eq. 5.1)	(measured)	(measured)
[#]	[MPa]	[MPa]	[MPa]	[MPa]
1	12.94	16.18	28.30	40.71
2	13.63	17.04	30.85	41.68
3	13.54	16.93	35.57	42.89
4				44.18
Average	13.37	16.71	31.57	42.37
StdDev	0.38	0.47	3.69	1.50
C.O.V.	2.83%	2.83%	11.68%	3.55%

It is again stated here, like in the previous section, that the major difference between the cast SHCC mix and the extrusion SHCC mix is the lower W/B ratio (W/B^{extrude} = 0.25) of the extrusion mix in comparison to the W/B ratio of the cast mix (W/B^{cast} = 0.4). As it was also previously stated, this lower W/B ratio results in an increased aggregate volume. It also results in a lower porosity, which coupled with the increased aggregate content will lead to an increased compressive strength. The increase in compressive strength is however beyond that which would be expected as a result of these mechanisms. It has however been shown [Powers 1958] that the relationship between the compressive strength and the porosity of a paste is as follows:

$$\sigma = k \cdot (1 - p^3) \hspace{5cm} (5.2)$$

where σ is the compressive strength, k is a constant and p is the porosity of the paste. When considering this equation, it can be argued that the increased compressive strength of the extruded SHCC in comparison to the cast SHCC is due to the significantly reduced porosity which is a result of the high extrusion pressure.

Here it is again evident that the higher ultimate strength is coupled with a lower ductility. The same argument that was followed in the previous section for this phenomenon can be followed here again. Both types of composites showed a type of strain softening behaviour after the ultimate compressive strength was reached, but still had significant energy absorbing capacity. The cast SHCC displayed a high ductility, while the extruded SHCC had a brittle failure similar to ordinary concrete. It is postulated that due to the random orientation of fibres within cast SHCC, these fibres can contribute to the post-peak ductility of the composite since these fibres can arrest splitting cracks. In the case of the extruded SHCC the fibres are orientated longitudinally and the slip-plane forms parallel to them, and thus the fibres can not contribute significantly to the post-peak ductility. Further investigation into the compressive behaviour, especially the post-peak behaviour, of cast and extruded SHCC remains to be performed in future research.

5.3 ELASTIC MODULUS OF SHCC

As it was mentioned in Chapter 2, the E-modulus of cast SHCC is relatively low, between 7.5 and 10 GPa. This section describes a test program that was followed to determine the E-modulus of cast and extruded SHCC from tensile as well as compressive tests. The results of this test program are also provided and discussed.

5.3.1 TEST PROGRAM AND RESULTS

E-modulus values for extruded as well as cast SHCC were determined from the uni-axial compressive and tensile tests that are described in the previous two sections. Additional core specimens were however also tested for the purpose of determining the E-modulus of extruded and cast SHCC in compression. Two cast specimens and two extruded specimens were tested additionally. These specimens were only tested until the ultimate compressive strength was reached. All specimens had an aspect ratio of height to diameter of 2.

A secant method was applied to compute the E-moduli from the direct tensile responses at stress levels one third of the first cracking stress and a low pre-stress (σ_0 = 0.1 MPa) and the corresponding strains as follows:

$$E_c = \frac{\frac{1}{3}\sigma_{t,c} - \sigma_0}{\varepsilon_{(\frac{1}{3}\sigma_{t,c})} - \varepsilon_0}$$
(5.3)

The same method was applied to compute the E-moduli from the direct compressive responses, but at stress levels one third of the ultimate compressive strength and a low pre-stress ($\sigma_0 = 0.1$ MPa) and the corresponding strains. The results for the E-moduli computed from the tensile and compressive responses are given in Table 5.7 and Table 5.8 respectively along with the average values, the standard deviations and the coefficients of variation. All E-modulus values were determined at an age of 14 days.

.

Table 5.8: E-modulus values for cast and extruded SHCC computed from uni-axial tensile tests.

| Specimen | Cast specimens | Extruded Specimens | |
| | Cast | Cut from plate | Cut from beam |
[#]	[GPa]	[GPa]	[GPa]
1	9.53	24.20	23.10
2	9.71	24.37	24.95
3	9.94	24.63	25.62
4	10.02	26.37	25.94
5	10.32	26.86	25.97
6	11.39		
7	12.08		
Average	10.43	25.29	25.12
StdDev	0.95	1.23	1.20
C.O.V.	9.09%	4.88%	4.77%

Table 5.9: E-modulus values for cast and extruded SHCC computed from uni-axial compressive tests.

| Specimen | Cast Specimens | Extruded Specimens |
[#]	[GPa]	[GPa]
1	9.24	20.71
2	9.55	21.32
3	10.71	22.47
4	10.84	22.59
5	11.84	23.82
Average	10.44	22.18
StdDev	1.05	1.21
C.O.V.	10.08%	5.45%

5.3.2 DISCUSSION

The average values of all the computed E-moduli are summarized in Figure 5.16 along with maximum and minimum values. It can be seen from Figure 5.16 that the E-moduli that were

computed from the tensile and compressive responses compare fairly well for the cast and extruded SHCC's respectively. The E-modulus of the extruded SHCC is however significantly higher than that of the cast SHCC.
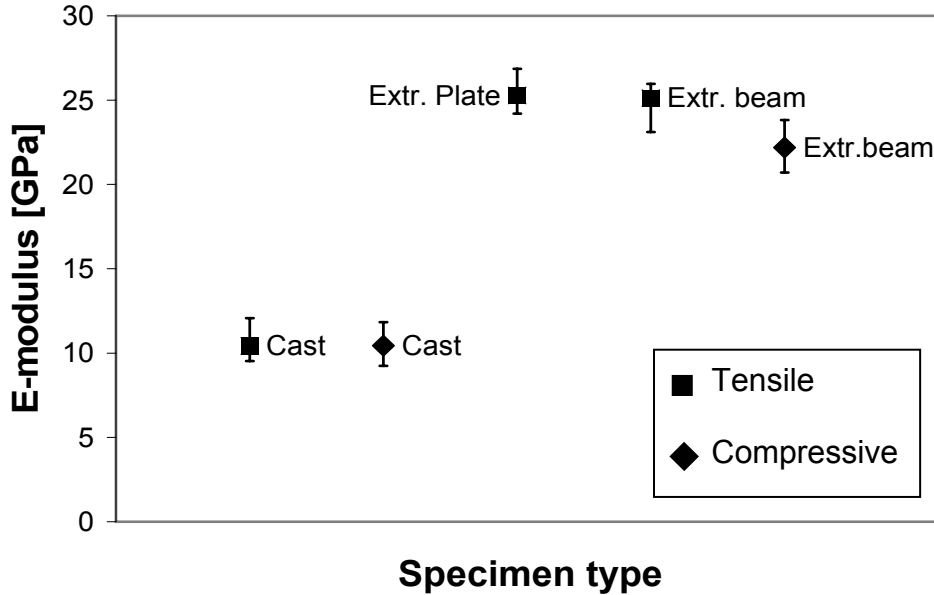
Figure 5.16: E-modulus of cast and extruded SHCC computed from tensile and compressive responses.

When considering the volume portions of the main phases in SHCC to be that of the matrix (V_m) and the fibres (V_f) with respective elastic moduli E_m and E_f, the composite E-modulus can be expressed as follows:

$$E_c = V_m E_m + \eta V_f E_f \tag{5.4}$$

based on homogenisation of the stress and strain fields in the two phases. A fibre efficiency coefficient (η) provides for the fact that the fibres are discontinuous and not all aligned in the main stress direction. To study the influence of the heterogeneities in the matrix, it is further subdivided into an aggregate volume (V_a) and a paste volume (V_p), with respective E-moduli E_a and E_p. Considering only the matrix, the E-modulus of the matrix (E_m) can be expressed as follows [Hashin 1962]:

$$E_m = \frac{(1+V_a)E_a + V_p E_p}{V_p E_a + (1+V_a)E_p} E_p \tag{5.5}$$

An alternative formulation is based on a representative matrix volume with a central concentration of solid aggregate surrounded by hardened cement paste:

$$\frac{1}{E_m} = \frac{(1-\sqrt{V_a})}{E_p} + \frac{\sqrt{V_a}}{E_a\sqrt{V_a} + E_p(1-\sqrt{V_a})} \tag{5.6}$$

Eq. (5.4) shows that a low volume of PVA fibres ($V_f = 2\%$) insignificantly contributes to composite E-modulus, even when considering an upper bound of $\eta = 1$. This was confirmed by results of uni-axial tensile tests of cast SHCC specimens of the same mix design as was used in this research study, but with fibre volumes of 2% and 2.5% [Shang 2007]. However, the inclusion of aggregate in proportions such as in this research study ($V_a^{cast} = 0.194$ and $V_a^{extrude} = 0.23$) significantly contributes to the matrix E-modulus (E_m), cf. eq. (5.5) or eq. (5.6), and thus to the E-modulus of the composite (E_c), cf. eq. (5.4). As it was mentioned in Chapter 2, this was confirmed by experimentally determined E_c [van Zijl 2005] of cast SHCC of the same type as was used in this research study, but with varying aggregate content, Figure 5.17. In Figure 5.17 the E-moduli computed from eq. (5.5) or eq. (5.6) and eq. (5.4) for various A/B ratios are also shown. Due to the uncertainty of E_a for aggregate used, two values ($E_a = 72$ GPa and $E_a = 100$ GPa) are used, along with $E_p = 5.3$ GPa, which produces $E_c = 6$ GPa as suggested by the E-modulus measured for the case A/B = 0.
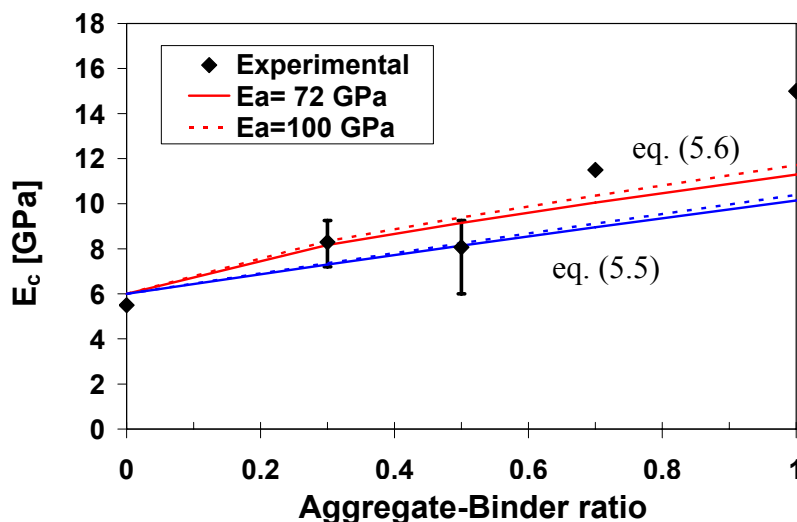

Figure 5.17: Influence of aggregate content on the E-modulus of cast SHCC [van Zijl 2005].

A significant dependence of E_c on aggregate content is apparent. The computed values underestimate the measured increase in E_c in the higher A/B range. All the E-moduli reported here

were determined with tests conducted after 14days of curing. Figure 5.18 shows the evolution of E_c, the cast SHCC used in this research study (A/B = 0.5), confirming that the 28 day E-modulus is significantly higher than the 14 day value [van Zijl 2005].
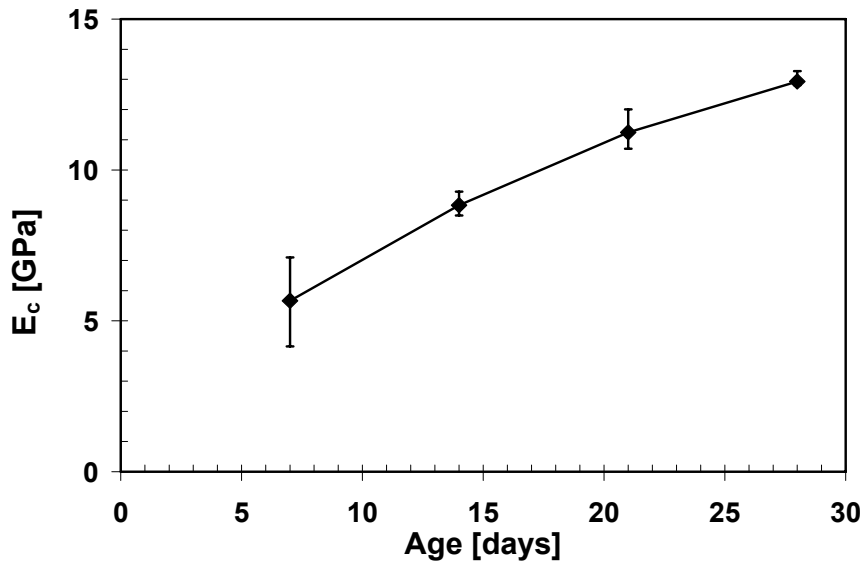
Figure 5.18: Influence of aging (A/B = 0.5) on the E-modulus of cast SHCC [van Zijl 2005].

As it was stated in the earlier chapters, the extruded SHCC has a lower W/B = 0.25 ratio than the cast SHCC (W/B = 0.4) to ensure the correct extrusion rheology. Thereby the aggregate content in the extrusion mix is effectively increased ($V_a^{extrude}$ = 0.23). This aggregate volume portion can be achieved in a cast mix with W/B = 0.4 and A/B = 0.625. For such a mix Figure 5.17 suggests E_c to be in the region of 8 – 10 GPa. This is slightly higher than the E_c shown for the same cast SHCC mix as the one used in this research study (A/B = 0.5). However, the E_c that was measured for the extruded SHCC is between 22.18 GPa and 25.29 GPa. To explain this significant difference, another mechanism is considered, namely paste porosity.

It is known that a reduced W/B ratio is linked to reduced porosity (p) and thus increased E-modulus of hardened cement paste. The governing mechanism of reduced porosity here however is the extrusion pressure, where by air is forced from the paste. Experimental evidence indicates a cubic relation between the paste E-modulus and porosity [Helmuth et al. 1996]:

$$E_p = E_p^*(1-p)^3 \tag{5.7}$$

where E_p^* is the paste modulus for zero porosity (p = 0). When assuming that the extruded SHCC has a porosity of 0% and by substituting E_p = 5.3 GPa into eq. (5.7), a porosity of 31.23% and

30.59% respectively is computed from eq. (5.5) and eq (5.6) for the cast SHCC pastes. Furthermore, keeping in mind that this is the porosity of the paste, which comprises 75% of the composite ($V_p^{extrude}$ = 0.75), an overall void content of 23.42% (eq. (5.5)) and 22.92% (eq. (5.6)) respectively is suggested. Air content values of about 15% have been measured for fresh SHCC mix with V_f = 2% at the University of Stellenbosch in the past. It is postulated that the extrusion process forces entrained air from the composite, and is thereby the main mechanism of increased stiffness of the hardened SHCC produced by extrusion. It is suggested that the quantification of the porosities and air content of cast versus extruded SHCC be investigated in future research. An indication of reduced porosity through extrusion is given by the increased density of extruded SHCC specimens in comparison to cast SHCC specimens [de Koker 2004].

6 BENDING MODEL FOR SHCC

This chapter is concerned with the development of a simple model that can be used to predict the maximum moment resistance of an SHCC member and from that the maximum force that can be applied to the SHCC member. Unlike ordinary concrete, there are currently no design guidelines for SHCC flexural members like beams and beam-columns and thus the need for a simple bending model was identified, to assist in the design of such flexural members. The principles of the bending model will be discussed in this chapter along with a comparison between results that were obtained with the use of the model and that of actual bending tests.

6.1 MODEL DESCRIPTION

The proposed bending model uses the compressive and tensile stress-strain responses of SHCC that were determined in Chapter 5 to calculate the stress distribution on a cross section of an SHCC member. This is done based on the assumption that the strain is distributed linearly over the given cross section.

The stress distribution on a cross section is obtained for a given strain distribution over the cross section. The cross section is divided into layers of equal height and the stress at the mid-point of each layer is determined from the stress-strain distribution. A force is then calculated for each layer by multiplying the area of the layer with the stress at the midpoint of the layer. The sum of all these forces is computed and, if the sum equals zero, the stress distribution is valid, as static equilibrium exists. If equilibrium does not exist, the neutral axis is adjusted, in other words the strain distribution is adjusted until equilibrium is reached. Once the correct strain distribution is found that ensures equilibrium, the moment resisted by the cross section is computed by adding together all the moments about the neutral axis caused by the layer forces. This concept is illustrated in Figure 6.1 for a rectangular beam.

Force for layer 1: $F_1 = \sigma_1 * h_1 * w$
Moment for layer 1: $M_1 = F_1 * d_1$
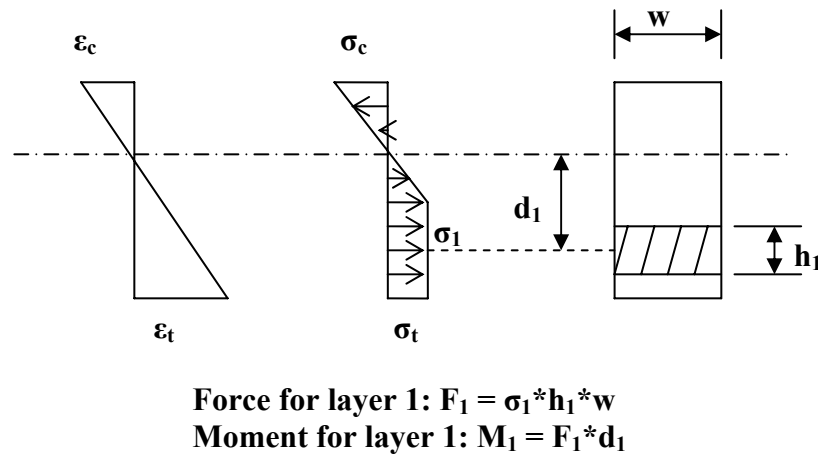
Figure 6.1: Diagram of the strain and stress distribution of an SHCC cross section.

For this research, the bending model described above was implemented in a Microsoft Excel [MS Office 2006] spreadsheet. This was done to first test the model. It can be implemented in a programming environment that is better suited for automated computation, like MATLAB [The Mathworks 2006], at a later stage.

The program requires as user defined input the tensile and compressive properties of the specific type of material. The dimensions of the cross section and the number of layers into which the cross section has to be divided, also have to be given as input. Note that a cross section with varying width over its height can also be accommodated. The maximum tensile strain, i.e. the strain at the lower edge then has to be specified, for which equilibrium and the accompanying moment resisted by the cross section is computed with the use of the solver function of Excel.

6.1.1 COMPRESSIVE AND TENSILE STRESS-STRAIN MODEL

Universal, simple best-fit curves were found to represent the stress-strain responses of the various materials used in this research, namely SHCC produced by casting and extrusion, as well as reinforcing steel.

The tensile stress-strain model for SHCC is shown in Figure 6.2. The parameters that are shown in this figure are used as input values for the bending model. The strain softening part of the curve, after the ultimate tensile stress is reached, should not be expressed as a strain, since this is a localized event where one crack localizes and starts opening up. This part can however be expressed as a strain when one considers the crack spacing between two cracks of the composite to be the gauge length and that the maximum amount that a crack can open up is half of the fibre length.

Then the maximum tensile strain of the composite in the gauge length spanning the localised crack can be expressed as follows:

$$\varepsilon_{t\max} = \varepsilon_{tu} + \frac{0.5L_f}{c}$$

(6.1)

where ε_{tu} is the strain corresponding to the ultimate tensile stress (σ_{tu}), L_f is the length of the fibres and c is the crack spacing between the fibres. The crack spacing for cast SHCC was previously determined [Boshoff 2006] to be 1.3 mm. It is assumed that this is also the value for extruded SHCC.
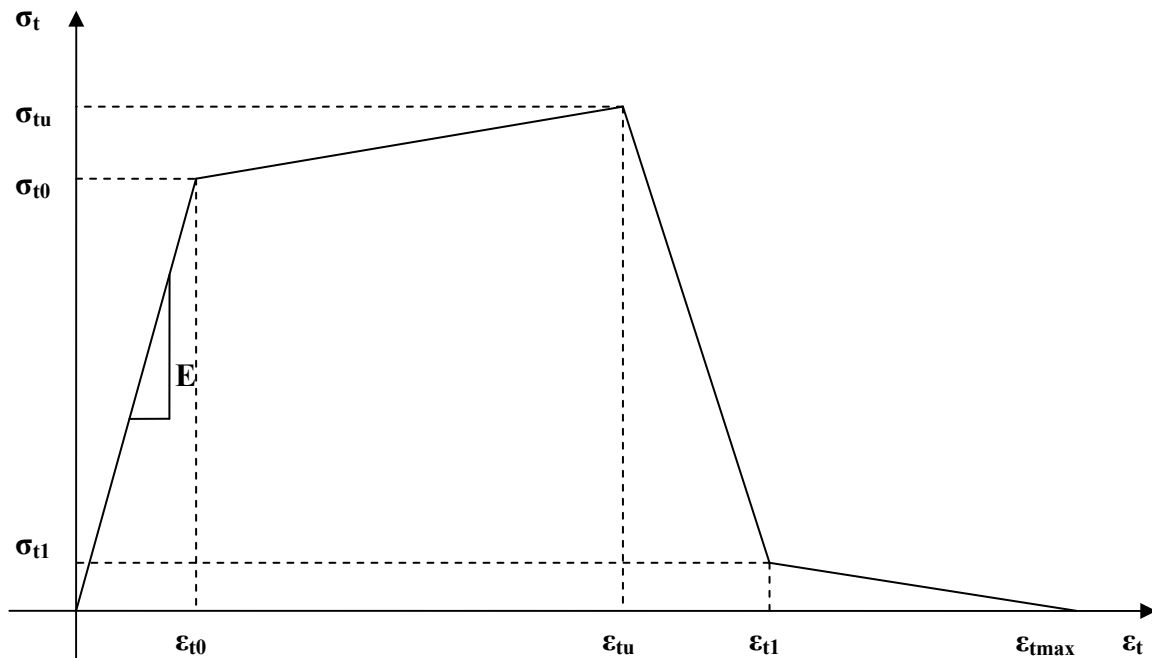
Figure 6.2: Tensile stress-strain model for SHCC material.

The parameter values for the tensile stress-strain model for cast and extruded SHCC are given in Table 6.1. These values were chosen based on average values for the E-modulus, ultimate strength and the ductility that were obtained in Chapter 5 and on a best fit to the stress-strain curves that were also obtained in the same chapter. The curves that were fitted to the uni-axial tensile test results for the cast and extruded SHCC with these values are shown in Figure 6.3.

Table 6.1: Parameter values for the tensile stress-strain model for cast and extruded SHCC.

	E [MPa]	σ_{t0} [MPa]	σ_{tu} [MPa]	σ_{t1} [MPa]	ε_{tu} [%]	ε_{t1} [%]	L_f [mm]	c [mm]
Cast:	10400	2.35	3.20	0.15	4.00	5.25	12	1.3
Extruded:	23000	4.40	4.20	0.25	1.10	2.75	12	1.3
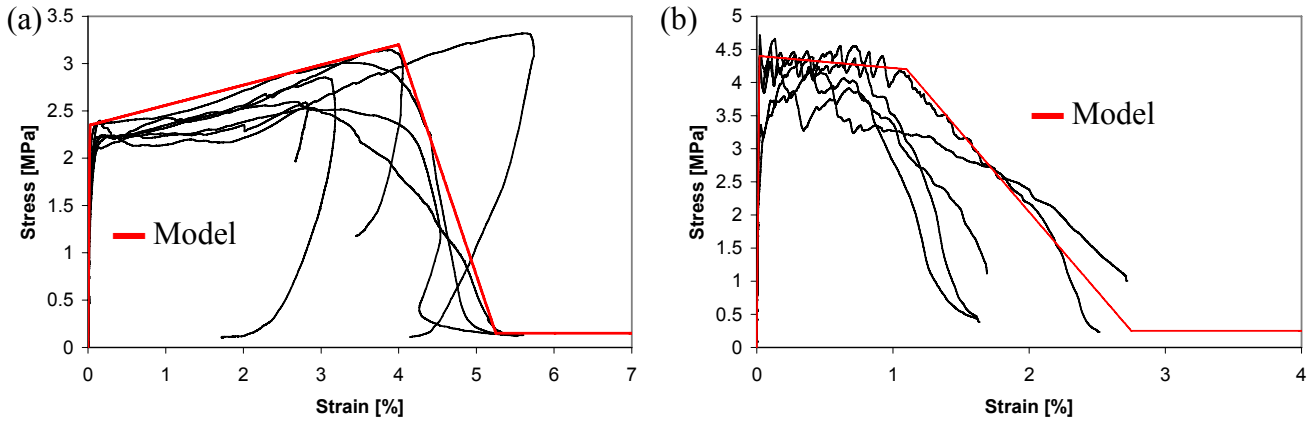
Figure 6.3: Tensile stress-strain curve fitting for (a) cast SHCC and (b) extruded SHCC.

The compressive stress-strain model for SHCC is shown in Figure 6.4. The parameters that are shown in the figure are also used as input values for the bending model. The strain softening part of the curve, after the ultimate stress is reached, should in actual fact not be shown as a strain since this is a localized event as discussed in Chapter 2. The results of the uni-axial compressive tests were however used directly and the strain-softening part of the curve was just fitted accordingly.
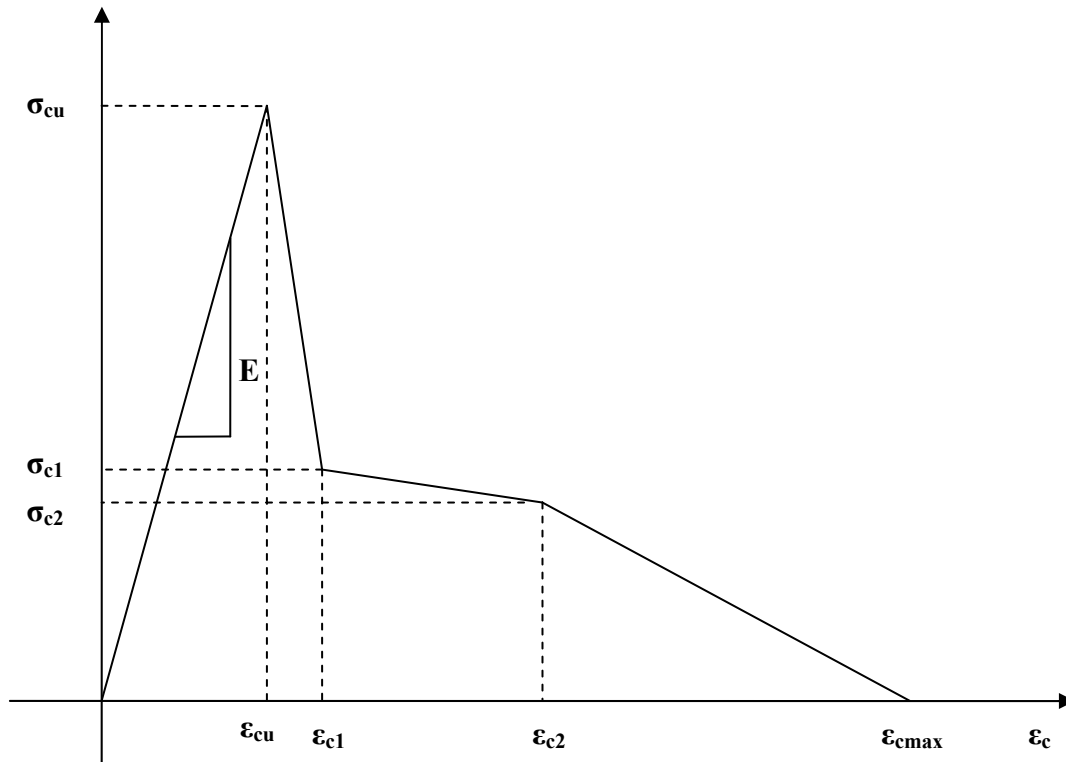
Figure 6.4: Compressive stress-strain model for SHCC material.

The parameter values for the compressive model were obtained by fitting curves to the results that were obtain from the uni-axial compressive tests that were preformed on core specimens. In this case the results that were obtained from the compressive tests that were conducted on cores with an

aspect ratio of 2 are used. These results are seen as a more accurate representation of the type of compression that is expected in the bending of beams, as the boundary effects that are associated with compressive specimens with an aspect ratio of 1 (core and cubes) are reduced for compressive specimens with an aspect ratio of 2. The parameter values for the compressive stress-strain model for cast and extruded SHCC are given in Table 6.2. The curves that were fitted to the uni-axial compressive test results for the cast and extruded SHCC are shown in Figure 6.5.

Table 6.2: Parameter values for the compressive stress-strain model for cast and extruded SHCC

|	E [MPa]	σ_{cu} [MPa]	σ_{c1} [MPa]	σ_{c2} [MPa]	ε_{c1} [%]	ε_{c2} [%]	ε_{cmax} [%]
Cast:	10400	14.0	11.5	8.0	3.00	4.00	7.00
Extruded:	23000	34.0	13.0	9.0	0.40	0.57	2.50
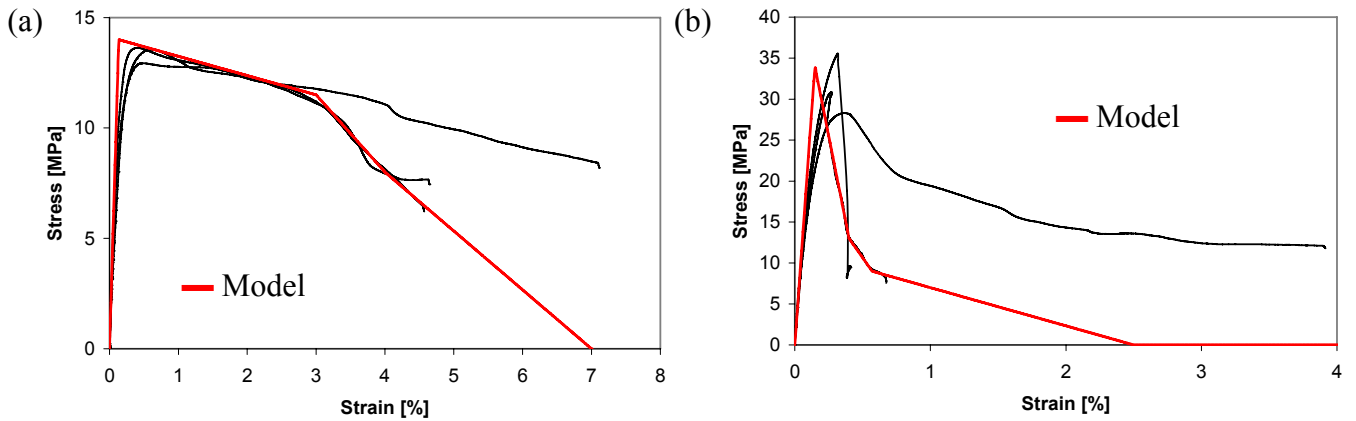
Figure 6.5: Compressive stress-strain curve fitting for (a) cast SHCC and (b) extruded SHCC

6.1.2 STEEL STRESS-STRAIN MODEL

The proposed bending model is also used to calculate the moment resistance of R/SHCC. To compute the steel force, the strain is determined at the midpoint of the steel from the given strain distribution in the cross section. The stress in the steel is then determined form the tensile stress-strain model for the steel and is subsequently multiplied by the area of the steel to calculate the steel tensile force. Now equilibrium of axial force on the cross section must be sought including the steel force. Then, the contribution of the steel to the moment resistance is calculated by multiplying the tensile force in the steel with the lever arm form the neutral axis to the centre of the steel.

As the maximum resistance only is computed by this model, the exact shape of the steel stress-strain curve is not important. However, to accurately account for the ultimate steel force, which is activated in "under-reinforced" elements, it must be known whether the steel is plastic and non-hardening. This was not established in this research, as the available extensometer used in the steel

test setup is intended only for the elastic range, as it has a limited deformation range and may be damaged in case of steel rupture. The linear elastic-perfect plastic tensile stress-strain model was assumed for the reinforcing steel [SABS 0100-1 2000]. The exact parameter values for the model were determined. These values were determined according to SABS 920 [2005] and SABS 054 [1994] with the use of uni-axial tensile tests on the reinforcing bars that were used in this research. Figure 6.6 shows the tensile stress-strain model for the reinforcing steel and the parameter values for this model are given in Table 6.3. These parameter values along with the reinforcing steel bar diameter, the number of bars and the concrete cover to the reinforcing steel have to be given as input values to the bending model when calculating the R/SHCC moment of resistance.
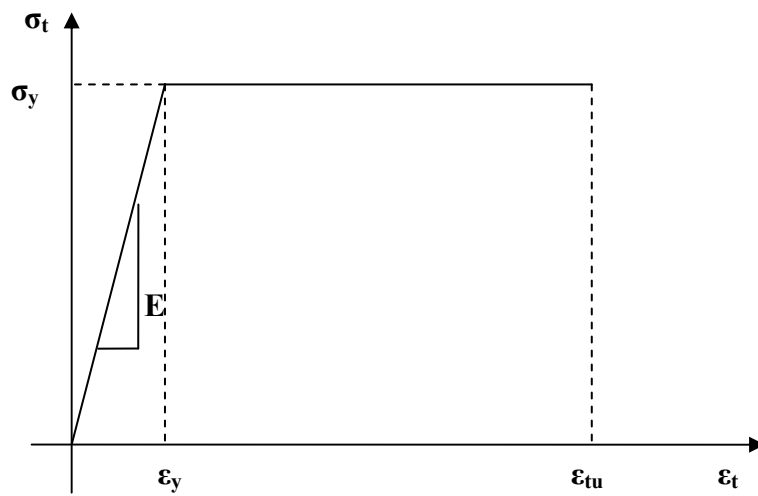
Figure 6.6: Tensile stress-strain model for reinforcing steel.

Table 6.3: Parameter values for the tensile stress-strain model for the reinforcing steel.

E [MPa]	σ_y [MPa]	ε_{tu} [%]
200 000	550.0	12.0

6.2 BENDING CALCULATIONS AND RESULTS

An analysis was conducted using the proposed bending model and the parameter values from the previous section to calculate the resistance moment of thin cast and extruded plates (15 mm X 70 mm) as well as the resistance moment of cast and extruded SHCC and cast and extruded R/SHCC beams (100 mm X 100 mm). Figure 6.7 and Figure 6.8 show the computed resistance moment plotted against the maximum tensile strain, in other words the strain at the bottom of a specimen.
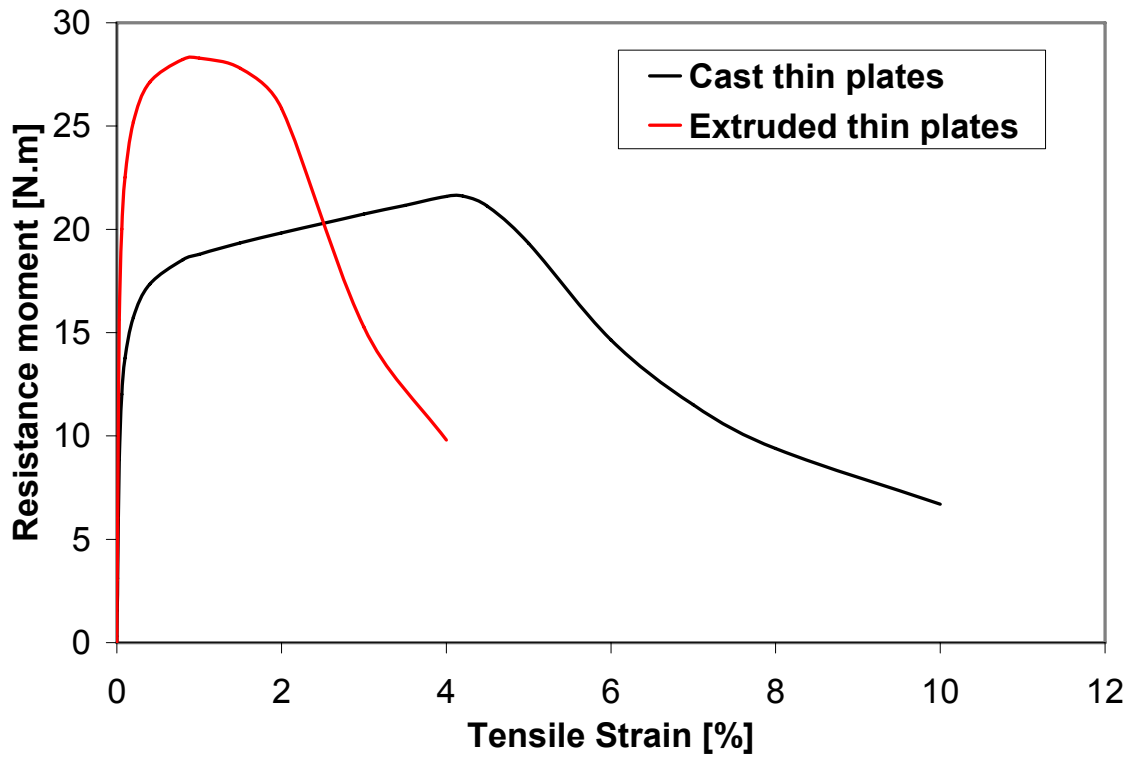
Figure 6.7: Computed resistance moment of thin cast and extruded SHCC plates (15 mm X 70 mm).
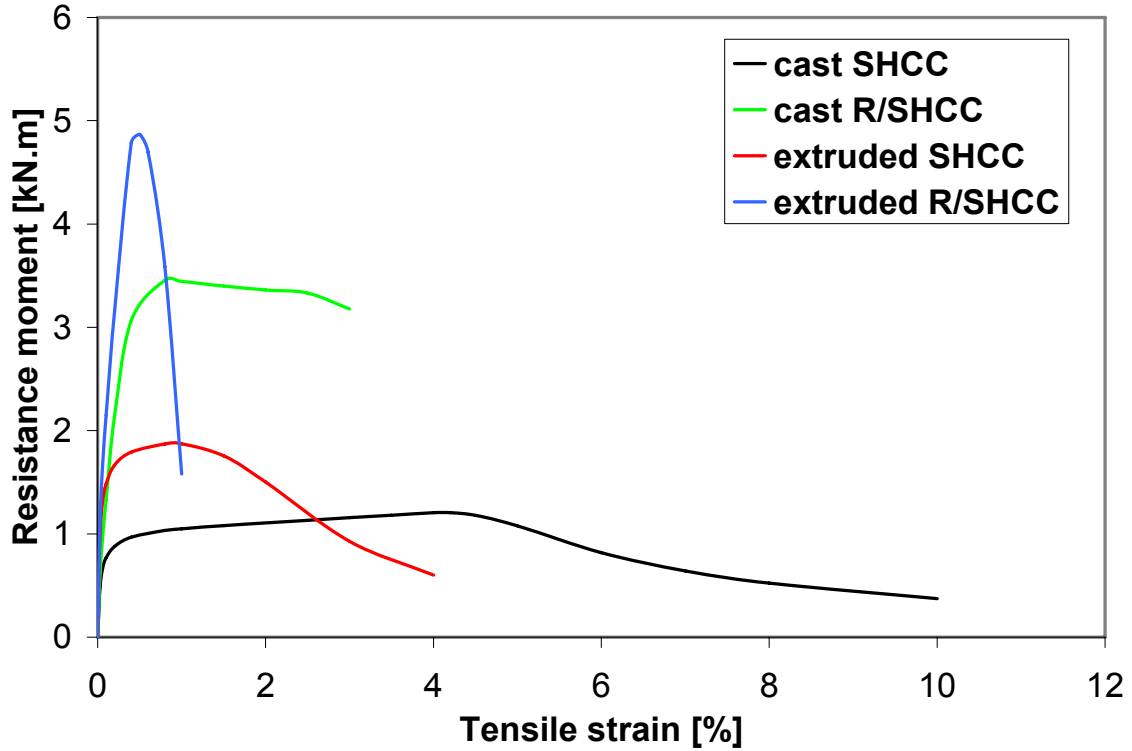
Figure 6.8: Computed resistance moment of cast and extruded SHCC and R/SHCC beams (100 mm X 100 mm).

From the resistance moment of an element the corresponding force that can be applied to the element can be calculated. For instance, for three-point bending tests the maximum moment is in the middle of the element and the applied mid-span force P can be calculated as follows:

$$P = \frac{4M}{L}$$
(6.2)

where M is the maximum moment and L is the distance between the supports.

The ultimate resistance moment for the various composites along with the ultimate applied mid-span force for three-point bending is given in Table 6.4 and Table 6.5. These values are compared with the values of the ultimate applied mid-span forces that were previously determined from three-point bending tests in this research study, reported in Chapter 5. The values for the thin cast SHCC and extruded SHCC plates were taken from previous research studies [Boshoff 2006, Visser 2005].

Table 6.4: Ultimate moment resistance and ultimate applied forces for thin SHCC plates

	Bending model		Test results
	M_{max} [N.m]	F_{max} [N]	F_{max} (average) [N]
Cast SHCC:	21.61	216.1	255.0
Extruded SHCC:	28.28	282.8	298.7

Table 6.5: Ultimate moment resistance and ultimate applied forces for SHCC and R/SHCC beams

	Bending model		Test results
	M_{max} [kN.m]	F_{max} [kN]	F_{max} (average) [kN]
Cast SHCC:	1.206	12.06	15.78
Cast R/SHCC:	34.54	34.54	32.23
Extruded SHCC:	1.872	18.72	20.17
Extruded R/SHCC:	48.69	48.69	49.15

6.3 DISCUSSION

It can be seen from the resistance moment results calculated with the bending model that the model somewhat underestimates the resistance moment capacity of the unreinforced cast and extruded SHCC composites. The calculated resistance moment for the thin cast SHCC plates is 84.7% of the experimentally determined average value, while calculated resistance moment for the thin extruded SHCC plates is 94.7% of the experimentally determined value. On the other hand, the calculated resistance moment for the cast SHCC beams (100 mm X 100 mm) is 76.4% of the experimentally

determined average value, while calculated resistance moment for the extruded SHCC beams (100 mm X 100 mm) is 92.8% of the experimentally determined value.

This underestimation can be due to the inherent assumptions that are incorporated in the bending model. The strain distribution is assumed to be linear over the cross sections at all times, in actual fact the strain distribution does not stay linear and thus the stress distribution will also change which could result in a different stress profile over the cross section. This in turn will lead to a different, higher maximum moment resistance capacity of the element. The dependence of SHCC on the loading rate [Boshoff 2006] is also not taken into account with the model, which may be another source of inaccuracy. When a specimen is subjected to bending, the deformation rate across the cross section is not uniform, with this rate increasing towards the bottom edge of the specimen. As it was shown by Boshoff [2006] the resistance of a specimen increases with increased loading or deformation rate, thus it is postulated that the specimen should have a higher resistance at its bottom edge than is afforded to it by the model. By not taking this phenomenon into consideration the resistance moment of the specimen is underestimated. The above mentioned reasons for underestimation will be more pronounced in specimens with a larger cross section as is evident from the results.

Another possible reason why the unreinforced cast SHCC's moment resistance is underestimated by the model is because it does not take account of the orientation of the fibres at the bottom of the cast specimens. The fibres at the bottom edge of the specimens are horizontally orientated due to the mould boundary influence. The bottom fibres are thus aligned to better resist the loading of the specimen. In Chapter 5 tensile specimens were cut from extruded beams to establish exactly this fact, namely whether the fibres are differently orientated closer to the lower boundary than in the centre. No significant difference was found. The same procedure was not followed for the cast specimens, as the focus is on extrusion here. Nevertheless, the beam resistance results present evidence in the form that the under-prediction of the beam model is significantly more for cast beams (average ultimate load 76.4% of the experimental load) than for extruded beams (92.8%). Furthermore, for the 15 mm thin plates this difference is not as significant between the cast (84.7% of the experimental load) and extruded (94.7%) specimens. Although it was argued by Boshoff [2006] that this boundary effect is present even in such (15 mm) thin plate specimens, the current research results indicate that it is not as pronounced as in the case of 100 mm thick beams. However, this must be further studied and confirmed.

The characterization of the cast SHCC was done over a period of more than two years and by two different researchers. The tensile tests and the bending tests on the thin plates were conducted by Boshoff [2006], while the compression tests and the bending tests on the 100 mm X 100 mm beams were conducted in this research study. Although the same mix design and preparation procedures were used, this use of different ingredient materials and a slight variability in test procedure can cause differences in material properties. This can be cited as the main cause for underestimation of the cast SHCC resistance moment. The prediction of the resistance moment of extruded SHCC is fairly accurate and it is postulated that the reason for this is the fact that the characterization of the extruded SHCC was done using the same materials and was done by one researcher.

The resistance moments of the cast and extruded R/SHCC as determined with the bending model can not directly be compared with the experimentally determined values of Chapter 4. The reinforced beams tested in Chapter 4 failed in a combination of flexure and shear and the bending model does not take account of the shear stresses and capacity of the SHCC and thus cannot predict failure in shear. These calculated resistance moment values can however be seen as the predicted resistance moment of the reinforced composites, should they have failed in flexure. It can then also be postulated that these values are also an underestimation, when following the same reasoning as for the unreinforced composites.

The bending model can however be deemed to be sufficient for design purposes. It is a very simple model that can be used very easily once the compressive and tensile model parameter values of a composite are known. The model was implemented in Microsoft Excel for this research study to enable easy changes to the model and to first test the model. It can be implemented in a more suitable and powerful program like MATLAB in a future research study. This can enable the user to predefine the tensile strain range over which the maximum moment resistance should be determined and the program can then automatically determine the corresponding compressive strains and the maximum moment resistance and draw a curve. Another prospect is to convert the strains into deflections so that this can be compared directly with measured values of deflection.

7 CONCLUSIONS AND RECOMMENDATIONS FOR FUTURE RESEARCH

7.1 CONCLUSIONS

The main objective of this research study was to investigate the effects that the piston-driven extrusion of SHCC have on the mechanical and structural behaviour thereof. To this end a new piston-driven extruder facility with the ability to extrude reinforced as well as unreinforced SHCC structural elements was designed and built. Subsequently a comparative study, based on the flexural behaviour of beams, was undertaken, where SHCC and R/SHCC beams produced by casting and extrusion as well as reinforced beams cast from ordinary concrete were tested in three-point bending. It was found that the superior mechanical behaviour of SHCC and R/SHCC in flexure when compared to that of R/C in flexure can be enhanced even more with extrusion.

The mechanical behaviour of extruded SHCC was also tested in uni-axial tension and compression and compared with the mechanical behaviour of cast SHCC. It was postulated that the reduced porosity of extruded SHCC is the main source for increased strength in compression and tension as well as its higher E-modulus. A bending model, based on these uni-axial tests, was also proposed for SHCC and the results from this model were compared to results that were obtained from experimental testing.

The following significant conclusions can be drawn from the work presented in this thesis:

7.1.1 COMPARATIVE STUDY

- Extruded SHCC display superior flexural properties in terms of first cracking strength and ultimate strength but with a reduced ductility when compared to cast SHCC. This was also observed with the reinforced SHCC's. This reduction in ductility is due to the increased

cracking strength of extruded SHCC which leads to less micro-cracking, which is the source of ductility.

- R/SHCC is a far superior construction material to R/C in terms of flexural characteristics. Although the R/SHCC specimens failed in a combination of flexure and shear they still have a higher shear resistance than R/C, which in fact reduces and in some instances may eliminate the need for shear reinforcement. The R/SHCC specimens also displayed higher ultimate strength and better ductility than the R/C specimens.

- The shear resistance of extruded SHCC is higher than that of cast SHCC because of the better fibre orientation of extruded SHCC. There are more fibres that can bridge and arrest the cracks that form in the matrix and this causes several shear cracks to form before the composite fails. Cast SHCC can also form multiple shear cracks, but fail earlier than extruded SHCC since not enough fibres are available to effectively bridge and arrest these cracks due to the random alignment of the fibres.

- The fibre orientation in extruded specimens is not significantly different in the lower boundary area from that in the beam at middle height. However, for cast specimens a significant difference in fibre orientation is believed to exist in these two regions, to which fact the under-prediction of the cast beam resistance by the beam model developed in this research is ascribed. However, this postulation remains to be studied and proven.

7.1.2 MECHANICAL CHARACTERISTICS OF EXTRUDED SHCC

- Extruded SHCC has a higher tensile first cracking strength and ultimate strength than cast SHCC. This is due in part to the difference in W/B ratio and the orientation of fibres in the direction of loading, but mainly due to the densification and thus reduced porosity of the composite as a result of the high extrusion forces.

- Extruded SHCC however has a lower tensile ductility in comparison to cast SHCC. This is in agreement with micro-mechanical considerations whereby increased crack tip toughness relative to fibre pull-out complementary energy requires a larger critical fibre volume to ensure tensile strain-hardening and ductility.

- Extruded SHCC also displays a significantly higher ultimate compressive strength than cast SHCC. This is due to a combination of a reduced W/B ratio and a reduce paste porosity.

- The elastic modulus of SHCC elements is increased when produced with extrusion. This is due to the higher aggregate content and a lower porosity of extruded products.

7.1.3 BENDING MODEL

- A simple bending model was proposed to predict the resistance moment of cast and extruded SHCC specimens. The results of the model compare fairly well with experimentally determined results. The model however somewhat under estimates the resistance moment of the composites, especially that of the cast SHCC.

- It is postulated that this underestimation is due to the inherent assumptions of the model and the fact that the rate effects of SHCC are not taken into account. Furthermore it is postulated that material properties can also vary over the cross section of cast SHCC specimens, but this still remains to be investigated. It was however shown in Chapter 4 that this is not the case with extruded SHCC specimens, which is ascribed to the optimised mix rheology and the internal pressure in the extruder transition zone

- R/SHCC composites were also modelled and their resistance moments calculated. These could however not be compared to the experimental results since the specimens failed in a combination of flexure and shear. It is however postulate that the actual resistance moment of these composites can be higher when following the same reasoning as for the SHCC composites.

7.2 FUTURE RESEARCH

The following issues were identified during this research study as possible inclusions in future research studies:

- In Chapter 3 design calculations, based on fluid flow, were used to design a new piston-driven extruder. The formulas that were derived to describe the change in pressure along the extrusion path were based on fluid flow and friction. A better model is needed to describe the flow of a viscous material and to set up formulas to describe the change in pressure along the extrusion path. These formulas can then be used for future design optimisation of extruders.

- The effects of different die lengths and transition lengths and angles should be investigated. By such study (i) the mechanical properties and surface finish of the extrudate can be optimised, and (ii) data for an improved model to describe the flow of material through the extruder may be obtained.

- When large cross sections of SHCC are extruded, the specimens settle under their own weight in the fresh state. This causes the specimens to be somewhat deformed and a solution

to this problem needs to be found. The rheology can be changed to ensure a stiffer mix or deformed specimens can be extruded which settles into the correct shape.

- The current extrusion set-up is only suitable for academic research. If this process is to be used in a factory it needs to be industrialized. Possible issues that can be addressed are the continuous feeding of the SHCC material, the feeding of reinforcement steel into the extruder and to handling of the extrudate once it exits the extruder.

- Experiments can be conducted to investigate the bond between SHCC and reinforcing steel. This can assist in the design of R/SHCC flexural elements where the bond length needs to be specified. It can also be used in the more accurate determination of the resistance moment of R/SHCC.

- Other possible applications for extruded SHCC can be identified and tested. Research can also be conducted where the extruded SHCC is modified to have a somewhat more random alignment of its fibres which will enable the use of extruded SHCC in bi-axial loading.

- The bending model can be refined to be implemented in a more suitable computer program. The model can also be modified to calculate the deflections of specimens corresponding to the moment resistance.

8 REFERENCES

Abrishami, H.H. and Mitchell, D. "Influence of Steel Fibres on Tension Stiffening", *ACI Structural Journal*, V.94, No.6, p. 769-776, November/December 1997.

Addis, B. *"Fundamentals of concrete"*, Chapter 8, p.101.Cement and Concrete Institute, 1998.

Avenant, P., *"Engineered Cement-based Composites (ECC) for the application of permanent formwork"*, Final Year Research Project, University of Stellenbosch, June 2005.

Boshoff, W.P. *Time-Dependant Behaviour of Engineered Cement-based Composites*. PhD Thesis, University of Stellenbosch, 2006.

de Koker, D., *"Manufacturing processes for Engineered Cement-based Composite material products"*, MScEng Thesis, University of Stellenbosch, 2004.

Fantilli, A.P., Mihashi, H. and Vallini, P., "The Role of HPFRCC in Compression on the Post-Peak Response of Structural Members", In *Proceedings of the Fifth International RILEM Workshop, High Performance Fiber Reinforced Cement Composites (HPFRCC5)*, p.147 – 154, 2007.

Farhat, F.A. and Karihaloo, B., "RC beams retrofitted with CARDIFRC – Behaviour after thermal cycling", In *Proceedings of the Fifth International RILEM Workshop, High Performance Fiber Reinforced Cement Composites (HPFRCC5)*, p.409–417, 2007.

Fischer, G. and Li, V.C. "Influence of Matrix Ductility on Tension-Stiffening Behavior of Steel Reinforced Engineered Cementitious Composites (ECC)", *ACI Structural Journal*, V.99, No.1, p.104-111, January/February 2002.

Fisher, G. and Li, V.C., "Effect of matrix ductility on deformation behaviour of steel-reinforced ECC flexural members under reversed cyclic loading conditions", *ACI Structural Journal*, V.99, No.6, p.781-790, November/December 2002.

Goodchild, C.H., "Best Practice Guidelines for Hybrid Concrete Construction" *The Concrete Centre*, Surrey, United Kingdom, 2004.

Hashin Z., "The elastic moduli of heterogeneous materials", *J Appl. Mech. 29*, p.143-150, 1962.

Helmuth, R.A. and Turk, D.M., Symposium on Structure of Portland Cement Paste, *Special Report 90*, National Academy of Science, Washington, 1996.

Horikoshi, T. et al. "Properties of polyvinylalcohol fibre as reinforcing materials for cementitous composites", In V. C. Li, G. Fischer, editor, *International RILEM workshop on HPFRCC in structural applications*, page 147. Rilem, S.A.R.L., 2006.

Illston, J.M. and Domone, P. J. L., editors. *Construction Material*, Chapter 13, page 104. Spon Press, 2001.

Illston, J.M. and Domone, P. J. L., editors. *Construction Material*, Chapter 14, page 112. Spon Press, 2001.

Iosipescu, N., "New accurate method for single shear testing of metals, *Journal of Materials*, 2(3), p.537-566, 1967.

Jurgens, C.J. and Wium, J.A., "Investigation into the feasibility of Hybrid Concrete Construction in South Africa", *CIBD Conference*, South Africa, 2006.

Kabele, P. "Fracture Behaviour of Shear-Critical Reinforced HPFRCC Members", *Proceedings of the Workshop on HPFRCC in structural applications*, Honolulu, Hawaii, USA, May 2005.

Kabele, P. and Kanakubo, T., "Experimental and numerical investigation of shear behaviour of PVA-ECC in structural elements", In *Proceedings of the Fifth International RILEM Workshop, High Performance Fiber Reinforced Cement Composites (HPFRCC5)*, p.137 – 145, 2007.

Kabele, P., "*Assessment of Structural Performance of Engineered Cementitious Composites by Computer Simulation*", A habilitation thesis, Czech Technical University, Prague, 2000.

Kanda, T., Kanakub, T., Nagai, S. and Maruta, M., "Technical Consideration in Producing ECC Pre-Cast Structural Element" In *Proceedings of HPFRCC Conference*, Hawaii, 2005.

Krstulovic-Opara, N., Watson, K.A. and LaFave, J.M. "Effect of Increased Tensile Strength and Toughness on Reinforcing-Bar Bond Behaviour", *Cement & Concrete Composites*, V.16, p.129-141, 1994.

Kong, F.K. and Evans, R.H., "*Reinforced and Prestressed Concrete*", Third Edition, Chapter 2, p.25, Spon Press, 2001.

Li, V.C. "On engineered cemetitous composites (ecc) a review of the material and its applications", *Journal of advanced concrete technology*, 1(3), p.215-230, November 2003.

Li, V.C. "Reflections on the research and development of ecc". In *Proceedings of the JCI International Workshop on Ductile Fiber Reinforced Cementitious Composites (DFRCC), Application and Evaluation (DFRCC-2002)*, p.1-21, 2002.

Li, V.C., Mishra, D.K. and Wu, H.C. "Matrix design for pseudo-strain-hardening fibre reinforced composites", *Materials and Structures 28*, p.586-595, 1995.

Li, V.C., Mishra, D.K., Naaman, A.E., Wigh, J.K., Lafave, J.M., Wu, H.C. and Inada, Y. "On the shear behaviour of engineered cementitious composites", *Journal of Advanced Cement Based Materials*, 1(3), p.142-149, 1994.

Li, V.C., and Yang, E.H., "Self-Healing in Concrete Materials", in print, *in Self-Healing Materials*, Ed. S. van der Zwaag, Springer, 2007.

Mackechnie, J.R., Alexander, M.G. and Jaufeerally. Structural and durability properties of concrete made with corex slag. Technical report, University of Cape Town, University of Witwatersrand, 2003.

Microsoft, "Microsoft Office 2006", *Microsoft Excel*, 2006.

Ohno, K. and Arakawa, T. "Shear tests of reinforced concrete beams by special type of loading", *Transactions of Architectural Institute of Japan*, p.581 − 584, 1957. (In Japanese)

Østergaard, L., Walter, R. and Oleson, J.F., "Method for determination of tensile properties of ECC II: Inverse analysis and experimental results." In *Proceedings of HPFRCC Conference*, Hawaii, 2005.

Powers T.C., "Structure and physical properties of hardened cement pastes", *Cement and Concrete Research 5*, 2, p.153 -162, March 1958.

Shah, S.P. and Peled, A. "Processing Effects in Cementitious Composites: Extrusion and Casting", *Journal of Materials in Civil Engineering © ASCE*: p.192-199, March/April 2003.

Shang, Q. and van Zijl, G.P.A.G.., "Characterising the shear behaviour of SHCC", *Journal of the South African Institution of Civil Engineers*, 49(2): p.16-23, 2007.

Shang, Q., *Shear behaviour of Engineered Cement-based Composites*. MScEng. Thesis, University of Stellenbosch, 2006.

Shimizu, K., Kanakubo, T., Kanda, T. and Nagai, S., "Shear behaviour of PVA-ECC beams", *International RILEM Workshop on High Performance Fiber Reinforced Cementitious Composites in Structural Applications,* RILEM Publications SARL, p.443-451, 2006.

South African Bureau of Standards. "Code of practice for tensile testing of metallic materials.", *SABS 054*, 1994.

South African Bureau of Standards. "Concrete tests − The drilling, preparation, and testing for compressive strength of cores taken form hardened concrete", *SABS method 865*, 1994.

South African Bureau of Standards. "Standard specifications for steel bars for concrete reinforcing", *SABS 920*, 2005.

South African Bureau of Standards. "The structural use of concrete; Part 1: Design", *SABS 0100-1*, Edition 2.2, 2000.

South African Bureau of Standards. "The structural use of concrete; Part 2: Materials and execution of work", *SABS 0100-2*, Edition 2, Table 5, 1992.

South African Bureau of Standards. "Detailing of steel reinforcement for concrete", *SABS 0144*, Edition 2, Annex D, 1995.

Stander, H., "*Interfacial bond properties of ECC overlay systems*" MScEng. Thesis, University of Stellenbosch, 2007.

Stang H. and Li, V.C., "Extrusion of ECC-material", p.1-10, 1999.

Suwada, H. and Fukuyama, H., "Nonlinear Finite Element Analysis on Shear Failure of Structural Elements Using High Performance Fiber Reinforced Cement Composites", Journal of Advanced Concrete Technology, Vol.4, No.1, p.45-57, February 2006.

The Mathworks, "The Language of Technical Computing", *MATLAB R2006a*, 2006.

Van Zijl, G.P.A.G., "The role of aggregate in HPFRCC", *Concrete / Beton 110*, p.7-13, 2005.

Visser, C.R., "*Rheological and Mechanical Optimisation of ECC Manufactured by Extrusion*", Final Year Research Project, University of Stellenbosch, November 2005.

Yamada, K., Saijo, R., Furumura, T. and Tanaka, S., "Application of extrusion moulded DFRCC to permanent form", *International RILEM Workshop on High Performance Fiber Reinforced Cementitious Composites in Structural Applications,* RILEM Publications SARL, p.253-260, 2006.

Yang, Y., M. Lepech and Li, V.C., "Self-Healing of Engineered Cementitious Composites Under Cyclic Wetting And Drying", Proc. *Int. Workshop on Durability of Reinforced Concrete under Combined Mechanical and Climatic Loads (CMCL),* Qingdao, China, p.231-242, 2005.